Thermodynamic Concepts in Adaptive Resolution Simulations.

Dissertation

zur Erlangung des Grades

"Doktor der Naturwissenschaften"

am Fachbereich Physik

der Johannes Gutenberg-Universität

in Mainz

Simón Poblete

geboren in Santiago (Chile)

Mainz, November 2010

Datum der mündlichen Prüfung: 20. Januar 2011

Zusammenfassung

Diese Arbeit befasst sich mit den konzeptionellen und technischen Entwicklung des "Adaptive Resolution Scheme" (AdResS) , einer Methode der Molekulardynamik, welche die gleichzeitige Simulation eines System in unterschiedlichen Auflösungen, ermöglicht. Die Simulationsdomäne teilt sich in einen Bereich mit höherer und einen Bereich mit geringerer Auflösung. Gekoppelt sind sie durch einen Übergangsbereich, indem die Moleküle frei diffundieren können.

Der erste Teil der Dissertation ist auf die thermodynamische Konsistenz der Methode fokussiert, die an einem flüssigen Modell aus tetraedrischen Molekülen getestet und verifiziert wurde. Die Ergebnisse erlauben die Einführung des Konzepts der *Thermodynamischen Kraft*, bei dem ein externes Feld unphysikalische Dichtefluktuationen im Übergangsbereich, die in üblichen AdResS Simulationen auftreten, korrigiert. AdResS wird auch auf ein System angewandt, bei dem sich zwei unterschiedliche Darstellungen mit identischem Auflösungsniveau gegenüberstehen. Dieser einfache Test erweitert die Anwendbarkeit der Methode von einem Schema mit adaptiver Auflösung zu einem Schema mit adaptiver Darstellung, in dem unterschiedliche Kraftfelder, die auf thermodynamischen Konsistenzargumenten basieren, gekoppelt werden können. Die Methode der *Thermodynamischen Kraft* wurde in dem hier dargestellten Beispiel erfolgreich angewandt.

Ein alternativer, auf konstantem Druck basierender Ansatz für die Deduktion der Thermodynamischen Kraft, ermöglicht die Interpretation des AdResS als ersten Schritt hin zu einer molekulardynamischen Simulation im großkanonischen Ensemble. Ausserdem hilft eine solche Definition die Thermodynamisches Kraft, die in der bekannten tetraedrischen Flüssigkeit getestet wird, einfacher zu bestimmen. Die Effekte von AdResS und deren Korrektur im atomistische Bereich der Simulation wurden durch die Untersuchung der lokalen Verteilung der Geschwindigkeiten, Radialverteilungsfunktionen, Druck und Schwankung der Partikelanzahl, analysiert. Deren Vergleich mit analogen Ergebnissen aus rein atomistichen Simulationen zeigt eine gute Übereinstimmung, die unter dem Einfluss des externen Feldes noch gesteigert wird.

Ein weiterer Schritt in der Entwicklung des AdResS, der für verschiedene Anwendungen in der Biophysik und Materialkunde nötig ist, setzt seine Anwendung zu Multikomponentensystemen voraus. In dieser Hinsicht wird die Darstellung in höherer Auflösung eines binären Mischungsmodells gegen seine vergröberte (coarse-grained) Darstellung systematisch parametrisiert. Dabei bringt die Methode der Thermodynamischen Kraft zufriedenstellende Ergebnisse, auch wenn ihre Entwicklung eine noch feinere Bearbeitung benötigt.

Schließlich wurde das AdResS in Systemen mit zweikörper-gebundenen Kräften durch die Simulation von einem Modellpolymer, dem es erlaubt ist, seine Darstellung adaptiv zu verändern, getestet. Es wird gezeigt, dass die Verteilung der Funktionen, die die Polymerstruktur charakterisieren, in der Praxis durch eine Veränderung der Auflösung nicht beeinflusst wird.

Die Erläuterung der technischen Details für die Ausführung von AdResS im ESPResSo Softwarepaket bildet den letzten Teil dieser Dissertation.

Summary

This thesis work is devoted to the conceptual and technical development of the Adaptive Resolution Scheme (AdResS), a molecular dynamics method that allows the simulation of a system with different levels of resolution simultaneously. The simulation domain is divided into high and low resolution zones and a transition region that links them, through which molecules can freely diffuse.

The first issue of this work regards the thermodynamic consistency of the method, which is tested and verified in a model liquid of tetrahedral molecules. The results allow the introduction of the concept of the Thermodynamic Force, an external field able to correct spurious density fluctuations present in the transition region in usual AdResS simulations. The AdResS is also applied to a system where two different representations with the same degree of resolution are confronted. This simple test extends the method from an Adaptive Resolution Scheme to an Adaptive Representation Scheme, providing a way of coupling different force fields based on thermodynamic consistency arguments. The Thermodynamic Force is successfully applied to the example described in this work as well.

An alternative approach of deducing the Thermodynamic Force from pressure consistency considerations allows the interpretation of AdResS as a first step towards a molecular dynamics simulation in the Grand Canonical ensemble. Additionally, such a definition leads to a practical way of determining the Thermodynamic Force, tested in the well studied tetrahedral liquid. The effects of AdResS and this correction on the atomistic domain are analyzed by inspecting the local distribution of velocities, radial distribution functions, pressure and particle number fluctuation. Their comparison with analogous results coming from purely atomistic simulations shows good agreement, which is greatly improved under the effect of the external field.

A further step in the development of AdResS, necessary for several applications in biophysics and material science, consists of its application to multicomponent systems. To this aim, the high-resolution representation of a model binary mixture is confronted with its coarse-grained representation systematically parametrized. The Thermodynamic Force, whose development requires a more delicate treatment, also gives satisfactory results.

Finally, AdResS is tested in systems including two-body bonded forces, through the simulation of a model polymer allowed to adaptively change its representation. It is shown that the distribution functions that characterize the polymer structure are in practice not affected by the change of resolution.

The technical details of the implementation of AdResS in the ESPResSo package conclude this thesis work.

Contents

Introduction

Computer simulations have become a major topic in physics during the last decades and a powerful tool to inquire into the details of complex systems. They can provide detailed information that is not accessible from an experimental perspective, or allow the study of a system under conditions that are difficult or unfeasible to achieve in real experiments. Additionally, molecular simulations can be the key to obtaining a more complete picture of systems where theoretical models can only provide qualitative information about their properties.

However, the same complexity that requires this treatment can become a challenge to simulate. For example, when the time that a system needs to reach equilibrium demands simulations over times that are far beyond the current capabilities, an exhaustive description is prohibitive. Therefore, the problem can be addressed through a simpler approach by removing the faster degrees of freedom, and effectively reintroducing them, keeping the relevant physics from the original picture. The simplification leads to a *coarse-grained* representation, where the number of degrees of freedom has been reduced, resulting in a model that is less computationally expensive. Furthermore, it also permits the removal of specific details in order to analyze their importance in the phenomena of interest. By this means, it is possible to treat each scale of a system separately, bridging them in a hierarchical way.

Another possible approach is to simulate a system where the detailed description is restricted to a limited region while the rest is treated in a coarser manner. Several methods have been proposed with the aim of linking different representations described by quantum, classical or continuum mechanics. The Adaptive Resolution Scheme (AdResS), the method of concern in this work, falls into this category. It allows the performance of molecular dynamics simulations of different classical representations of the same system, through which particles can freely diffuse.

The present work contributes to its development by studying its thermodynamic consistency, and improving its results by means of these principles through the definition of the Thermodynamic Force. It also states the principles that allow AdResS to be interpreted as a first step towards the simulation of open systems.

The thesis is composed of eight chapters.

- Chapter 1 introduces basic concepts of statistical mechanics that will be

useful for the latter chapters. It also provides the basics of molecular dynamics simulations that will orient the reader in the context of the following work.

- Chapter 2 is concerned with coarse-graining in simulations of soft matter systems. The main concepts and the methods employed in this thesis are described here.

- Chapter 3 is dedicated to the Adaptive Resolution Scheme. The equations of motion are presented, and the interpretation of thermodynamic quantities in a system with a variable number of degrees of freedom is introduced, based on the principles of fractional calculus. The nature of the equations and their consequences are also explained. The chapter is concluded with the analysis of a well studied model system: a medium dense liquid of tetrahedral particles. It presents the main features of an AdResS simulation, its advantages and the effects of the equations of motion in the region where the two resolutions are matched.

- Chapter 4 introduces the concept of the Thermodynamic Force, an external field able to correct the spurious effects that AdResS can produce in the density of the system, which development is based on thermodynamic considerations. It is applied to the previously introduced tetrahedral system, and to a set of two one-site potentials, where the resolution does not change but the force fields do. A practical implementation is presented, based on an alternative interpretation that leads to the thermodynamic consistency with the grand canonical ensemble.

- Chapter 5 consists of the study of a model binary mixture. A coarse-grained set of potentials is developed and confronted with its atomistic representation in AdResS. In addition, the thermodynamic force is calculated for this system.

- Chapter 6 contains the first AdResS results of two-body bonded interactions from the study of a model polymer.

- Chapter 7 describes the implementation of AdResS in the ESPResSo simulation package, a more technical aspect that provides helpful insight into the equations of motion.

- Finally, the conclusions are presented in Chapter 8.

Chapter 1

Basic concepts

This chapter is composed of two sections that provide the main theoretical elements used in this thesis. The first part contains the basic statistical mechanics and distribution functions and their relation to thermodynamics. The definition of the Potential of Mean Force, a quantity of relevance in this work, is also introduced. The second section explains some basic concepts of molecular dynamics simulations and some features of the calculations presented in the later chapters.

1.1 The radial distribution function

The state of a classical system constituted of a large number of particles N is totally defined by the positions $\mathbf{r}^N$ and momenta $\mathbf{p}^N$ of its components at a certain time t. However, its exhaustive description is not only unfeasible, but unnecessary for the calculation of macroscopic properties. Therefore, a statistical treatment results more practical and meaningful. The average of a quantity $A(\mathbf{r}^N, \mathbf{p}^N)$ sampled over a trajectory is defined as

$$\langle A \rangle_t = \lim_{\tau \to \infty} \frac{1}{\tau} \int_0^\tau A(\mathbf{r}^N(t), \mathbf{p}^N(t)) dt \tag{1.1}$$

In addition, if it is assumed that in a trajectory position and momentum space is sampled thoroughly [1], the ensemble average of $A(\mathbf{r}^N, \mathbf{p}^N)$ is defined by [1,2]

$$\langle A \rangle = \int \int A(\mathbf{r}^N, \mathbf{p}^N) f(\mathbf{r}^N, \mathbf{p}^N) d\mathbf{r}^N d\mathbf{p}^N \tag{1.2}$$

where each point is weighted by the probability distribution $f(\mathbf{r}^N, \mathbf{p}^N)$ [2–4]. Such a function is determined by the thermodynamic quantities that characterize the macroscopic state of the system, providing a link between the microscopic and macroscopic levels of description. For the canonical ensemble, where the number of particles, temperature and volume are fixed, f is given in terms of

the Hamiltonian $\mathcal{H}$ of the system, by

$$f_{NVT}(\mathbf{r}^N, \mathbf{p}^N) = \frac{e^{-\beta\mathcal{H}(\mathbf{r}^N, \mathbf{p}^N)}}{Q_N(V,T)} \tag{1.3}$$

where $\beta = 1/k_B T$, with k_B the Boltzmann's constant. The normalization factor $Q_N(V,T)$ is the partition function [2–5]. f_{NVT} is a huge object that contains an enormous amount of information which is unnecessary for practical purposes. A way of distilling its physical meaning is to deal with *reduced* distribution functions.

The most simple case is to calculate the probability of finding a particle at some position $\mathbf{r}$, independent of the configuration of the rest of the system, given by [2, 4]

$$\rho(\mathbf{r}_1) = N \int \mathbf{r}_2 \ldots \int d\mathbf{r}_N \int d\mathbf{p}^N f(\mathbf{r}^N, \mathbf{p}^N) \tag{1.4}$$

where the prefactor N indicates that any particle can be chosen among the N indistinguishable particles.

In a homogeneous system, $\rho(\mathbf{r})$ is independent of $\mathbf{r}$ and becomes simply $\frac{N}{V}$. This is enough to describe the thermodynamics in an ideal gas, that lacks of structure. However, if the forces between the particles are relevant, the correlations induced by them must be considered for a proper description of the system. Further information can be extracted from the probability distribution by defining

$$\rho_N^{(2)}(\mathbf{r}_1, \mathbf{r}_2) = N(N-1) \int d\mathbf{r}^{(N-2)} \int d\mathbf{p}^N f(\mathbf{r}^N, \mathbf{p}^N) \tag{1.5}$$

the *pair density function* [2, 4]. This density gives the probability of finding two particles at $\mathbf{r}_1$ and $\mathbf{r}_2$, independent of their identity. It is remarkable that in a homogeneous system of non-interacting components, $\rho_N^{(2)}(\mathbf{r}_1, \mathbf{r}_2) = \rho^2\left(1 - \frac{1}{N}\right)$, that is simply ρ^2 for large N. It is thus convenient to measure the degree of correlation between two particles by comparing the pair density function with this reference value as

$$g_N^{(2)}(\mathbf{r}_1, \mathbf{r}_2) = \frac{\rho_N^{(2)}(\mathbf{r}_1, \mathbf{r}_2)}{\rho(\mathbf{r}_1)\rho(\mathbf{r}_2)} \tag{1.6}$$

If the system is homogeneous, $g_N^{(2)}(\mathbf{r}_1, \mathbf{r}_2)$ depends only on the distance $r = |\mathbf{r}_1 - \mathbf{r}_2|$ and it is denoted simply by $g(r)$, the *radial distribution function*. This function is of vital importance in the theory of liquids. It provides basic information about the microscopic structure, but it is also closely linked to the thermodynamics of the system and determines it completely when particles interact through pair potentials. Moreover, $g(r)$ can be measured experimentally [2,4,6].

In addition, higher order density functions can be defined as

$$\rho_N^{(n)}(\mathbf{r}^N) = N(N-1)\ldots(N-n+1) \int d\mathbf{r}_{n+1} \ldots d\mathbf{r}_N \int d\mathbf{p}^N f(\mathbf{r}^N, \mathbf{p}^N) \tag{1.7}$$

and the n-particle distribution functions are given by

$$g_N^{(n)}(\mathbf{r}^n) = \rho_N^{(n)}(\mathbf{r}_1, \mathbf{r}_2, \ldots, \mathbf{r}_n) / \prod_{i=1}^{n} \rho_N^{(1)}(\mathbf{r}_i) \tag{1.8}$$

For the cases considered in this thesis work, the analysis will be restricted to the radial distribution function $g(r)$ and pair potentials in liquids, with some exceptions that will be explained in detail when required.

1.1.1 Relation to Thermodynamics

The average of a function that depends on the position of two particles can be easily expressed in terms of integrals of $g(r)$. A typical example is the potential energy, that initially is written as a sum of many-body contributions [7]

$$U(\mathbf{r}^N) = \sum_i U^{(1)}(\mathbf{r}_i) + \sum_{i<j} U^{(2)}(\mathbf{r}_i, \mathbf{r}_j) + \sum_{i<j<k} U^{(3)}(\mathbf{r}_i, \mathbf{r}_j, \mathbf{r}_k) + \ldots \tag{1.9}$$

where the two-body contribution $U^{(2)}$ can be averaged over the positions $\mathbf{r}_1$ and $\mathbf{r}_2$ as

$$\langle U^{(2)} \rangle = \frac{1}{N(N-1)} \int \rho_N^{(2)} \left(\frac{1}{2} U^{(2)}(\mathbf{r}_1, \mathbf{r}_2) \right) d\mathbf{r}_1 d\mathbf{r}_2 \tag{1.10}$$

resulting, in terms of the pair distribution function, in

$$\langle v \rangle = 2\pi\rho^2 V \int g(r) v(r) r^2 dr. \tag{1.11}$$

A more general form for the average potential energy is

$$\langle U \rangle = \frac{\rho^2 V}{2} \int d\mathbf{r} U^{(2)}(\mathbf{r}) g(r) + \frac{\rho^3 V}{6} \int \int d\mathbf{r} d\mathbf{r}' U^{(3)}(\mathbf{r}, \mathbf{r}') g^{(3)}(\mathbf{r}, \mathbf{r}') + \ldots \tag{1.12}$$

The scalar pressure has an analogous relation once it has been expressed as the average of a function of pairs of coordinates. Such relation is described in terms of the *virial* [8,9], defined as

$$\Theta = -\frac{1}{2} \sum_{i=1}^{N} (\mathbf{r}_i \cdot \mathbf{F}_i) \tag{1.13}$$

The forces used in the sum have two sources: one comes from the intermolecular forces while the other, the external virial Θ_e, from the pressure exerted by the walls of the container that confine the system to its volume V. Hence, Θ can be written as

$$\Theta = \frac{1}{2} \sum_{i=1}^{N} \left(\mathbf{r}_i \cdot \nabla_i U(\mathbf{r}^N) \right) - \Theta_e \tag{1.14}$$

On average, the walls will exert a total force of $-p\mathbf{n}dA$ per unit area, where $\mathbf{n}dA$ is an infinitesimal unit of area pointing away from the container. Thus, from the external virial it is given

$$\langle \Theta_e \rangle_t = \frac{3}{2} pV \tag{1.15}$$

while its total average is

$$\langle \Theta \rangle_t = -\lim_{\tau \to \infty} \left[\frac{1}{\tau} \int_0^\tau \left(\sum_i \frac{d}{dt} (m_i \mathbf{r}_i \cdot \dot{\mathbf{r}}_i) - \sum_i m_i \dot{\mathbf{r}}_i^2 \right) d\mathbf{r} \right] \tag{1.16}$$

Assuming that velocities and displacements are bounded [10, 11], the first term in the right side of 1.16 vanishes in the limit $\tau \to \infty$. Consequently, it yields

$$\frac{3}{2} pV - \frac{1}{2} \sum_{i=1}^{N} \left(\mathbf{r}_i \cdot \nabla_i U(\mathbf{r}^N) \right) = \langle \sum_i m_i \dot{\mathbf{r}}_i^2 \rangle \tag{1.17}$$

By identifying the average kinetic energy per particle as $3Nk_BT$ [3], with k_B the Boltzmann's constant and T the temperature, it is possible to conclude that

$$p = \rho k_B T - \frac{1}{3V} \langle \nabla U \cdot \mathbf{r} \rangle_t \tag{1.18}$$

or

$$p = \rho k_B T - \frac{2}{3} \pi \rho^2 \int_0^\infty \frac{dv(r)}{dr} g(r) r^3 dr \tag{1.19}$$

while a more general formula involving many-body terms is given by

$$p = \rho k_B T - \frac{\rho^2}{6} \int d\mathbf{r} \frac{dU^{(2)}(r)}{dr} g(r) - \frac{\rho^3}{18} \int \int d\mathbf{r} d\mathbf{r}' r \frac{dU^{(3)}(\mathbf{r}, \mathbf{r}')}{dr} g^{(3)}(\mathbf{r}, \mathbf{r}') + \dots \tag{1.20}$$

1.1.2 The Potential of Mean Force

By fixing the position of two particles, it is possible to write the average force on one of them as a function of their distance, by integrating over the positions of the $N-2$ remaining particles. This force can be derived from a potential directly linked to the pair distribution function: the *potential of mean force* [2].

In fact, by labeling the fixed particles as 1 and 2, the force on the first one is

$$\langle -\nabla_1 U(\mathbf{r}^N) \rangle_{1,2} = \frac{\int d\mathbf{r}_3 \dots d\mathbf{r}_N \left(-\frac{\partial U}{\partial \mathbf{r}_1} \right) e^{-\beta U}}{\int d\mathbf{r}_1 \dots d\mathbf{r}_N e^{-\beta U}} \tag{1.21}$$

The previous quotient can be written as

$$-k_B T \frac{\nabla g(r)}{g(r)} \tag{1.22}$$

so, according to the previous definition, the potential of mean force is

$$U_{\mathrm{PMF}} = -k_B T \log g(r) \tag{1.23}$$

It can also be proven that $U_{\mathrm{PMF}}(r)$ approaches the potential $v(r)$ in the low density limit [2].

1.2 Molecular dynamics simulations

Computer simulations [12, 13] are a powerful tool for the study of phenomena difficult to characterize by experiment, and too complex to be treated in detail by theory. They also provide a good testing field for matching the microscopic laws of a system with its thermodynamic features; a numerical implementation of statistical mechanics.

This section contains the basic concepts of a simulation, followed by the basic relations to thermodynamics and concludes with a brief description of stochastic thermostats, a subject of relevance in the following work.

1.2.1 Equations of motion

A molecular dynamics simulation consists basically in the numerical solution of the equations of motion of a set of particles. In the most general form, the equations are (in terms of the positions $\mathbf{r}_i$ and momenta $\mathbf{p}_i$)

$$\dot{\mathbf{r}}_i = \frac{\mathbf{p}_i}{m_i} \tag{1.24}$$

$$\dot{\mathbf{p}}_i = \mathbf{f}_i \tag{1.25}$$

The forces can be written as

$$\mathbf{f}_i = -\frac{\partial}{\partial \mathbf{r}_i} U(\mathbf{r}^N) \tag{1.26}$$

for conservative systems, where a potential energy $U(\mathbf{r}^N)$ is well defined.

Equations 1.24 and 1.25 can be numerically solved, in order to obtain the configurations of positions and velocities of the system for a discrete set of times t_m. Thus, the time average of a function $A(\mathbf{r}^N, \mathbf{p}^N)$ can be estimated as

$$\lim_{\tau\to\infty} \frac{1}{\tau} \int_0^\tau A(t')dt' \approx \frac{1}{M} \sum_{m=1}^{T} A_m \tag{1.27}$$

where the sum is performed over the M configurations generated.

The equations of motion can be numerically solved by several schemes [12, 14–16]. Among them, the Verlet algorithm [17] is specially remarkable, due its efficiency and stability [14]. It is also time reversible, preserves the area of the phase space and displays low energy drifts throughout the simulation.

Specifically, the Velocity Verlet algorithm [18,19] will be used in this work. Its equations are

$$\mathbf{r}_i(t+\Delta t) = \mathbf{r}_i(t) + \mathbf{v}_i(t)\Delta t + \frac{1}{2m_i}\mathbf{f}_i(t)\Delta t^2 \tag{1.28}$$

$$\mathbf{v}_i(t+\Delta t) = \mathbf{v}_i(t) + \frac{1}{2m_i}\left(\mathbf{f}_i(t+\Delta t) + \mathbf{f}_i(t)\right)\Delta t \tag{1.29}$$

denoting by Δt the discrete time step. This variant of the original Verlet method generates trajectories with an accuracy of order Δt^4, as in the original Verlet scheme. However, it also allows a more accurate computation of the velocities, which requires the calculation of the forces twice per integration step.

For numerical reasons, it is usually convenient to use units suitable for the characteristic scales of the system [12, 14]. In practice, it is only necessary to have a unit of energy ϵ, length σ and mass m. Then, a reduced time t^* can be defined through the relation $t^* = t/\sqrt{(m\sigma^2)/\epsilon}$. The reduced energy can be written as $U^* = U/\epsilon$, while reduced pressure and temperature are $p^* = p\sigma^3/\epsilon$ and $T^* = k_B T/\epsilon$ respectively. The integration time step Δt is usually written in these reduced units as a small fraction of the smallest time scale present in the system.

1.2.2 Thermodynamic quantities

Temperature and pressure are fundamental thermodynamic quantities obtained as averages in a simulation once the system has reached equilibrium. From its definition [1, 3, 12, 14], the temperature is calculated as a time average of an instantaneous temperature T_m at time t_m defined as

$$T_m = \sum_{i=0}^{N} \frac{m_i \mathbf{v}_i^2(t_m)}{k_B N_f} \tag{1.30}$$

where N_f is the number of degrees of freedom.

Analogously, the pressure can be obtained from a time average of the instantaneous pressure π_m given by

$$\pi_m = \rho k_B T_m + \frac{1}{3V}\sum_{i<j} \mathbf{f}_{ij} \cdot \mathbf{r}_{ij} \tag{1.31}$$

where $\mathbf{f}_{ij}$ and $\mathbf{r}_{ij}$ are evaluated at time t_m.

1.2.3 Stochastic thermostats

In principle, the integration of Hamilton's equations of motion generates trajectories that conserve energy, number of particles and volume. Nevertheless, it is useful in most cases to perform simulations in the canonical ensemble, where the system is in contact with a heat reservoir. Several algorithms have been proposed for this [20–26].

Stochastic dynamics [27] provides a powerful tool to accomplish this task, that will be used here as a thermostat [28,29]. The idea consists of the addition of a random noise $\mathbf{f}^S$ and a friction $\mathbf{f}^f$ to the force on each particle. Under this scheme, the equations of motion adopt the form

$$\dot{\mathbf{r}}_i = \mathbf{v}_i \tag{1.32}$$

$$\dot{\mathbf{v}}_i = \frac{1}{m_i}\mathbf{f}_i^{\mathcal{H}} - \frac{\zeta_i}{m_i}\mathbf{v}_i + \frac{\sigma_i}{m_i}\mathbf{f}_i^S \tag{1.33}$$

where $\mathbf{f}^{\mathcal{H}}{}_i$ is the force acting on particle i coming from the conservative potential. The stochastic force must satisfy

$$\langle \mathbf{f}_i^S \rangle = \mathbf{0} \tag{1.34}$$

and

$$\langle f_i^S(t) f_j^S(t') \rangle = 2\delta_{ij}\delta(t-t') \tag{1.35}$$

for each of its components.

It can be proven that the system of Langevin equations of 1.33 generates the canonical distribution function in equilibrium [27, 30] provided that the fluctuation-dissipation theorem [30, 31]

$$\sigma_i^2 = k_B T \zeta_i \tag{1.36}$$

holds.

It is also known that, in general, this integration scheme stabilizes the equations of motion, allowing the use of longer time steps for integration [32, 33]. Equilibrium properties are not affected, but shear viscosities and diffusion coefficients are sensitive to the choice of the friction coefficient [34].

A major drawback of the equations shown above is that they do not conserve momentum, which is a crucial property for the reproduction of certain hydrodynamic phenomena [35]. This can be solved by applying the noise and friction forces in a pair-wise fashion, acting along the vector that joins two atoms. This implementation corresponds to the dissipative particle dynamics thermostat (DPD) [31, 34, 36–39], that preserves also the advantages of the stochastic dynamics. Thus, the friction can be rewritten as

$$\mathbf{f}_i^D = -\sum_j \zeta w^D(r_{ij}) \left((\mathbf{v}_i - \mathbf{v}_j) \cdot \hat{r}_{ij} \right) \hat{r}_{ij} \tag{1.37}$$

while the noise is redefined through

$$\mathbf{f}_i^S = \sum_j \sigma w^R(r_{ij}) \eta_{ij}(t) \hat{r}_{ij} \tag{1.38}$$

where $\mathbf{r}_{ij} = \mathbf{r}_i - \mathbf{r}_j = r_{ij}\hat{\mathbf{r}}_{ij}$. The noise η_{ij} must satisfy

$$\langle \eta_{ij} \rangle = 0 \tag{1.39}$$

and

$$\langle \eta_{ij}(t)\eta_{kl}(t')\rangle = 2(\delta_{ik}\delta_{jl} + \delta_{il}\delta_{kj})\delta(t-t') \tag{1.40}$$

analogous to the Langevin forces. The functions w^D and w^R are just weighting functions that vanish for $r > r_c$, a predefined cutoff radius. In order to satisfy the fluctuation-dissipation theorem, they must satisfy

$$[w^R(r)]^2 = w^D(r) \tag{1.41}$$

while the constants ζ and σ are related through Eq. 1.36.

Their form can be given by a smooth function of r [34]

$$w^D(r) = [w^R(r)]^2 = \begin{cases} (1-r/r_c)^2, & r \leq r_c \\ 0, & r > r_c \end{cases} \tag{1.42}$$

or a simpler expression

$$w^D(r) = [w^R(r)]^2 = \begin{cases} 1, & r \leq r_c \\ 0, & r > r_c \end{cases} \tag{1.43}$$

Additionally, it is required that $\eta_{ij} = \eta_{ji}$.

Langevin thermostats can also be used to tune transport properties, like diffusion coefficients or viscosities, by setting ζ properly, satisfying relation 1.36. For the case of DPD, such properties are quite insensitive to these changes. However, transport coefficients can be modified by adding noise and friction forces in a direction perpendicular to $\hat{\mathbf{r}}_{ij}$, whose ζ_T and σ_T coefficients are not necessarily the same as those used by the DPD forces. Such a *transverse DPD thermostat* has been successfully used to tune the diffusion and viscosity coefficients [40].

Chapter 2

Coarse-graining in soft matter simulations

Atomistic simulations are an indispensable tool for the characterization of many processes in physics that, due their complexity, are difficult to treat by analytic or experimental methods. By these means, it is possible to understand more deeply processes such as protein folding [41–45], the formation of micelles [46–51], the interaction of polymers with surfaces [52–56], or to simply obtain information about the equation of state [57–66] or to calculate of free energies of certain systems [67–72].

However, soft matter systems can be especially challenging to simulate. Their properties usually involve the interplay of several time and length scales, and their energy densities is in general low, of the order of the elastic constants. Accordingly, thermal fluctuations are a relevant factor in their configurational behavior, which demands long simulations in order to thoroughly sample the phase space.

This is usually the case for many complex liquids, biomolecular systems and polymer melts, where the presence of different time and length scales demands long simulations which makes the calculation extremely expensive, if not unfeasible in computational terms.

A more concrete example of this issue is the simulation of polyethylene, an illustrative case due its simplicity and wide number of industrial applications. While a single chemical bond between carbon atoms is of the order of 1 Å, the effective size of a polymer coil, expressed through its gyration radius, can be of the order of 100 Å at relevant thermodynamic conditions. Therefore, the system size required for a proper simulation must be beyond the longest characteristic length, containing millions of atoms. On the other hand, the characteristic vibration time of a bond is of the order of 10^{-13} seconds, which confines the integration step to around 10^{-15} seconds. However, the relaxation time of chains (composed approximately of 500 monomers) in melts is estimated to be around 10^{-5} seconds [73], a difference of at least ten orders of magnitude.

Hence, the relevant physics occurring at the mesoscopic scales can be difficult if not impossible to cover due to the prohibitive computational efforts required.

A possible way to avoid these limitations is by employing simplified models of the original system, where the details belonging to the fast scales are omitted in the integration, but properly reintroduced through effective interactions on the slower variables. The aim of such a *coarse-grained* representation is to reduce the number of degrees of freedom, capturing at the same time the essential physics required to describe the phenomena of interest as accurately as possible. As a consequence of this reduction, the time needed to simulate larger systems and to perform longer runs is reduced. In this spirit, the different levels of resolution can be simulated separately by different methods and consistently coupled for making a complete picture and obtain quantitative predictions.

The form of designing a coarse-grained model strongly depends on the physical quantities of relevance for the problem. In some simulations of lipid membranes in water, for example, it is useful to remove the solvent from the integration of the equations of motion and include it into the effective interactions of the solute particles [74–79]. However, the approach taken in this work consists of the clustering of a group of atoms onto a mapping point. The position of this *superatom* will be a function of the positions of its n components, written as $\mathbf{R}_i(\mathbf{r}_1, \mathbf{r}_2, \ldots, \mathbf{r}_n)$, while the mass and velocity are defined in a consistent manner. Consequently, the number of degrees of freedom is reduced. Figure 2.1 illustrates a water molecule mapped onto a structureless bead centered at its center of mass. Once mapping sites have been defined as a function of the atomistic positions, the effective interactions that govern them have to be determined to suitably resemble the aspects of interest of the original system.

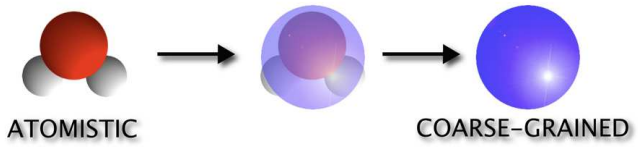

Figure 2.1: Water molecule mapped into its center of mass.

It is also of importance that the coarse-graining methods are not only an attempt to overcome the technical limitations found in the simulation of complex systems, but also, a way to distillate the essential physics that determines the process under study. In this framework, coarse-graining can also be considered to be an analysis tool [79–83].

Depending of the problem, a coarse-grained system can be designed to match, the total energy of the atomistic system [84], the instantaneous force at the mapping points [85, 86], or thermodynamic aspects in order to emulate certain biological functions [87]. In this work, however, the coarse-graining procedure will be focused on the mapping of the thermodynamics and some basic

structure functions. In the following sections, the reasons for this choice will be explained, followed by the description of the methods employed for this aim, to conclude with the limitations of such approaches.

2.1 Structure-based coarse-graining

The main feature of a structure-based coarse-graining is the close link between its configurations and that of its atomistic model. This allows a direct comparison with experiments, and makes possible, in some cases, the reinsertion of atomistic details when needed [88].

The goal of structural coarse-graining is to reproduce certain distribution functions, defined between the mapping points in the atomistic system. Typically, each distribution function is adjusted by the modification of its associated force field. In a simple liquid, for example, the basic structure is contained in the radial distribution function that is tuned through a non-bonded pair potential between the corresponding mapping points. In more complex structures, like polymers, the monomers can be represented by one or more units which are bonded by two, three or four-body potentials. Each of these force fields matches its respective distribution function, although more complex distributions could require more specific and sophisticated treatments [89].

Several techniques provide a way of generating these force fields. Nevertheless, in an ideal situation, the form of an effective pair potential should be independent of how it is obtained, as it has been rigorously proven by Henderson [90]. In his theorem it is stated that, in a simple liquid, two pair potentials that reproduce the same radial distribution function are identical up to a trivial constant.

However, it has been lately shown that significantly different force fields can produce distribution functions that are practically indiscernible [91]. This issue establishes a numerical dependence of the potential on the technical implementation of the coarse-graining procedure.

Iterative methods, like Reverse Monte Carlo (RMC) [92] or Iterative Boltzmann Inversion (IBI) [93] are easy to implement and they have been successfully tested on many systems. Reverse Monte Carlo employs a correction based on rigorous principles, and consequently, it generally converges faster than the Iterative Boltzmann Inversion, whose formula is inspired on phenomenological considerations. However, the former also requires better statistics on each step, that demands longer runs [91], and exhibits much more sensitivity to the system size. Hence, there is a balance between both methods in terms of computational time: while the first converges faster, the latter can be iterated with shorter simulations.

The Iterative Boltzmann Inversion is of main concern in this work, specifically in the cases of simple liquids, binary mixtures and model polymers that will appear in the following chapters. Its implementation is explained in the next section.

2.2 Technical implementation: the Iterative Boltzmann Inversion

The Iterative Boltzmann Inversion allows one to obtain a potential that reproduces its respective target structure function, previously obtained from experimental data or high-resolution simulations. For this aim, in a polymer system, the coarse-grained potential is usually decomposed into bonded and non-bonded contributions, which constitutes the first assumption in this approach. Their respective treatment is explained in the following sections.

2.2.1 Bonded interactions

The simplest coarse-grained polymer can be represented by a chain of structureless monomers. Its conformations are basically determined by the bond length r, that is the distance between two monomers, and the angles formed by the bonds shown in Fig. 2.2. The angle θ is defined as the angle formed by three consecutive monomers, while a torsion is the angle between the plane defined by the particles p_1, p_2 and p_3 and the plane defined by the particles p_2, p_3 and p_4. This implies the necessity of introducing three and four body potentials to adjust the distribution functions.

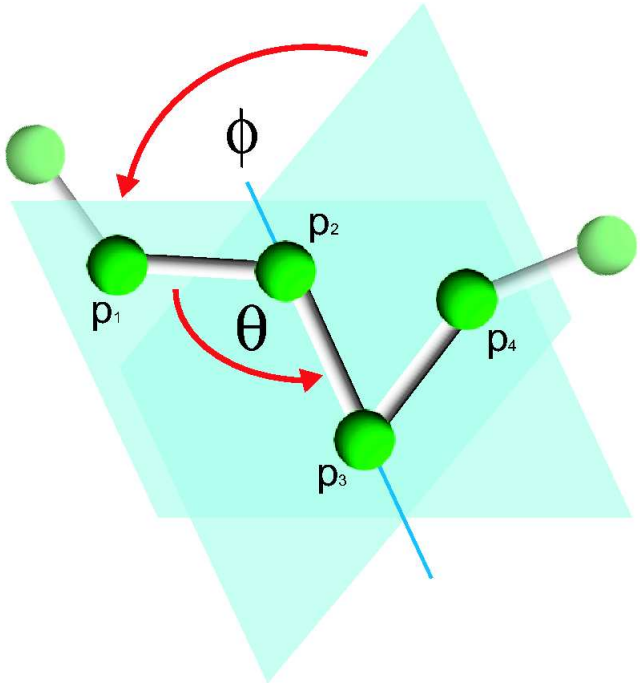

Figure 2.2: Angles and torsions in a model polymer.

A basic mapping of the structure expresses the probability distribution in terms of these parameters as $P(r, \theta, \phi)$. In addition, for practical purposes, a widely used simplification is to factorize it as $P^b(r)P^a(\theta)P^t(\phi)$, assuming that each coordinate is uncorrelated with the rest. The proper choice of the mapping points [94] can help to decorrelate such variables. In some cases, however, it is necessary to resort to more complex distribution functions [89].

A first guess for an effective interaction is the Boltzmann Inversion, that consists of starting from the mean force potential, defined as

$$U^b_{\mathrm{PMF}}(r) = -k_B T \log \frac{P^b_{\mathrm{target}}(r)}{r^2} + C_r \tag{2.1}$$

in terms of the target bond length distribution probability $P^b_{\mathrm{target}}(r)$ and the temperature T. Here C_r is an arbitrary constant that sets the minima of the potential, while the factor r^{-2} in the logarithm comes from the radial term of the Jacobian $r^2 \sin\theta$. This guarantees the proper normalization of the distribution functions, when they are obtained as simple normalized histograms sampled from the original data.

For the angular interactions, the inverted potential is given in terms of the target angle distribution $P^a_{\mathrm{target}}(\theta)$ by

$$U^a_{\mathrm{PMF}}(\theta) = -k_B T \log \frac{P^a_{\mathrm{target}}(\theta)}{\sin\theta} + C_\theta \tag{2.2}$$

The denominator of the argument of the logarithm contains a $\sin\theta$ factor to ensure the proper normalization of the probability. C_θ, as before, is an arbitrary constant.

In an analogous way, for the torsion angles the potential is

$$U^t_{\mathrm{PMF}}(\phi) = -k_B T \log P^t_{\mathrm{target}}(\phi) + C_\phi \tag{2.3}$$

where C_ϕ is an arbitrary shift and $P^t_{\mathrm{target}}(\phi)$ is the target distribution.

All these potentials can be refined iteratively by means of the recursion

$$U_{i+1}(r) = U_i(r) + k_B T \log \frac{P_i(r)}{P_{\mathrm{target}}(r)} \tag{2.4}$$

where $U_{i+1}(r)$ and $U_i(r)$ are the potentials of steps $i+1$ and i, respectively, while $P_i(r)$ is the corresponding distribution function obtained from the integration of the equations of motion using $U_i(r)$ as input. From the equation above, it is clear that the potential becomes more repulsive where there is an excess of particles in comparison with the target distribution, and vice versa.

2.2.2 Non-bonded interactions

Starting from a target distribution $g_{\mathrm{target}}(r)$, the pair correlation function between the mapping points in the atomistic system, the potential of mean force is defined as

$$U_{\mathrm{PMF}}(r) = -k_B T \log g_{\mathrm{target}}(r) \tag{2.5}$$

and corresponds to the Boltzmann Inversion of $g(r)$ [95]. Such a potential generates the target radial distribution function in the limit of an infinitely dilute system. However, this is usually not the case for medium and high density systems [96], and additional corrections have to be introduced iteratively, following Eq. 2.4.

When more species are present in the system, the procedure to follow is straightforward. The potential $U_{ij}(r)$ between the components i and j is associated with the corresponding radial distribution function $g_{ij}(r)$. Thus, the iterative refinement of Eq. 2.4 can be applied to the potential of mean force of Eq. 2.5 separately for each pair of species.

2.2.3 Pressure correction

In addition to the structure adjustment, it could also be necessary to fit the pressure at the density of the target system through the non-bonded pair potentials [93]. In this case, a small linear potential can be added, as

$$\Delta U(r) = V_0 \left(1 - \frac{r}{r_c}\right) \tag{2.6}$$

for $r < r_c$, where r_c is the cutoff radius of the pair potential and V_0 is a small corrective constant. The correction from Eq. 2.6 yields a constant force that makes the interaction more attractive if V_0 is negative, and more repulsive in the opposite case. Thus, the pressure can be controlled by initially choosing a small value (typically $0.1 k_B T$) and adding iteratively $\Delta U(r)$, consecutively decreasing V_0 for a higher accuracy.

A more precise form of estimating V_0 is to use the virial expression of the pressure in terms of the force field $F(r)$ and density ρ

$$p = \rho k_B T + \frac{2}{3}\pi\rho^2 \int_0^\infty F(r) r^3 g(r) dr \tag{2.7}$$

from which the contribution to the pressure p_c introduced by the correction can be written as

$$p_c \approx \frac{2}{3}\pi\rho^2 \frac{V_0}{r_c} \int_0^{r_c} r^3 g(r) dr \tag{2.8}$$

where it has been assumed that the $g(r)$ stays the same under the slight modification of the force field. This yields an estimate of V_0 of

$$V_0 \approx \frac{p_c}{\frac{2}{3}\pi\rho^2 \int_0^{r_c} r^3 g(r) dr} \tag{2.9}$$

as a function of p_c, that has to be evaluated as the difference of the pressure of the current coarse-grained system with the target value [97].

If V_0 is not small enough, the structure can be considerably modified, and hence, it will have to be readjusted, until a reasonable balance between the accuracy of the fit of the radial distribution function and pressure is reached after

a recursive alternation between these methods [93]. In most cases in the present work, however, the correction will be applied at each step of the Boltzmann iterations, in order to minimize its effects on the structure of the system.

It has been observed that the simultaneous adjustment of two or more properties in coarse-grained systems is a difficult task and is not always possible [98]. This trend is a well known disadvantage of any coarse-graining procedure, and it is briefly discussed in the next section.

2.3 Limitations of structure-based coarse-graining

In general, a coarse-grained model can not be expected to reproduce the physical properties of the atomistic model. A common conflict lies on the incompatibility between thermodynamics and structure [97]. The case of water models, for example, has been widely studied, displaying this mismatch between pair structure and pressure [98]. In addition, the compressibility, that in theory should be determined by the pair correlation function [2], has been shown to be unable to adjust simultaneously to the pressure [97] by means of pair potentials. Clearly, the simplification of the coarse-grained system does not consider multiple-body potentials, and therefore, correlation functions of order higher than two are not necessarily reproduced. It is expected then that a reduction of the number of degrees of freedom and the simplified form of the effective potential restrict the range of observables that the coarse-grained system can emulate.

Transferability problems are another limitation of coarse-grained approaches. The use of a coarse-grained force field on a different state point from where it has been constructed can lead to a mismatch of the adjusted properties with respect to the reference system. Such behavior has been observed, for example, in simulations of *ortho*-terphenyl [99] parametrized by means of the Iterative Boltzmann Inversion above and below the temperature of the glass transition. Both force fields produce qualitatively different behaviors at low temperatures: in the first case the system exhibits a glassy state while in the second, it crystallizes. Thus, a glass transition temperature in this case can not be defined consistently since the phase space depends on the state point of the reference system [99].

The origin of this dependence on the thermodynamics comes from a reduction of the faster degrees of freedom as an average effect on the rest of the system. This procedure makes implicit use of the probability distribution that depends of the macroscopic thermodynamic quantities. Consequently, a change in the state point will imply a new calculation of the effective interactions. This trend is a more general tendency shown every time that a many-body force field is reduced to an effective set of forces acting on a lower number of degrees of freedom. Such simplification is often performed in every field of physics when phenomenological constants are introduced. A simple example resides in the definition of the effective values of ϵ and σ in the usual Lennard-Jones potential for noble gases, since they are a simplification from the three-body Axilrod-Teller potential [100].

A final remark is the difference between the dynamical properties of atomistic and coarse-grained simulations. Normally, the coarse-grained systems display faster dynamics due to their smoother potential energy landscape. Such a trend can be used as an advantage, since longer effective integration time steps can be used, and the efficiency of the simulation is enhanced. However, transport properties such as diffusion coefficients or viscosities must be rescaled properly to have physical meaning [101].

Chapter 3

The Adaptive Resolution Scheme

Many soft matter systems involve a close relationship between several length and time scales which demands a fully atomistic description for their proper characterization. Such requirement can usually be addressed by means of a multiscale approach, where each scale is studied in detail separately. The consistency between them is imposed by using the output of the high resolution simulations as input for the lower resolution models in a hierarchical fashion [102–106].

However, if a detailed description is required in a specific region of the space, an approach that is able to deal simultaneously with several levels of resolution would be much more practical. A typical example of this situation is found in the study of solvation properties [81], where a high resolution model is necessary only in the solute and the first solvation shells while the bulk of the solvent can be treated in a less sophisticated way.

This is the aim of several methods [107,108] that couple, for example, quantum mechanical descriptions with classical ones, relegating the chemistry to a bound region while treating the less relevant surrounding particles in a coarser, classical manner. Additionally, several approaches have been designed to link mesoscale and atomistic descriptions [109–117], commonly used for the modeling of crack propagation in certain materials. However, in these cases, the regions of different resolution are rigidly defined and do not allow the exchange of particles between them, which, in fluctuating soft matter systems, is an important issue to consider.

The Adaptive Resolution Scheme (AdResS) [80, 96, 118, 119] is one of the molecular dynamics algorithms designed to fulfill these requirements [120,121]. It allows the description of a system divided in regions of different resolution across which particles can freely diffuse, changing smoothly their number of degrees of freedom. Such a transition from one level of resolution to another should not affect the global physics of the system, since only the representation of the species has changed but not its nature. Therefore, equilibrium conditions

such as pressure balance, thermal equilibrium and the absence of molecular flux [80] must be fulfilled.

Recently, the adaptive simulation of quantum/classical systems has also been extended to an adaptive scheme [122,123]. However, such approaches are beyond the scope of this work.

The present chapter begins exposing the equations of motion of AdResS. It follows the definition of the thermodynamic quantities of interest under the scheme and continues with the main features of the non-Hamiltonian nature of the equations, giving the main arguments that support the choice of their form. Finally, the method is illustrated through the application to a previously studied model of tetrahedral particles [96, 118, 119].

3.1 Equations of motion

It will be assumed along this work that the coarse-grained model consists of an interacting site mapped at the center of mass of the atomistic molecule. The interaction between these sites can be obtained by means of the methods mentioned in Chapter 2. Therefore, having the coarse-grained and atomistic force fields $\mathbf{F}^{CG}$ and $\mathbf{F}^{AT}$, the total force between two molecules α and β is given by

$$\mathbf{F}_{\alpha\beta} = w(\mathbf{R}_\alpha)w(\mathbf{R}_\beta)\mathbf{F}^{AT}_{\alpha\beta} + (1 - w(\mathbf{R}_\alpha)w(\mathbf{R}_\beta))\,\mathbf{F}^{CG}_{\alpha\beta}, \tag{3.1}$$

in terms of the *weighting function* $w(\mathbf{R})$. This function depends exclusively of the position of the mapping point of the molecule, denoted by $\mathbf{R}$, while its conforming atoms inherit its value. This function gives account of the degree of resolution of each particle, ranging from 0 to 1. From Eq. 3.1, it is straightforward that $w = 0$ yields a purely coarse-grained force field, while $w = 1$ leaves the purely atomistic contribution. The region where w has a non-integer value is called the *hybrid* or *switching* region. Figure 3.1 illustrates the implementation in a one-dimensional geometry.

In the hybrid region, the force felt by the molecules is a linear combination of the two force fields that ensures a smooth change of the representation of the molecules, and consequently, a gradual removal or inclusion of the degrees of freedom that are absent in the coarse-grained regime.

3.2 Consequences of a non-hamiltonian approach

As the number of degrees of freedom of each representation is not the same, thermodynamic quantities like the chemical potential will not necessarily match. Therefore, the system must be coupled to a local thermostat that provides (or removes) the required amount of heat in order to keep the system in equilibrium. Thus, every time that a molecule leaves the coarse-grained regime, its internal degrees of freedom are set up according an equilibrium distribution, while the thermostat takes care of keeping such distribution.

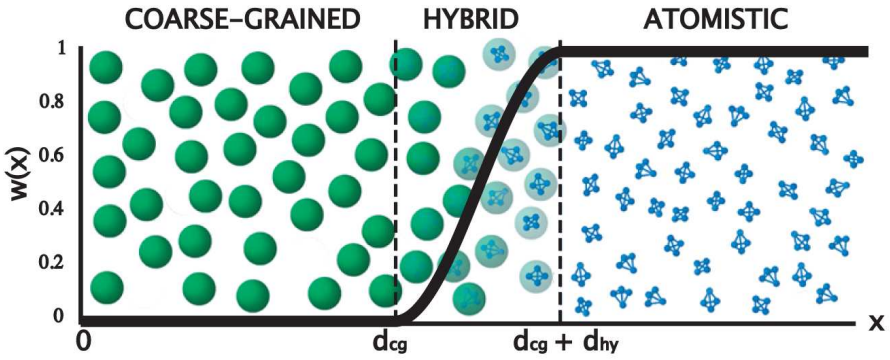

Figure 3.1: Pictorial representation of an x-dependent setup, $w(x) = sin^2\left[\frac{\pi x}{2d_{hy}}\right]$.

In this sense, an adaptive simulation can be seen (with certain limitations) as a geometrically induced phase transition, where the energy required to activate the internal degrees of freedom of a molecule is identified as a latent heat.

A second issue to be mentioned is the impossibility to deduce the forces of Eq. 3.1 from an energy-conserving approach. This can be easily seen by writing equations of motion coming from an interpolation of potentials,

$$U_{\alpha\beta} = w(\mathbf{R}_\alpha)w(\mathbf{R}_\beta)U^{AT}_{\alpha\beta} + (1 - w(\mathbf{R}_\alpha)w(\mathbf{R}_\beta))\, U^{CG}_{\alpha\beta} \tag{3.2}$$

that produce the AdResS forces and an additional drift force $\mathbf{F}^d$ proportional to

$$\mathbf{F}^d \propto (U^{CG} - U^{AT})\nabla w(\mathbf{R}) \tag{3.3}$$

From this very initial point it is possible to note that such approach would seriously depend on the shape of the weighting function. In addition, Newton's third law is violated. An attempt to remove this drift by the addition of an external field would lead to the set of equations

$$\begin{aligned} U^{CG}\nabla_\alpha f(\mathbf{R}_\alpha, \mathbf{R}_\beta) - U^{AT}\nabla_\alpha g(\mathbf{R}_\alpha, \mathbf{R}_\beta) &= 0 \\ U^{CG}\nabla_\beta f(\mathbf{R}_\alpha, \mathbf{R}_\beta) - U^{AT}\nabla_\beta g(\mathbf{R}_\alpha, \mathbf{R}_\beta) &= 0 \end{aligned} \tag{3.4}$$

denoting by ∇_i the gradient with respect to the position of particle i, and introducing $f(x, y)$ and $g(x, y)$ as the interpolation factors used Eq. 3.1, written in a more general way.

The requirements presented in Eq. 3.4 are clearly impossible to satisfy in general [119], since they consist of two boundary conditions for a system of differential equations of first order. Then, a Hamiltonian approach is possible only in trivial cases [119], although some efforts have been made in this subject [120,121].

3.3 Thermodynamic quantities

Since the number of degrees of freedom of a molecule changes in time as particles fluctuate between atomistic and coarse-grained regions, it is necessary to redefine temperature and pressure in a consistent way.

The pressure is expressed in terms of molecular interactions, since the number of molecules is constant throughout the simulation. Thus,

$$p = \rho_N k_B T + \frac{1}{3V} \sum_{\alpha} \sum_{\beta > \alpha} \mathbf{F}_{\alpha\beta} \cdot \mathbf{R}_{\alpha\beta} \tag{3.5}$$

where ρ_N is the density of molecules, T is the temperature and $\mathbf{F}_{\alpha\beta}$ and $\mathbf{R}_{\alpha\beta}$, the total force and radius-vector between molecules α and β.

The temperature, on the other hand, is well defined on purely atomistic or coarse-grained representations through the equipartition theorem [3]

$$T^{AT/CG} = 2\frac{\langle K^{AT/CG} \rangle}{N^{AT/CG}} \tag{3.6}$$

where the average kinetic energy per degree of freedom is $\langle K^{AT/CG} \rangle$ and their number is denoted by $N^{AT/CG}$ on the respective representation. It is clear that certain degrees of freedom, like the coordinates of the center of mass of the molecules, are present across the whole system, so Eq. 3.6 can be applied to them with no modifications. However, for a switchable degree of freedom q, it is necessary to take into account that its contribution to the statistics varies from the coarse-grained representation, where it is zero, to the atomistic one, where it has to be fully considered. Consequently, the number of degrees of freedom, statistically speaking, changes continuously as a function of space according the representation of the particles is changed. Moreover, the dimensionality of the phase space region belonging to q is a fractional number between 0 and 1 in the hybrid region.

The volume element of a space of fractional dimension w can be obtained by means of the fractional calculus [124],

$$dV_w = \frac{\Gamma\left(\frac{w}{2}\right)}{2\pi^{w/2}\Gamma(w)} d^w q = \frac{|q|^{w-1}}{\Gamma(w)} dq = \frac{1}{w\Gamma(w)} dq^w \tag{3.7}$$

with $\Gamma(w)$ the usual Γ function [125]. Hence, the ensemble average of the kinetic energy associated is

$$\langle K_q \rangle_w = \frac{\int_0^\infty e^{-\beta p_q^2} q^{w+1} dq}{\int_0^\infty e^{-\beta p_q^2} q^{w-1} dq} \tag{3.8}$$

that is [124]

$$\langle K_q \rangle_w = \frac{w}{2} \beta^{-1} \tag{3.9}$$

Such result is called the *generalized equipartition theorem*, that states that the average of a quadratic function of a fractional degree of freedom is proportional to its dimensionality.

3.4 AdResS simulation of tetrahedral liquid

The AdResS applied to a liquid of tetrahedral molecules has been previously studied [96,118,126]. Here, the main results are reproduced due to the relevance of the model for the later chapters.

A tetrahedral molecule is composed of four atoms of mass m_0. All the atoms interact through a purely repulsive Weeks-Chandler-Andersen (WCA) potential of the form

$$U^{WCA}(r_{i\alpha j\beta}) = \begin{cases} 4\epsilon[(\sigma/r_{i\alpha j\beta})^{12} - (\sigma/r_{i\alpha j\beta})^{6}] + \frac{1}{4}, & r_{i\alpha j\beta} \leq 2^{1/6}\sigma \\ 0, & r_{i\alpha j\beta} > 2^{1/6}\sigma \end{cases} \tag{3.10}$$

where $r_{i\alpha j\beta}$ is the distance between atom i of molecule α and atom j of molecule β. From now on, ϵ and σ will be the reference units of energy and length used.

In a molecule, atoms are bonded via a finite extensible nonlinear elastic (FENE) potential

$$U^{FENE}(r_{i\alpha j\alpha}) = \begin{cases} -\frac{1}{2}kR_0^2 ln[1 - (r_{i\alpha j\alpha}/R_0)^2], & r_{i\alpha j\alpha} \leq 2^{1/6}\sigma \\ \infty, & r_{i\alpha j\alpha} > 2^{1/6}\sigma \end{cases} \tag{3.11}$$

being $R_0 = 1.5\sigma$ and $k = 30\epsilon/\sigma^2$m the divergence length and the stiffness respectively. By construction, the bond length is approximately 1.0σ at temperature $k_BT = \epsilon$.

In the coarse-grained representation, the molecule is mapped into a bead located at its center of mass [96,118]. The effective interaction was obtained at a molecular density of $\rho = 0.175\sigma^{-3}$ using the Iterative Boltzmann Inversion in order to reproduce the radial distribution function. Additionally, the pressure was adjusted with a simple pressure correction at each step [96].

AdResS simulations were performed in a box of dimensions $36 \times 20 \times 20\sigma^3$ with periodic boundary conditions, using a time step of 0.005τ, where $\tau = (\epsilon/m_0\sigma^2)^{-1/2}$ is the reduced unit of time. After an equilibration of 2500τ, a production run of 7500τ was performed saving the configuration of the system every 1000 steps. A Langevin Thermostat, presented in Chapter 1, was employed using the value $\Gamma = 0.5\tau^{-1}$.

The weighting function is given in terms of the box length L_x along the x direction and h, the half of the hybrid zone width a,

$$w(x) = \begin{cases} 0, & h < x < L_x/2 - h \\ 1, & h + L_x/2 < x \leq L_x - h \\ \sin^2[\frac{\pi}{4h}(x - L_x + h)], & L_x/2 - h \leq x \leq L_x/2 + h \\ \cos^2[\frac{\pi}{4h}(x - L_x + h)], & L_x - h < x \leq h \\ \cos^2[\frac{\pi}{4h}(x + h)], & 0 \leq x \leq h \end{cases} \tag{3.12}$$

plotted on Fig. 3.2.

Figure 3.3 shows the radial distribution function between the centers of mass of all particles, regardless their representation, and the density profile of an

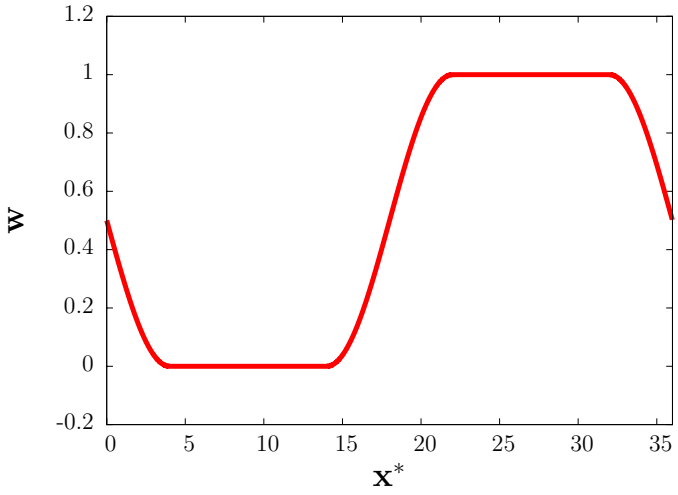

Figure 3.2: Weighting function

AdResS simulation with $h = 2\sigma$. Note that this function slightly deviates from the result of a purely atomistic simulation. Such deviation depends on the size of the hybrid region as reported previously [96,118]. On the other hand, the density profile displays the same value in both resolution domains, but its drop observed in the hybrid region is a clear artifact of the force interpolation on it. Since the

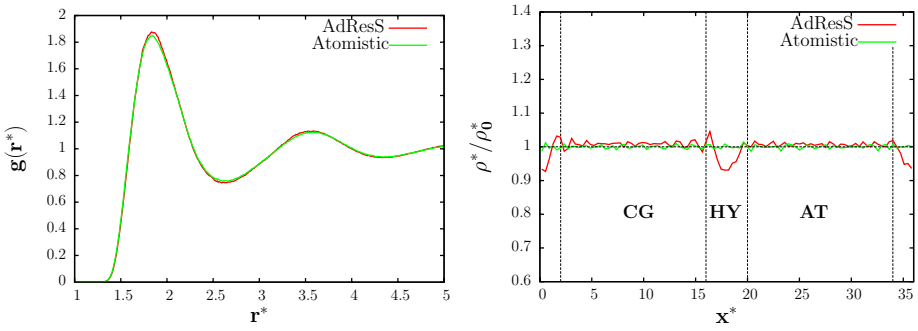

Radial distribution function Density profile

Figure 3.3: Equilibrium properties of an AdResS simulation.

equations of motion couple the representations in this zone, it is expected that their main effects will be manifested there. The explanation lies on the fact that if two potentials have the same state point at certain temperature, a linear interpolation of forces will not necessarily produce the same thermodynamics.

The pressure in reduced units, that has a value of 1.98 ± 0.02 and 1.98 ± 0.02 in atomistic and coarse-grained simulations respectively, increases to 2.04 ± 0.03 in the AdResS simulation. Such disagreement becomes more pronounced with the size of the switching region, what means that this zone affects not only the structure, but also the thermodynamics of the whole system.

Despite these effects, particles can freely diffuse across the simulation box. Figure 3.4 shows the diffusion profile for a set of particles located initially in the coarse-grained and atomistic regimes, which confirms this statement. However, transport properties must also be analyzed carefully. It is well known that in general, diffusion coefficients and viscosities do not necessarily match between atomistic and coarse-grained representations, since the smoother energy landscape in the latter leads usually to a faster dynamics [101]. In consequence, particles can diffuse in an inhomogeneous way during the simulation.

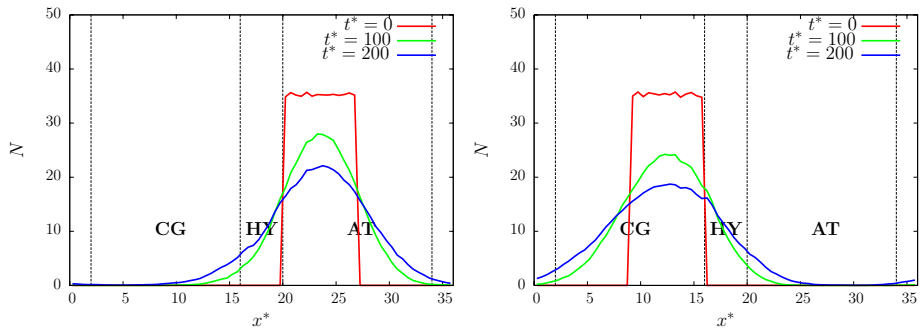

Atomistic Coarse-grained

Figure 3.4: Diffusion profile for particles located initially in atomistic and coarse-grained regimes.

A possible solution to this problem is the use of a position-dependent stochastic thermostat [127]. It is well known that transport coefficients can be tuned from the friction coefficient [40, 127]. Therefore, the coarse-grained dynamics can be slowed down by a local increase of the friction coefficient of the thermostat in order to match the behavior of the atomistic system, as it has already been tested on adaptive water simulations [127]. However, this procedure is usually avoided.

3.5 Interface correction

A first attempt to reduce the unphysical behavior in the hybrid region consisted of replacing the coarse-grained force field by

$$\mathbf{F}_{\alpha\beta}^{CG,corrected} = s\left(w(\mathbf{R}_\alpha)w(\mathbf{R}_\beta)\right)\mathbf{F}_{\alpha\beta}^{CG} + \left[1 - s\left(w(\mathbf{R}_\alpha)w(\mathbf{R}_\beta)\right)\right]\mathbf{F}_{\alpha\beta}^{CG,HY} \quad (3.13)$$

where $\mathbf{F}_{\alpha\beta}^{CG,HY}$ is a coarse-grained potential able to match the thermodynamics and structure of a system at **constant weighting function** $w_0 = 0.5$. It has been pointed that in this system [96], the disagreement with the reference properties is maximum around this point. $s\left(w(\mathbf{R}_\alpha)w(\mathbf{R}_\beta)\right)$ is, on the other hand, the *correction function*. Its choice requires $s(0) = 1$ and $s(w_0) = 0$. A tested form is given by [119]

$$s(x) = 4(\sqrt{x} - 1/2)^2 \tag{3.14}$$

The radial distribution function and density profile are plotted on Fig. 3.5. The improvement is notorious, considering that the pressure in reduced units is of 1.99 ± 0.02, closer to the reference value.

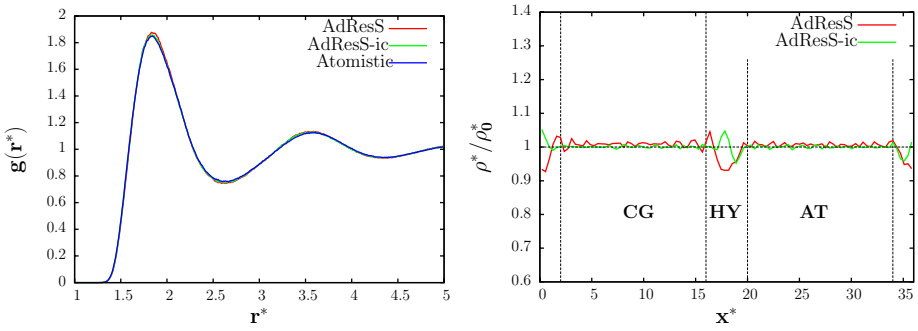

Radial distribution function Density profile

Figure 3.5: Equilibrium properties compared for atomistic, AdResS and AdResS-corrected simulations.

The main drawback of this procedure is the high computational cost required for reparametrization of the interactions under a purely hybrid representation, since it involves several simulations of a double-resolution system. In addition, it is only a local correction, unable to correct effects that arise from the intrinsic difference between the thermodynamics of the atomistic and coarse-grained representations. In such cases, it could be necessary to correct the density by means of external forces, an approach presented in the next chapter.

Chapter 4

The concept of thermodynamic force: one component system

The *thermodynamic force* can be seen as an external field applied in the hybrid region that leads to a homogeneous density ρ_0 across the whole system. Its determination is based on thermodynamic consistency considerations.

Nevertheless, the introduction of this concept is not only justified by technical reasons or to check thermodynamic consistency of AdResS, since it also makes possible the coupling between different representations on which the number of degrees of freedom is not necessarily different. This issue greatly extends the idea behind the method and situates it in a much more general framework.

The chapter begins with the presentation of the approach based on the adjustment of the chemical potential and the comparison with the previously developed interface correction [119]. The method is also tested on the coupling of two one-site pair potential with satisfactory results. Later on, an alternative approach based on the consistency of the pressure is introduced, together with a practical way of obtaining the thermodynamic force. It will be numerically shown that such corrections (and AdResS by itself) do not affect the local distribution functions in the atomistic region. Finally, an interpretation of the force in terms of an analogy with the Grand Canonical Ensemble concludes this chapter.

4.1 Chemical potential approach

It was already shown that AdResS simulations display a stationary state where the density is inhomogeneous in space. Such effect can be corrected by applying an external force that provides the right amount of work to each molecule.

In this framework, the thermodynamic force is defined as

$$\mathbf{f}_{th} = \nabla \mu^{\text{eff}} \tag{4.1}$$

where μ^{eff} is the effective chemical potential in an AdResS system, calculated on a configuration at constant density ρ_0.

For its determination, the chemical potential of a molecule is decomposed into two contributions, as [2]

$$\mu = \mu_{id} + \mu_{ex} \tag{4.2}$$

μ_{id} is the ideal gas contribution, the chemical potential of a noninteracting particle. μ_{ex}, on the other hand, is the excess chemical potential due exclusively to the intermolecular interactions. Later on, it will be shown that only the latter contribution has to be corrected.

4.1.1 Development of the thermodynamic force

Equation 4.2 requires the knowledge of the chemical potential profile along the hybrid region. A way of estimating it is by dividing such region into N slabs, as illustrated in Fig. 4.1 for a one dimensional setup. At each slab i, it is associated a weighting function w_i and an excess chemical potential $\mu_{ex}(w_i)$. The latter is obtained from an independent simulation of a bulk system at density ρ_0 in the canonical ensemble. The intermolecular forces used in these system correspond to the AdResS interpolation of forces from Eq. 3.1 at constant weighting function w_i. Such forces come from the Hamiltonian

$$\mathcal{H}_i = w_i^2 \mathcal{H}^{AT} + (1 - w_i^2)\mathcal{H}^{CG} \tag{4.3}$$

that is nothing less than a linear interpolation of $\mathcal{H}^{AT}$ and $\mathcal{H}^{CG}$. Under this setup, it is evident that the spurious drift that emerges from the interpolation of Hamiltonians in Eq. 3.3 is now zero. Therefore, the existence of a Hamiltonian allows the calculation of the excess chemical potential by means of conventional methods like the test particle insertion [2] since μ_{ex} is in these cases a well defined quantity. The excess chemical potentials calculations were performed in the GROMACS simulation package [128].

Having a numerical expression for $\frac{\partial \mu_{ex}}{\partial w}$, it is possible to evaluate $\frac{\partial \mu_{ex}}{\partial w} \nabla w$ making use of the analytic form of the weighting function. The result is, of course, a first approximation, since it does not consider the interaction between subsystems with different weighting functions.

4.1.2 Role of the thermostat

A local thermostat must keep thermalized the atoms and centers of mass in the whole system. The internal degrees of freedom of a molecule that are added when it passes from coarse-grained to hybrid resolution, must also be introduced properly [118, 129]. Hence, the local thermostat keeps the molecules thermalized regardless their resolution. A practical interpretation, consistent with the

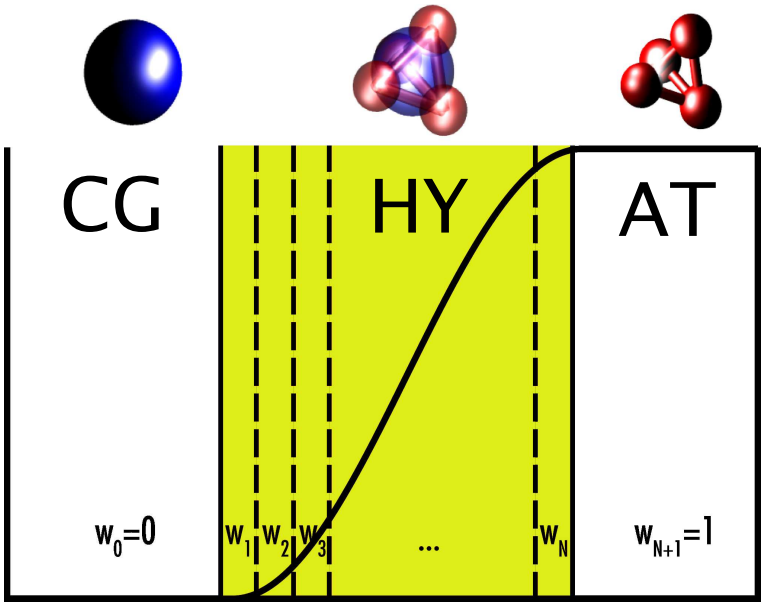

Figure 4.1: Partition of the simulation domain for the calculation of the thermodynamic force.

numerical implementation explained in detail in Chapter 7, is to consider the whole AdResS simulation as a double-resolution system. Hence, molecules contain the atoms and center-of-mass positions and velocities, while the change of resolution is exclusively attributed to the interpolation of intermolecular forces of Eq. 3.1. Clearly, the atomistic degrees of freedom do not play any role in the physics of the coarse-grained region, since they are decoupled from the dynamics and their integration can be omitted for practical purposes. The initialization of the internal degrees of freedom is discussed with more detail in Chapter 7.

From the theoretical point of view, the ideal chemical potential can be written in terms of the dimensionality of the phase space at each point of the space. The phase space integral associated to the kinetic contribution of a fractional degree of freedom is proportional to

$$\int e^{-\beta p^2} d^w p \tag{4.4}$$

(without considering constants such as the mass), where $d^w p = p^{w-1} dp/\Gamma(w)$ is the fractional volume element [96]. Therefore, the chemical potential associated is

$$-k_B T \frac{w}{2} \log T - k_B T \log \frac{\Gamma\left(\frac{w}{2}\right)}{\Gamma(w)} \tag{4.5}$$

The second term, considering the classical temperature regime, is negligible.

Since in these approach, the contribution of a degree of freedom is statistically weighted according to its degree of resolution given by w. Statistically speaking, this means that the amount of free energy has to be properly counted, so in both cases, the work provided by the thermostat to a particle has to be independent of the resolution.

A numerical test of this assertions is depicted on Fig. 4.2, calculated in a tetrahedral system composed of 2520 molecules in a box of $36 \times 20 \times 20\sigma^3$, with a hybrid region of width 12σ. The work done by the thermostat on the atoms subtracting the work done on the center of mass [130] on a molecule is defined as

$$W = \sum_i \mathbf{f}_i \cdot \Delta\mathbf{r}_i - \sum_i \mathbf{f}_i \cdot \frac{1}{M} \sum_j m_j \Delta\mathbf{r}_j \tag{4.6}$$

where $\mathbf{f}_j$ is the force exerted by the thermostat on atom j and $\Delta\mathbf{r}_i$, the displacement of atom i at the same integration step. This quantity has been calculated for simulations of 5000τ, sampled every 100 iterations. The plot shows W as a function of the coordinate x, along which the representation of the molecules change. There is no difference between purely atomistic and AdResS simulations.

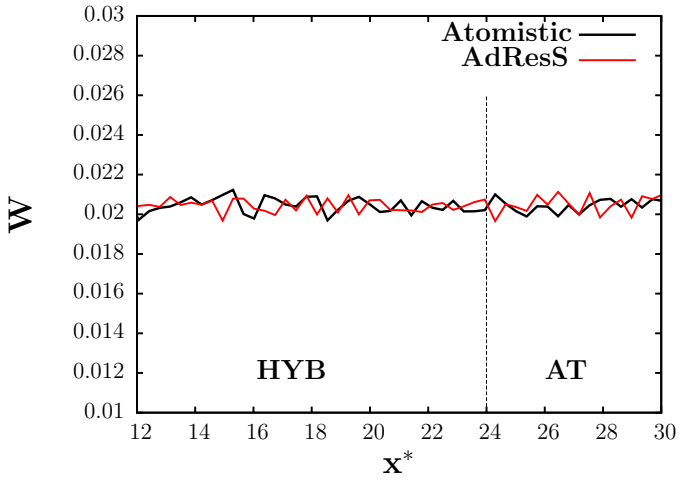

Figure 4.2: Work performed by the Langevin thermostat on each molecule, subtracting the work on the center of mass.

4.1.3 Application to the tetrahedral system

The thermodynamic force is calculated and applied to a system of tetrahedral molecules at a density of $0.175\sigma^{-3}$. The chemical potential profile is displayed on Fig. 4.3, as a function of the weighting function. Each point was obtained

from a simulation of 10000τ in a box of dimensions $20 \times 20 \times 20\sigma^3$ with 10^6 insertions. Error bars were obtained using Jackknife analysis [131].

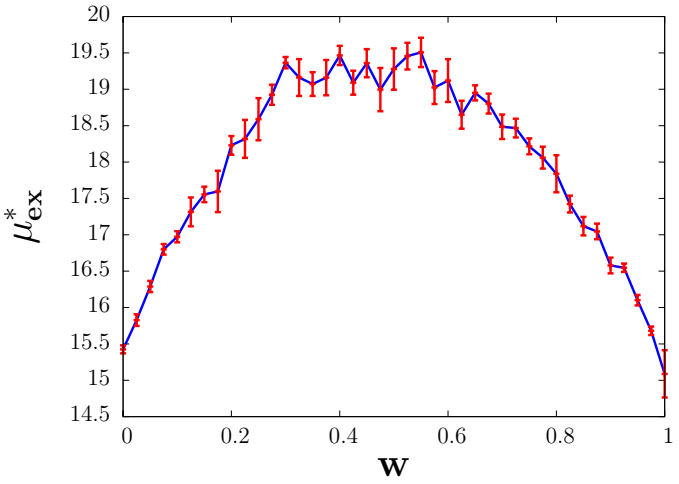

Figure 4.3: Excess chemical potential in terms of the weighting function.

As expected, the chemical potential has its maximum around $w = 0.5$, where the density hole of AdResS simulations is typically located(see previous chapter). In addition, the chemical potentials of the atomistic and coarse-grained representations are consistent. This is not surprising since their state points are the same and, more generally, their equations of state have a very similar shape as shown in Fig. 4.4. Small differences are expected in their thermodynamic properties under these circumstances.

After applying a smoothing procedure on the chemical potential profile, the thermodynamic force is calculated from $f_{th} = \frac{\partial \mu}{\partial w}\frac{\partial w}{\partial x}$. Its final form is shown in Fig. 4.5, compared with a sinusoidal fit.

The thermodynamic force is applied to a system of 2520 molecules in a box of $36 \times 20 \times 20\sigma^3$, with a hybrid region width of 12σ. The density profile of this simulation, plotted in Fig. 4.6, shows a clear improvement with respect to the uncorrected AdResS simulation.

The radial distribution function function and state point are practically not perturbed by the application of the force. Figure 4.7 compares the center of mass radial distribution function between a purely atomistic simulation, an uncorrected AdResS simulation and an AdResS simulation under the effect of the thermodynamic force, averaged over the whole simulation box. It is clear that the effects on the structure coming from the hybrid regime are not removed by the thermodynamic force. Analogously, the virial pressure in reduced units, that counts only the intermolecular contributions, does not change considerably: its value of 2.15 ± 0.03 of an uncorrected AdResS simulation increases slightly to 2.17 ± 0.04 under the effect of the force.

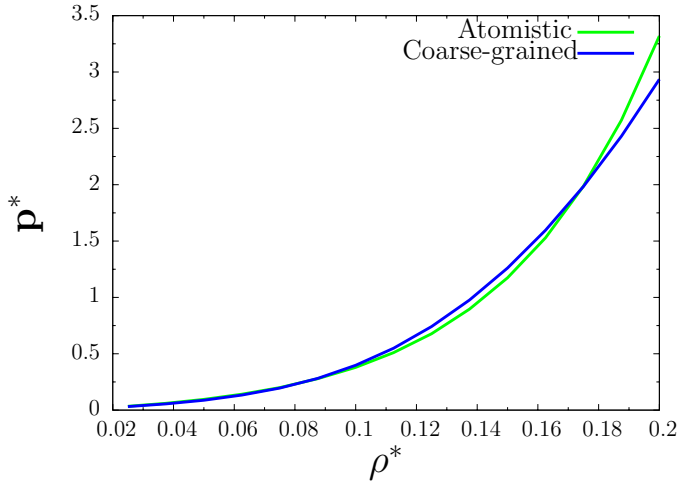

Figure 4.4: Equation of state of atomistic and coarse-grained representation of the tetrahedral model.

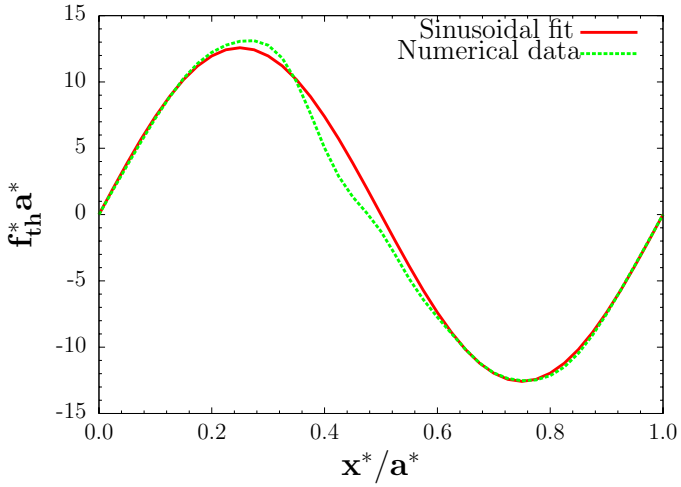

Figure 4.5: Thermodynamic force for the tetrahedral system.

4.1.4 Finite size effects

Spurious effects on the density profile are expected when the width of the hybrid region is too small. Under these circumstances, the strength of the thermodynamic force can become too high, since the field must now provide the difference of chemical potential in a much smaller region. In addition, the construction of

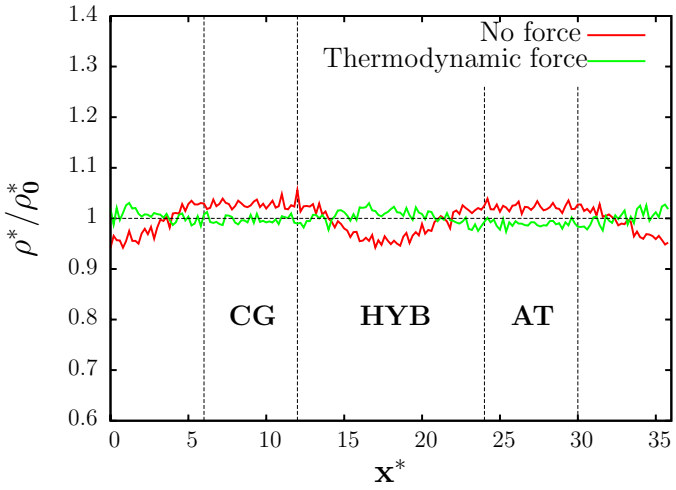

Figure 4.6: Density profile under the effect of the thermodynamic force.

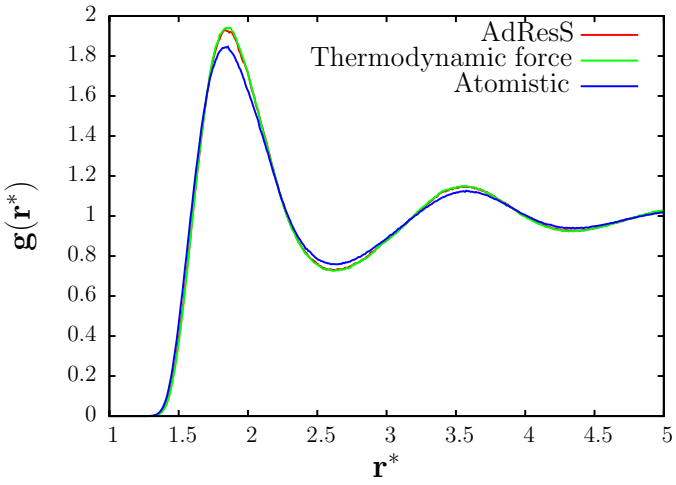

Figure 4.7: Center of mass $g(r)$ for AdResS and atomistic simulations.

the thermodynamic force has been make on the assumption that, at each point, the chemical potential can be estimated from a bulk simulation at the corresponding weighting function. The reduction of the hybrid zone can eventually break down this ansatz.

The effects of the width of the hybrid region on simulations under the effect of the thermodynamic force are analyzed below. Figures 4.8 show the density

profiles for a box of size $36 \times 20 \times 20\sigma^3$ and hybrid regions of 4σ and 8σ. The

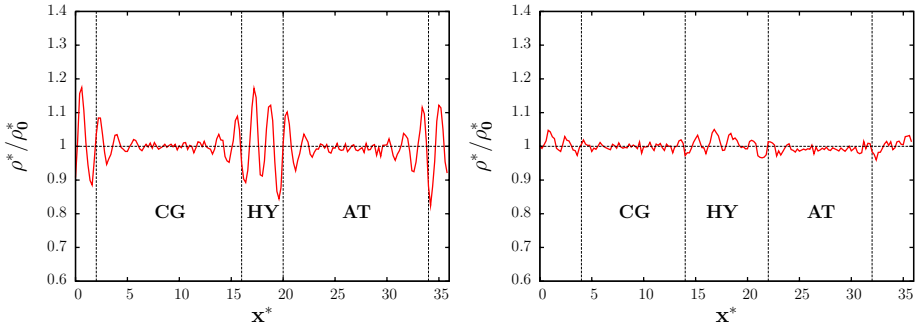

Width = 4σ. Width = 8σ.

Figure 4.8: Density profiles for the same box, with narrower hybrid regions.

results show that particles tend to agglomerate in the hybrid region, forming a *layered* pattern that becomes more pronounced as the hybrid region becomes narrower.

The numerical evidence of this *layering effect* plus the arguments aforementioned suggest that the thermodynamic force requires a minimum size of the region where it is applied.

On the other hand, an increase of the size of the hybrid region does in practice not affect the density profile. Figure 4.9 shows that the density is almost homogeneous, displaying a small bump in the hybrid zone that is also present in the first application.

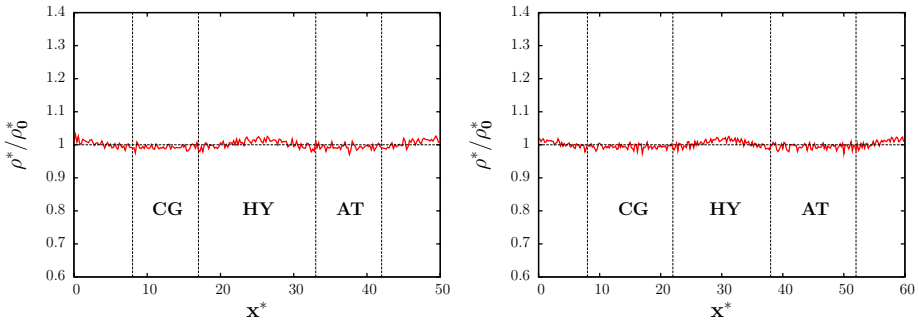

Box length = 50σ. Box length = 60σ.

Figure 4.9: Density profiles for hybrid region width of 16σ.

The increase of the size of the atomistic or coarse-grained domains improves the agreement of the radial distribution function and pressure with their atomistic references as reported previously [118]. Simulations with a hybrid region

L_{at}	p^*
6	2.17 ± 0.04
13	2.12 ± 0.02
18	2.1 ± 0.02
Atomistic	1.98 ± 0.02

Table 4.1: Pressure at hybrid width = 12σ.

width of 12σ and atomistic (and coarse-grained) widths of 6σ, 13σ and 18σ give pressures listed in Table 4.1 and radial distribution functions plotted in 4.10 in agreement with the previous results. The thermodynamic force does not change this general trend.

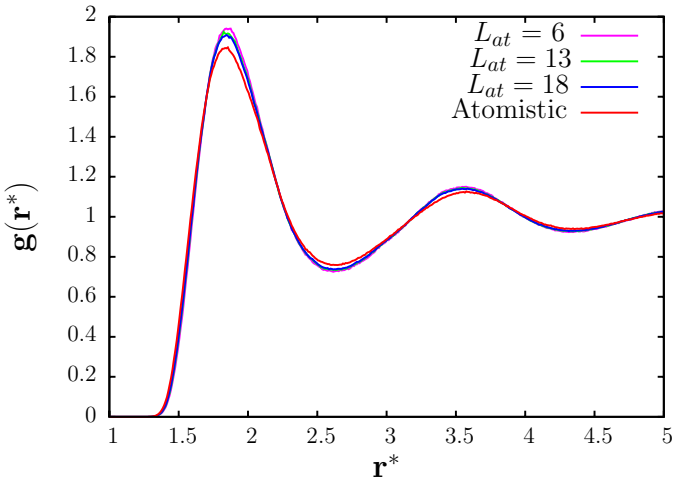

Figure 4.10: Center of mass $g(r)$ for AdResS and atomistic simulations.

4.1.5 Interfacing two generic force fields: example in a one-site model

The interpolation of forces that characterizes the equations of motion can be generalized to two arbitrary force fields. In this context, the change of resolution is merely a specific case of the coupling between two levels of representation.

An illustrative example is to interface two coarse-grained models of the tetrahedral system that have been derived at different thermodynamic state points. Figure 4.11 shows the equation of state of the tabulated potential adjusted around $\rho = 0.175\sigma^{-3}$ with an analytical Morse potential adjusted at $\rho = 0.1\sigma^{-3}$ [118]. The potentials are interfaced in an AdResS simulation at an

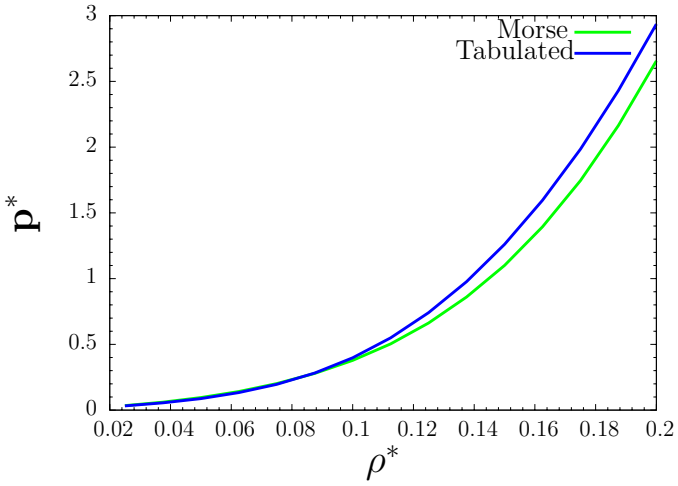

Figure 4.11: Equation of state of two coarse-grained representations of the tetrahedral liquid.

intermediate density of $0.135\sigma^{-3}$. Here there is a clear mismatch between their equations of state. The profile of chemical potential and the force produced from it are plotted in Fig. 4.12, obtained from simulations in a box of dimensions $20 \times 20 \times 20\sigma^3$ with 1080 molecules. The integration was over 25000τ with 5×10^6 insertions for the test particle insertion method.

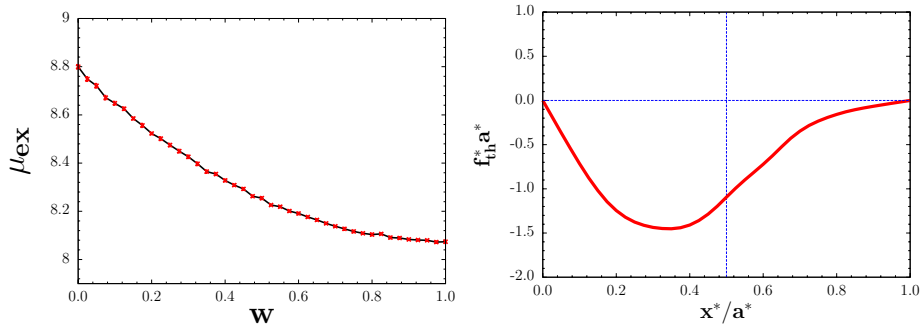

Chemical potential. Thermodynamic force.

Figure 4.12: Corrective elements for the confrontation of two coarse-grained parametrizations. Values $w = 0$ and $w = 1$ are assigned to the tabulated and Morse potentials respectively.

The density profile obtained from the application of this force is shown in Fig. 4.13, compared with the result of an uncorrected AdResS simulation. As

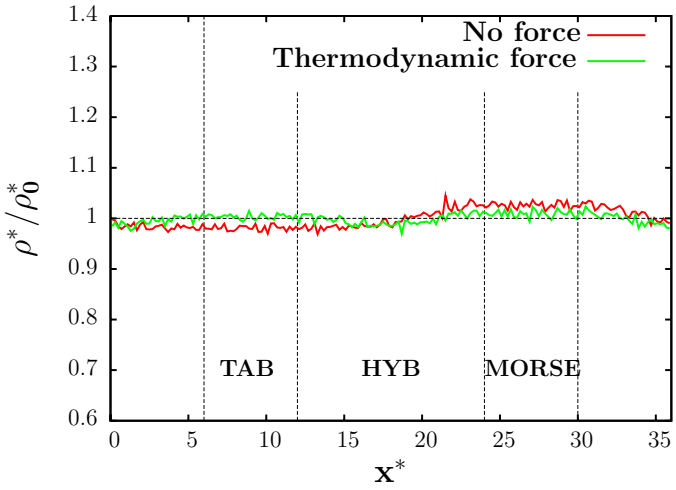

Figure 4.13: Density profiles with and without thermodynamic force.

in the previous case, the density is considerably improved under the application of the force.

This short test is a first step towards the conceptual extension of the AdResS to a more general approach that allows the coupling between different representations through thermodynamic considerations, which is clearly far beyond the original AdResS idea.

4.2 Iterative approaches

In this section, a more practical way to deduce the thermodynamic force is presented, starting from the assumption that in a stationary situation, an AdResS system will evolve to a configuration where **the pressure is the same throughout the whole box** [132]. Pressure is a well defined quantity since it can be defined in terms of the intermolecular forces, provided the existence of an equilibrium state [2]. In AdResS, however, the averages of thermodynamic quantities are taken over stationary states that have been numerically observed [96, 118, 119, 124, 126].

It is well known that a homogeneous pressure configuration displays a non homogeneous density profile in the absence of corrections [96, 118]. This can be tested numerically by calculating the pressure profile, using the expression proposed by Todd, Evans and Davis [133] for the pressure tensor

$$\bar{p}_{\beta\alpha}(\alpha) = \frac{1}{2A_\alpha \Delta\alpha}\left\langle \sum_{\alpha-\Delta\alpha\leq\alpha_i\leq\alpha+\Delta\alpha} m_i v_{i\beta} v_{i\beta} \right\rangle + \frac{1}{2A_\alpha}\left\langle \sum_{i=1}^{N} F_{i\beta} sgn(\alpha_i - \alpha) \right\rangle \tag{4.7}$$

where A_α is a cross-sectional area perpendicular to the direction α. The first term is the ideal gas contribution calculated in a slab centered at α of thickness $2\Delta\alpha$, and the second represents the contribution of the intermolecular interactions.

In the case of two-body forces, the second sum is reduced to the count of the forces that cross the area A_α. Particles at distances bigger than the maximal cutoff of the non-bonded interactions do no contribute to the sum. In the same spirit, it is possible to note that this way of counting the forces per area is not affected by the periodic boundary conditions provided that the sides of the simulation box are longer than the longest range of the interactions.

Figure 4.14 shows the component p_{xx} of the pressure tensor along the x direction, on which the change of resolution occurs. The profile is plotted for three systems: a purely atomistic liquid and two AdResS simulations with hybrid regions of width 4σ and 12σ. In all cases, p_{xx} is practically constant, even though in the AdResS simulations the density profiles are not. Its average value, however, is higher in these cases with respect to the atomistic reference, and increases with the size of the hybrid region. This is not surprising since hybrid particles increase the pressure, as it has been reported in this tetrahedral system [96, 118].

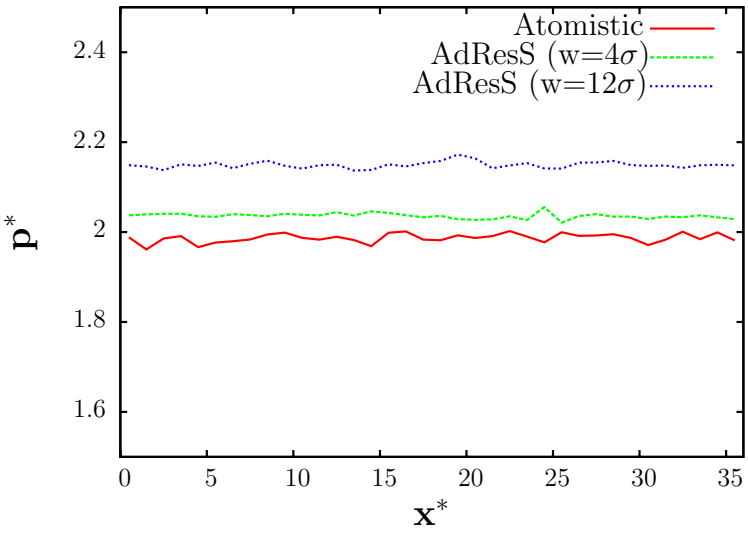

Figure 4.14: Pressure profile $p_{xx}(x)$ for AdResS and pure atomistic simulations.

In an analogous way, a flat density profile will require the application of an external force to remain stationary. Knowing the pressure profile p_f of a flat density configuration, the thermodynamic force can be written as

$$\mathbf{f}_{th} = \frac{1}{\rho_0}\nabla p_f \tag{4.8}$$

where ρ_0 is the value of the homogeneous density. This force can be estimated by the same slab procedure used in the chemical potential approach. By dividing the simulation domain into several subsystems centered at x_i, the pressure at each point is approximated as the value obtained from a hybrid simulation performed at constant weighting function $w(x_i)$.

However, this procedure, rather tedious, can be difficult to achieve in systems like water, where accurate estimations of the pressure demand long runs [97]. It is recommendable then to devise a simpler and faster way to estimate $\mathbf{f}_{th}$ in an accurate and less expensive manner, making use of the density profile of an uncorrected AdResS simulation.

Starting from the stationary density profile of an uncorrected AdResS simulation, the pressure can be written as $p(\rho(\mathbf{r}))$, assuming that it depends locally on the density. Therefore, expanding to first order at each point

$$p(\mathbf{r}) = p_f(\mathbf{r}) + (\rho(\mathbf{r}) - \rho_0) \left[\frac{\partial p}{\partial \rho}\right]_{\rho=\rho_0} + \mathcal{O}([\rho(\mathbf{r}) - \rho_0]^2) \tag{4.9}$$

Hence, by taking the gradient at both sides of 4.9, and knowing that $\nabla p = 0$, it yields

$$\nabla p_f(\mathbf{r}) \approx -\nabla \left[\frac{1}{\rho_0 \kappa_T}(\rho(\mathbf{r}) - \rho_0)\right] \tag{4.10}$$

by using the isothermal compressibility κ_T, as in

$$\left[\frac{\partial p}{\partial \rho}\right]_{\rho=\rho_0} = \frac{1}{\rho_0 \kappa_T} \tag{4.11}$$

and neglecting higher order terms. For simplicity, the compressibility is taken as a constant, that can be its atomistic (or coarse-grained) value. Such choice will later be proven to be a good approximation in the tetrahedral liquid. Thus, the first guess of the thermodynamic force is

$$\mathbf{f}^0_{th}(\mathbf{r}) = -\frac{1}{\rho_0^2 \kappa_T^{at}} \nabla \rho(\mathbf{r}) \tag{4.12}$$

The inclusion of higher order derivatives in the equation of state would require the knowledge of the coefficients of the whole expansion, which is a non trivial, if not prohibiting problem. To overcome this situation, the force can be iteratively corrected as

$$\mathbf{f}^{i+1}_{th}(\mathbf{r}) = \mathbf{f}^i_{th}(\mathbf{r}) - \frac{1}{\rho_0^2 \kappa_T^{at}} \nabla \rho^i(\mathbf{r}) \tag{4.13}$$

until a flat density profile is reached.

The effects of the thermodynamic force calculated from the pressure profile on the local pressures can be seen in Fig. 4.15. In the corrected AdResS simulation, p_{xx} shows a sizeable bump increase in the hybrid region, while in the atomistic and coarse-grained regimes it matches the reference values. Such

inhomogeneities are compensated by the thermodynamic force, as it can be seen by monitoring the quantity $p_{xx} + \rho_o \phi$, where ϕ is the potential associated to the external field. Its value across the x axis is practically constant, similar to the atomistic profile.

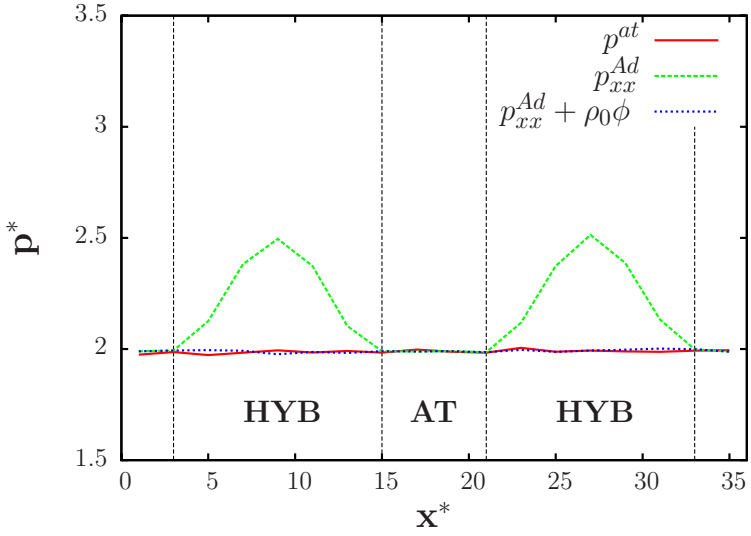

Figure 4.15: Pressure profile of a purely atomistic simulation compared with AdResS under the thermodynamic force. It also includes the profile corrected, adding the contribution of the thermodynamic force. Note that in the uncorrected case, the local pressure at the atomistic region matches the atomistic value.

The other components of the pressure tensor p_{yy} and p_{zz} are expected to display an analogous profile to p_{xx}, since in equilibrium, the pressure tensor must satisfy

$$p_{xx} = p_{yy} = p_{zz} \tag{4.14}$$

However, Eq. 4.7 permits the calculation of $p_{yy}(y)$ and $p_{zz}(z)$, but not their profiles across the x direction. Therefore, the validity of 4.14 can only be assumed and numerically tested by comparing the averages of p_{yy} and p_{zz} along the directions y and z respectively. Their profiles, in Figs. 4.16, are flat, with averages of $\langle p^L_{yy} \rangle_y = 2.161 \pm 0.003$, $\langle p^L_{zz} \rangle_z = 2.161 \pm 0.002$ in reduced units. These values match the average $\langle p^L_{xx} \rangle_x = 2.2 \pm 0.2$, in agreement with Eq. 4.14. If such equation holds, it is possible to conclude that

$$\frac{p}{\rho_0} + \phi \tag{4.15}$$

is constant across the whole space in an AdResS simulation.

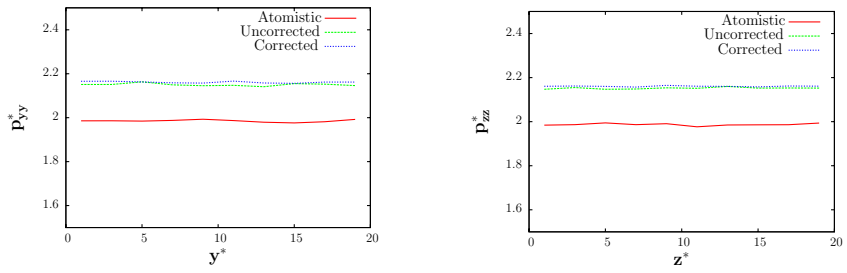

$p^L_{yy}(y)$ $p^L_{zz}(z)$

Figure 4.16: Pressure profiles along the y and z directions for corrected and uncorrected simulations, compared with the atomistic result.

The presented approach is also relevant from a conceptual point of view, since it establishes that the pressure, and consequently, $-pV$, are constant in the whole simulation domain independent of the representation. The thermodynamic force, as shown in Fig. 4.15, imposes a flat density profile by compensating this quantity. Therefore, in the thermodynamic limit, such force can be identified with the derivative of the Grand Canonical potential divided by the number of particles. An AdResS simulation can then be numerically consistent with an open system where the region of interest is the atomistic one. Thus, the system can be divided into various subvolumes with different molecular representation that can be approximated as a particle reservoir for the adjacent subvolumes.

4.2.1 Iterative thermodynamic force on tetrahedral liquid

The iterative procedure can be tested with the compressibility of the atomistic or coarse-grained representations that do not differ substantially, due to the similarity between their equations of state. The prefactor $C = \frac{1}{\rho_0^2 \kappa_T}$ is $C_{AT} = 236.86\epsilon\sigma^3$ and $C_{CG} = 190.62\epsilon\sigma^3$ for each representation. The forces produced by the first iterations using these coefficients are displayed in Fig. 4.17. It takes in both cases two steps to obtain a flat density profile, as depicted in Fig. 4.18. The final shape of the force is compared with the previous calculated thermodynamic force, using both the chemical potential and pressure profiles in Fig. 4.19, with the respective density profiles in Fig. 4.20.

Clearly, the density displays a uniform profile after a few AdResS simulations, without the necessity of simulating several hybrid systems. It is also noticeable that the small excess of particles in the hybrid region produced by the application of the thermodynamic force coming from the chemical potential approach is now absent.

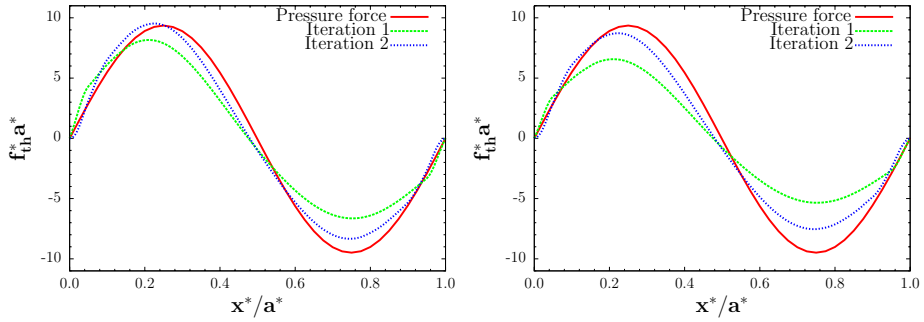

Atomistic Coarse-grained

Figure 4.17: First iteration of the thermodynamic force using atomistic and coarse-grained compressibilities.

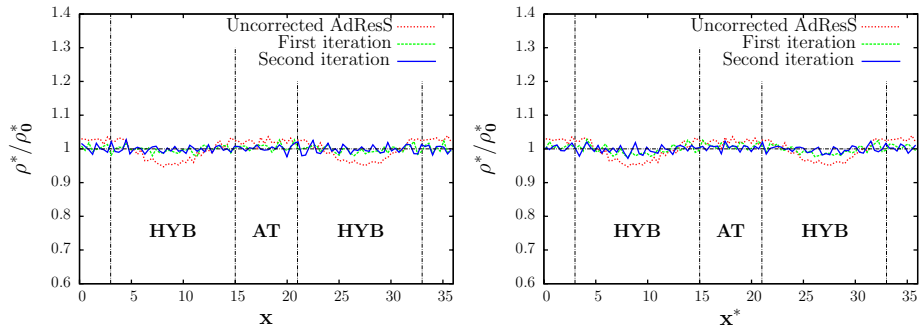

Atomistic Coarse-grained

Figure 4.18: Density profile for first two iterations, applying thermodynamic forces calculated with atomistic and coarse-grained compressibilities.

4.2.2 Comparison with Interface Pressure Correction

The density profiles obtained can be compared with the old approach of the interface correction. As shown on Fig. 4.21, the thermodynamic force produces a flatter distribution of particles. Another advantage is that it can be used to match representations that do not have the same state point, while the interface correction is just able to correct the density locally in the hybrid region. However, the thermodynamic force does not affect notoriously the radial distribution function of the whole system, as it will be shown in the next subsection.

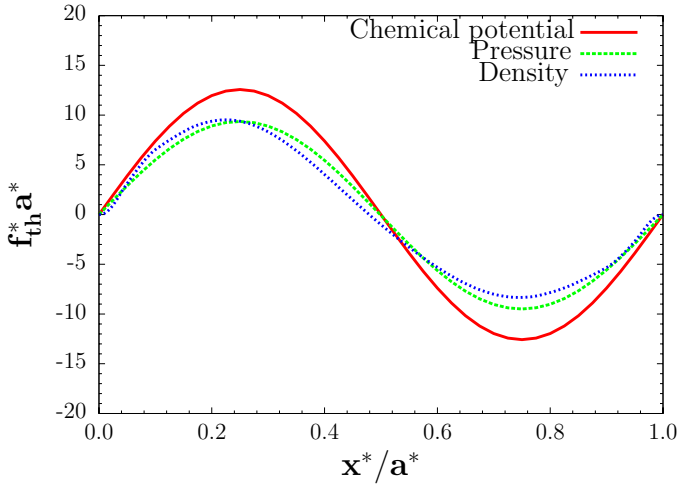

Figure 4.19: Final shape of the iterated thermodynamic force compared with the other approaches.

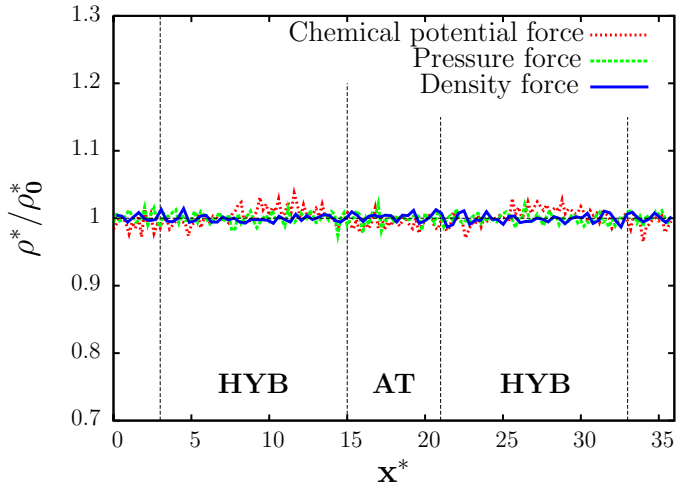

Figure 4.20: Final shape of the density profile of the iterative thermodynamic force compared with the other approaches.

4.2.3 Distribution functions

It is important to show that the recently developed corrections do not alter the physics of the atomistic region. This can be checked by monitoring the velocity distribution and pair correlation function in that region, and comparing it

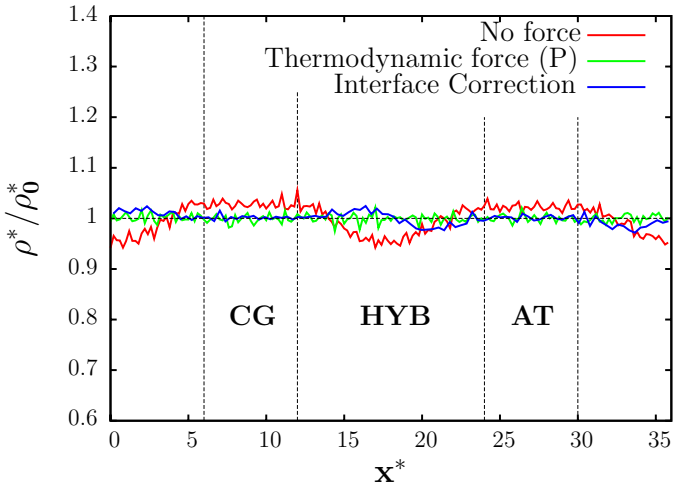

Figure 4.21: Density profiles of AdResS simulations under different approaches.

with the purely atomistic results. Figure 4.22 shows the velocity distribution of the atoms of the atomistic domain of an AdResS simulation with and without thermodynamic force. The comparison with the distribution taken in a subdomain of the same dimensions from a purely atomistic simulation shows good agreement.

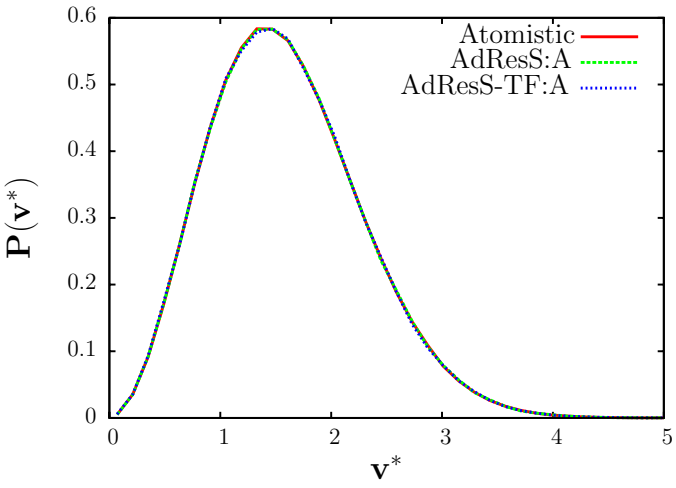

Figure 4.22: Velocity distribution of atoms in the atomistic domain.

It is also of interest to observe the behavior of the velocities in the hybrid re-

gion. Figure 4.23 shows the distribution of velocities for particles with weighting function between 0.4 and 0.6, compared with the analytic expression. Again, it is observed that both curves match in the numerical precision.

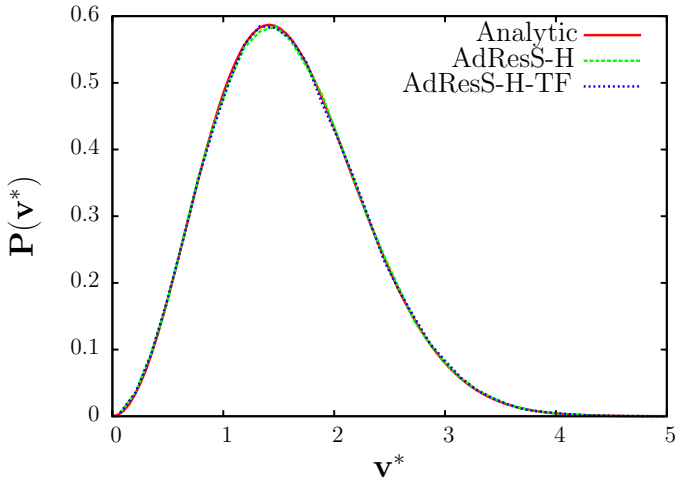

Figure 4.23: Velocity distribution of atoms, hybrid region.

Consequently, in a stationary situation, the thermostat is able to keep the regions of interest thermalized independent of the application of the thermodynamic force.

Concerning the configurational distribution, it is possible to evaluate part of its information through the local analysis of the radial distribution function. It is well known that the particles in the hybrid region distort it; however, it is important to see if this effect is not propagated over the atomistic regime.

Figures 4.24 show the radial distribution function of particles restricted to the atomistic domain in AdResS simulations. An analogous calculation on purely atomistic simulations gives distributions that are in excellent agreement with the previous results. The decay of the functions for long distances is due the size of the atomistic region.

4.2.4 Particle number fluctuations

Finally, Table 4.2 displays the particle number fluctuations in the AdResS and atomistic systems. It is clear that this quantity, within the error bars, is not affected by AdResS nor its corrections.

Therefore, it is possible to conclude that the thermodynamic force can be used to obtain a flat density profile, restoring the local state point of the atomistic domain. It also does not affect the local velocity distribution and radial

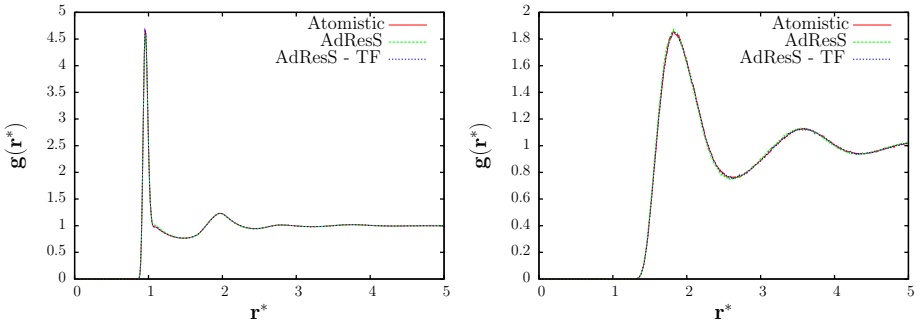

Atoms Centers of mass

Figure 4.24: Local radial distribution function.

Table 4.2: Number of particles and fluctuations of atomistic regions.

System	N	$\sigma^2(N)$
Atomistic	420	25.8 ± 0.8
AdResS	429	26.1 ± 1.1
AdResS-PF	420	25 ± 0.7

distribution functions, while the particles fluctuate in this region in a consistent manner with purely atomistic systems. The fact that the differences in the thermodynamics can be compensated with the thermodynamic force allows the use of coarse-grained models that do not fit the chemical potential of their atomistic counterparts, but focus in other physical quantities like the basic structure.

Chapter 5

Thermodynamic force on a binary mixture.

The simulation of more realistic situations requires the generalization of AdResS to multicomponent systems. However, the development of a coarse-grained model in this cases represents a challenge by itself. This chapter addresses both issues in a binary mixture consisting of spherical solutes solvated in the already studied tetrahedral molecules. It begins with the description of the system and the procedure followed for the reparametrization of the interactions are presented below. Later on, the firsts tests on the AdResS simulation of multicomponent systems are discussed, to conclude with the applications of the interface correction and thermodynamic force.

5.1 System setup

The binary mixture consists of a minor component (solute) represented by spherical particles and a major component represented by the aforementioned tetrahedral molecules. The solute particles interact between themselves through a repulsive Weeks-Chandler-Andersen potential

$$U_s^{WCA}(r) = \begin{cases} 4\epsilon_s[(\sigma_s/r)^{12} - (\sigma_s/r)^6 + \frac{1}{4}] & ,r \leq 2^{1/6}\sigma_s \\ 0 & ,r > 2^{1/6}\sigma_s \end{cases} \tag{5.1}$$

where the parameters σ_s and ϵ_s can be written in the previously introduced Lennard-Jones units as $\sigma_s = 1.8\sigma$ and $\epsilon_s = \epsilon$. Their interaction with the solvent atoms obeys Lorentz-Berthelot [126] rules, that is, a Weeks-Chandler-Anderson potential with the parameters $\sigma_{ts} = 1.4\sigma$ and $\epsilon_{ts} = \epsilon$.

The systematic approach chosen for the parametrization of the interactions will make use of several mixtures at different concentrations, which are listed on Table 5.1. The cubic box size L has been adjusted to obtain the same pressure

Table 5.1: Concentration c and pressure of the mixtures.

c	L^*	N	M	p^*
0.007	20.05	1400	10	1.99 ± 0.05
0.034	20.265	1400	50	1.98 ± 0.04
0.125	21.01	1400	200	1.98 ± 0.04

as the pure tetrahedral liquid previously studied, once the number of solute and solvent particles have been fixed.

The steps followed in the procedure are described in detail in the following section.

5.2 Development of Interactions

The coarse-graining model of the mixture aims to reproduce of the radial distribution function of the species and the total pressure. This is achieved by means of the successive reparametrization of the interactions in systems of increasing concentration. The procedure is schematized in Fig. 5.2.

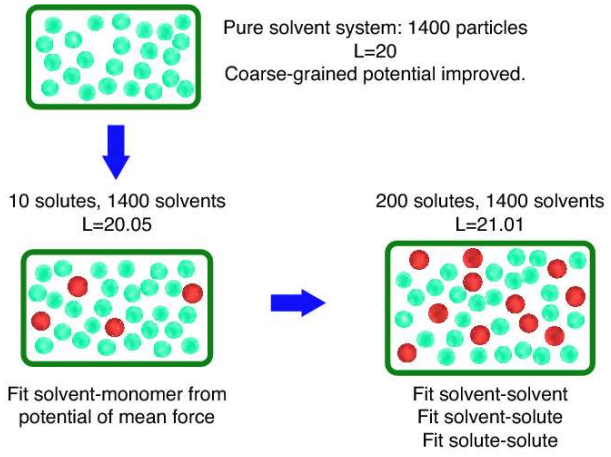

Figure 5.1: Scheme of reparametrization of the interactions.

The systematic approach consists of three steps:

- The refinement of the interaction between solvents in a pure system, starting from the potential used in the previous systems. The pressure is simultaneously adjusted.
- Tune the force between solvents and solutes in the most diluted system

with the iterative Boltzmann inversion. In this case, the force field between the solutes is the same as in the atomistic representation.

- Finally, the potentials for the solvent-solvent, solvent-solute and solute-solute are corrected in the most concentrated mixture. Technical details are described below.

For the first step, the system consisted of 1400 molecules on a box of $20 \times 20 \times 20\sigma^3$. Between the solvents, the Iterative Boltzmann Inversion was applied over the existent interaction for 8 steps, where each simulation consisted of 1000τ and 2500τ of equilibration and production respectively. A smoothing procedure over the potential was applied 5 times per each step. The pressure was simultaneously corrected using $\Delta V = 0.01\epsilon$, giving a final value of 1.98 ± 0.01 reduced units, consistent with the target pressure. The slight difference between the radial distribution functions is plotted in Fig. 5.2, while the potentials are depicted in Fig. 5.3.

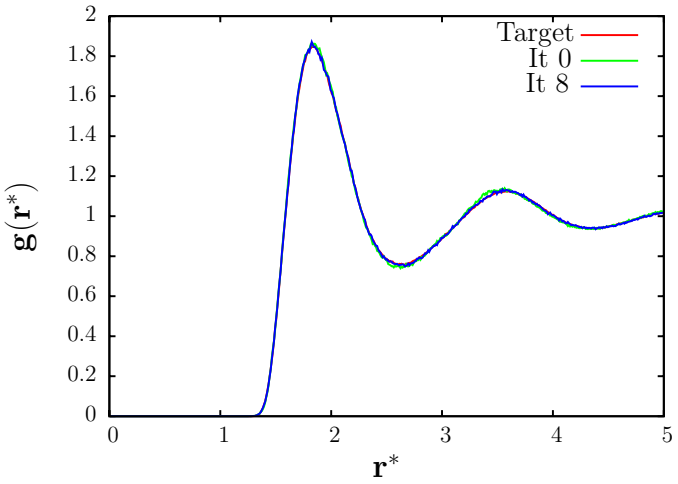

Figure 5.2: Radial distribution function improvement for the pure solvent after 8 IBI steps.

For the second step of the procedure, the interaction between solvent and solute starts from the potential of mean force. The force between the solvents used was the previously developed one, while the solute interaction interacted through the WCA potential defined in Eq. 5.1. The cutoff radius was of 3.59375σ, that matches the second maxima of the solvent-solute radial distribution function. This choice resulted the effective since at that point the force is zero. Besides, it was observed that by using a smaller cutoff radius, the radial distribution function could not be fitted properly. The use of longer cutoffs produced problems as well in the fit of the first peak of the radial distribution function. The

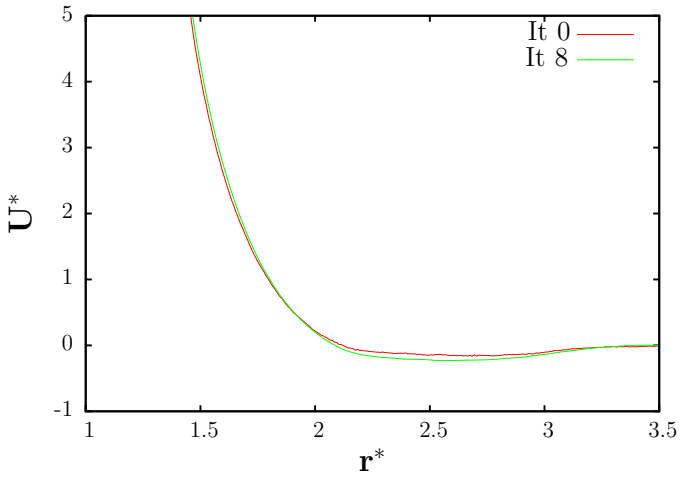

Figure 5.3: Potentials for the solvent interaction in pure solvent system.

solvent-solute radial distribution function is shown in Fig. 5.4, compared with its target shape. The pressure was adjusted with a value of $\Delta V = 0.01\epsilon$, until its value was of 1.98 ± 0.01 reduced units. The initial and final potentials are shown in Fig. 5.5.

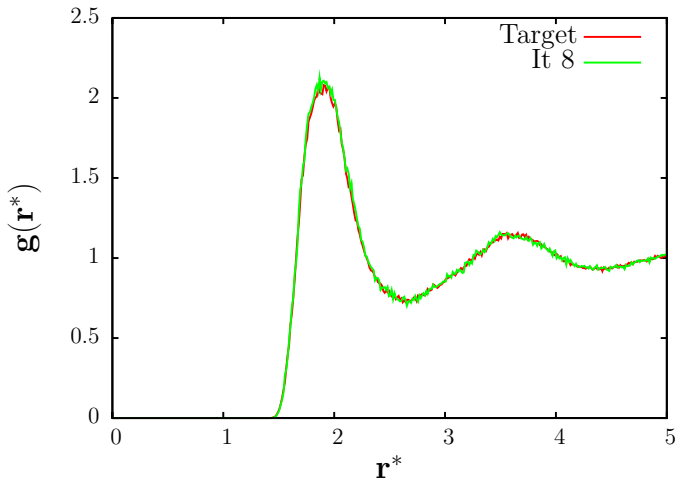

Figure 5.4: Solvent-solute radial distribution function the most dilute mixture after IBI.

The last step consists of three reparametrizations in the most concentrated

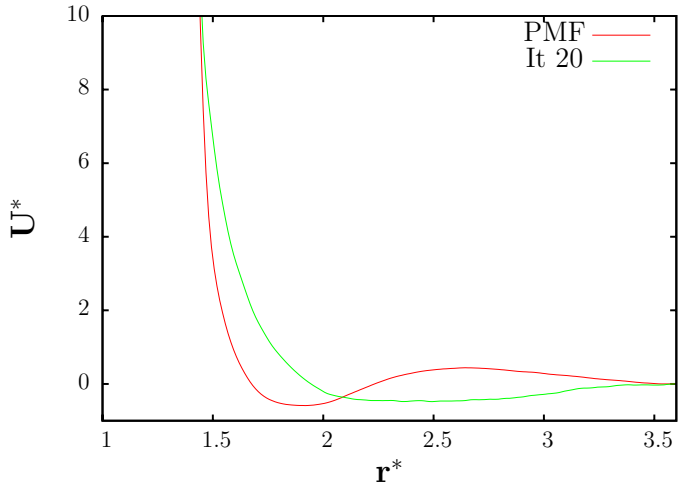

Figure 5.5: Solvent-solute potentials for the most diluted mixture. The initial function is the Potential of Mean Force (PMF).

system, whose features are shown in Table 5.1. It begins with the refinement of the solvent-solvent force field by means of the iterative Boltzmann inversion and the pressure correction with $\Delta V = 0.01\epsilon$, smoothing the potential 5 times per step. Equilibration simulations were of 500τ while production runs were of 5000τ. In 20 steps of the Iterative Bolztmann method, there was no improvement observed in the radial distribution function. However, the shape of the potential keeps changing in the initial iterations, until reaching a fixed form at iteration 10. Therefore, the last iteration was selected for the later parametrizations. The pressure in the last iteration was of 1.89 ± 0.01 reduced units, whose value did practically not change in the successive iterations, although the target value was of $1.98\epsilon\sigma^{-3}$. This suggests that the pressure must be corrected by tuning the solvent-solute or solute-solute interaction.

The solvent-solute interaction was then reparametrized for this system. It took 10 steps to obtain a good agreement of the radial distribution function, while the pressure was of 1.98 ± 0.02 reduced units. The potential was smoothed one time per Boltzmann step to give the shape shown in Fig. 5.8, while the pressure was corrected using a value of $\Delta V = 0.01\epsilon$. Initial and final radial distribution functions are displayed in Fig. 5.7.

Finally, the potential between the solutes is corrected, starting from the atomistic excluded volume interaction. The force field was corrected after one step, without pressure correction. The force is slightly modified (shown in Fig. 5.9, increasing its cutoff radius (based on the same criteria as for the previous interactions) to $3.69\ \sigma$.

The final pressure obtained was of 1.98 ± 0.02 reduced units in agreement with the total pressure of the mixture. The final radial distribution functions

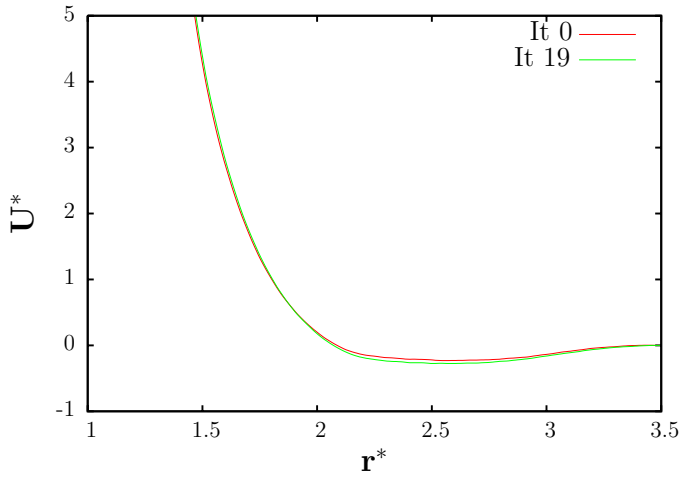

Figure 5.6: Solvent-solvent potentials for the most concentrated mixture.

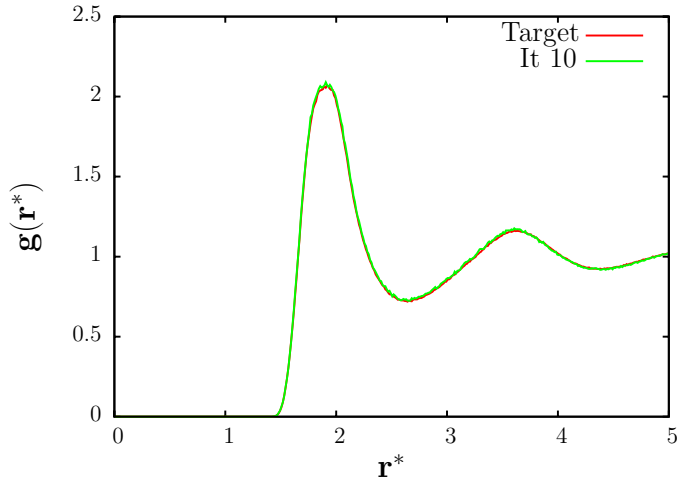

Figure 5.7: Solvent-solute radial distribution function the most concentrated mixture after IBI.

are listed in Fig. 5.10. They also are able to reproduce these functions for the lower concentrations as shown in Figs. 5.11 and 5.12, and match the pressures as well. The latter quantities are displayed in Table 5.2.

The AdResS simulations using the developed coarse-grained representation are discussed in the following sections.

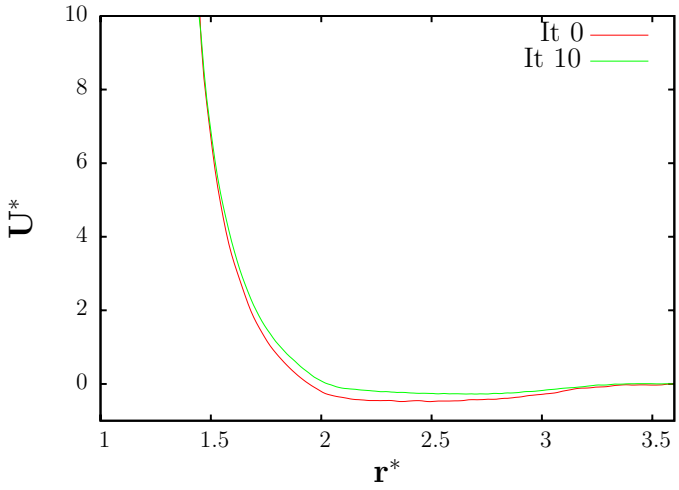

Figure 5.8: Solvent-solute potentials for the most concentrated mixture.

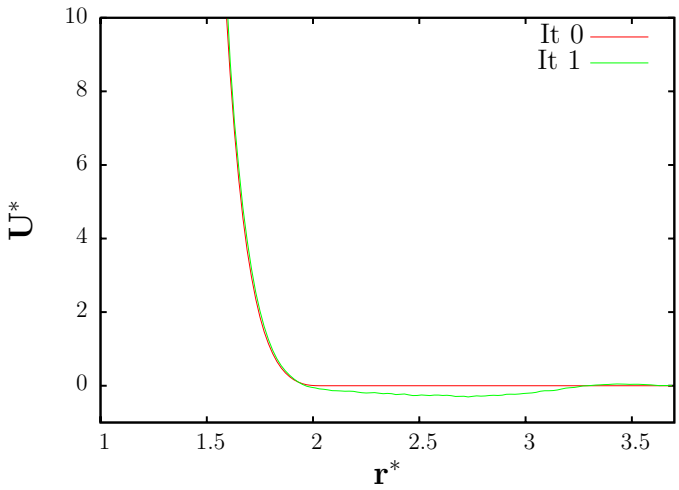

Figure 5.9: Solute-solute potentials for the most concentrated mixture.

5.3 AdResS simulations

AdResS simulations have been performed for the three different concentrations in boxes of the respective dimensions. The hybrid region width was of 4σ, while the weighting function is the same as in the pure solvent case, changing the resolution along the x direction. Equilibration simulations of 500τ were followed by

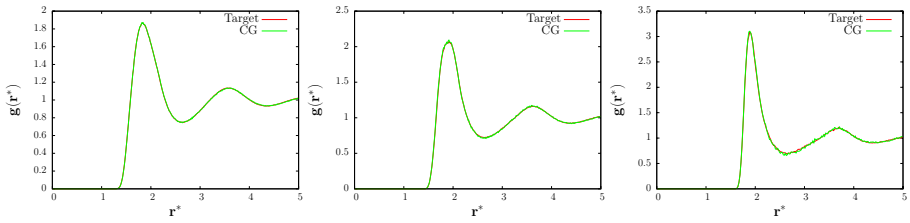

Solvent-Solvent Solvent-Solute Solute-Solute

Figure 5.10: Radial distribution function for 200 solute particles system.

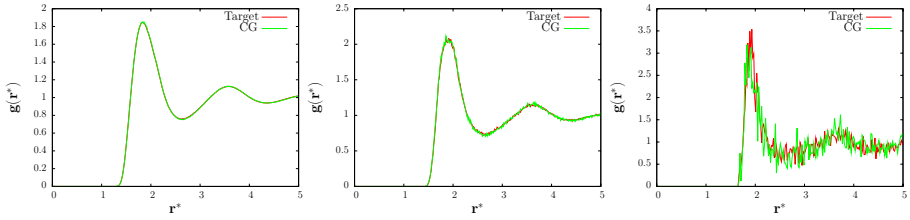

Solvent-Solvent Solvent-Solute Solute-Solute

Figure 5.11: Radial distribution function for 10 solute particles system.

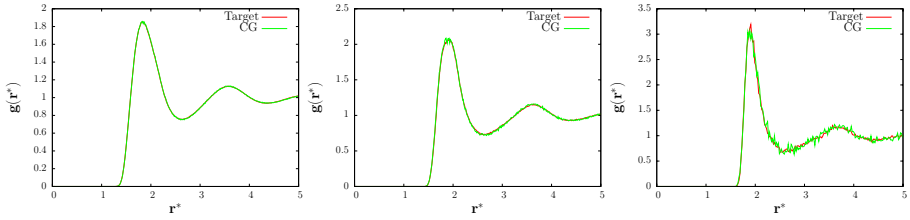

Solvent-Solvent Solvent-Solute Solute-Solute

Figure 5.12: Radial distribution function for 50 solute particles system.

production runs of 5000τ. Their density profiles are shown in Fig. 5.13, while the pressures are listed in Table 5.3. As expected, the solvent particles tend to concentrate in the atomistic and coarse-grained regions, displaying the typical density hole in the hybrid zone. However, the solute particles, whose representation does not change substantially as the other component, compensate this lack of solvent, agglomerating in the switching region. This trend is common for lower concentrations, as shown on Figs. 5.14.

In addition, a set of corrected force fields has been developed for the application of the interface correction at $w = 0.5$. The potentials have been reparametrized for purely hybrid simulations by iterative Boltzmann inver-

c	p
0.007	1.99 ± 0.01
0.034	1.982 ± 0.007
0.125	1.98 ± 0.02

Table 5.2: Pressures using final coarse-grained potentials.

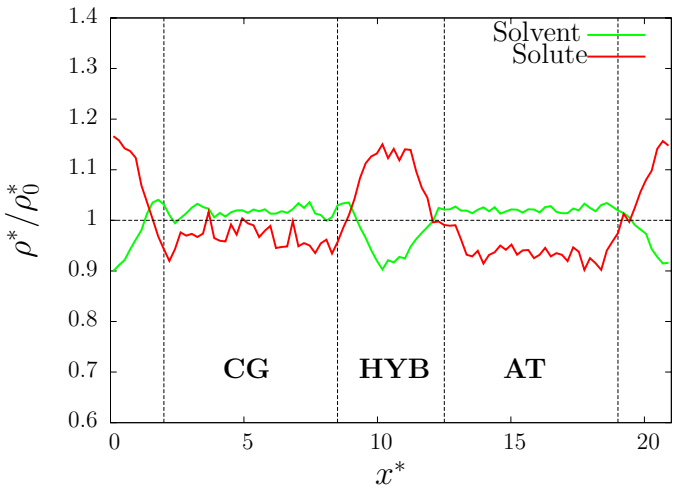

Figure 5.13: Density profiles of solvent and solute for the highest concentration system.

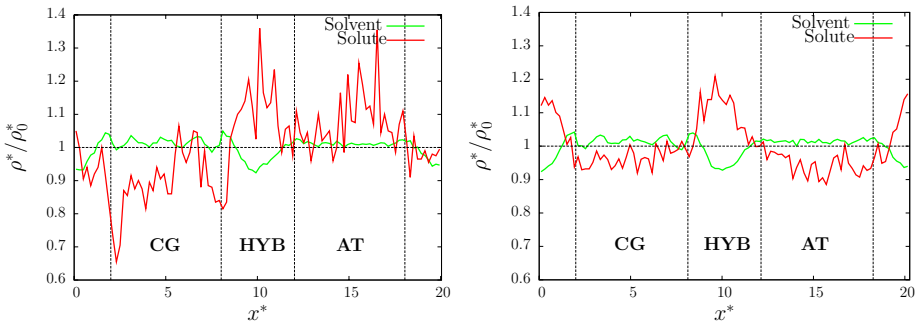

Lowest concentration Medium concentration

Figure 5.14: Density profiles of solvent and solute for lower concentrations.

sion, correcting at the same time the pressure with coefficients $\Delta V_{tt} = 0.1\epsilon$,

c	p^*
0.007	2.07 ± 0.03
0.034	2.06 ± 0.03
0.125	2.05 ± 0.03

Table 5.3: Pressures for AdResS systems.

$\Delta V_{ts} = 0.05\epsilon$ and $\Delta V_{ss} = 0.01\epsilon$ according to their respective contribution to the virial pressure. The correction was performed simultaneously on all interactions. The initial force field was the purely coarse-grained potential for all cases, with the exception of the solvent-solvent interaction. The iteration for this one has started from the corrected potential for the pure solvent previously developed [96]. After three iterations it was possible to observe a reasonable agreement between the radial distribution functions, improving the pressures with a last step where $\Delta V_{tt} = 0.075\epsilon$, $\Delta V_{ts} = 0.06\epsilon$ and $\Delta V_{ss} = 0$. The resulting radial distribution functions and pressures are plotted and listed, respectively, in Fig. 5.15 and Table 5.3 for atomistic and purely hybrid simulations using the coarse-grained and corrected coarse-grained potentials.

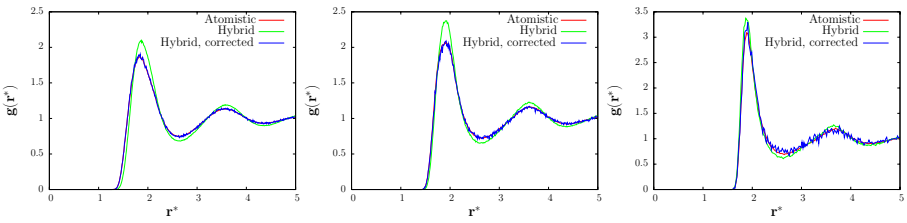

Solvent-Solvent Solvent-Solute Solute-Solute

Figure 5.15: Radial distributions function for 200 solute particles system.

Pressure	Atomistic	Purely hybrid	Purely hybrid-corrected
Total	1.98 ± 0.04	2.45 ± 0.03	1.98 ± 0.03
Solvent-solvent	1.36 ± 0.04	1.74 ± 0.03	1.36 ± 0.03
Solvent-solute	0.41 ± 0.02	0.5 ± 0.02	0.41 ± 0.01
Solute-solute	0.032 ± 0.005	0.039 ± 0.006	0.035 ± 0.006

Table 5.4: Total molecular pressure and its contributions to the virial, compared between atomistic systems and the corrected hybrid simulations for the highest concentration.

For the AdResS simulations, the correction function used was

$$s[x] = \begin{cases} (1-2x) & x \leq 0.5 \\ 0 & x > 0.5 \end{cases} \tag{5.2}$$

that produces a linear interpolation between the normal and corrected coarse-grained potentials for $x < 0.5$, keeping its corrected shape for higher values.

The resultant density profiles are shown in Fig. 5.16. Radial distribution functions show a better agreement with the reference functions, as illustrated in Fig. 5.17.

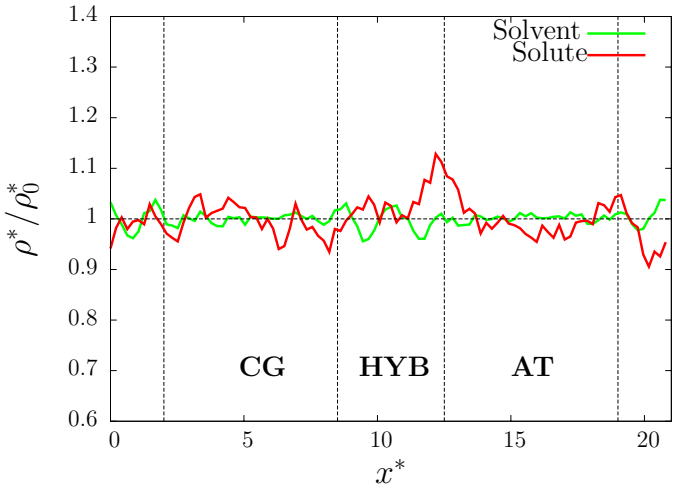

Figure 5.16: Density profiles of solvent and solute for the highest concentration system, with the old corrective approach, the interface correction.

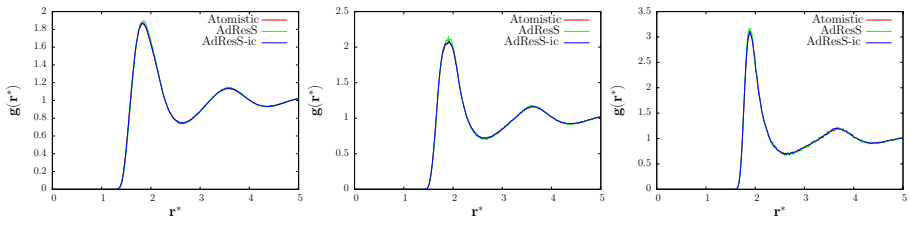

Solvent-Solvent Solvent-Solute Solute-Solute

Figure 5.17: Radial distribution functions for 200 solute particles system under AdResS with and without interface correction.

5.4 Thermodynamic Forces

The application of the thermodynamic force in this system is slightly more complicated [134], since special care must be taken for the treatment of the mixing contributions. Consequently, the chemical potentials are expressed as

$$\mu^{mix}_{solvent} = \mu^{0}_{solvent} + kT\log[c_{solvent}] + f^{mix}_{int}(c_{solvent}, c_{solute}) \tag{5.3}$$

$$\mu^{mix}_{solute} = \mu^{0}_{solute} + kT\log[c_{solute}] + g^{mix}_{int}(c_{solvent}, c_{solute}) \tag{5.4}$$

where μ^0 is the chemical potential of the pure component at the same density. The logarithmic term is the part coming from the entropy of mixing, that depends on the concentration c_i. $f^{mix}_{int}(c_{solvent}, c_{solute})$ is, on the other hand, the contribution of the molecular interactions for the solvent and equivalently g for the solute. Both f and g functions are unknown.

The procedure followed to determine the full thermodynamic force is based in two steps:

- The chemical potential profile is calculated for each component separately, at the same density of the AdResS simulation. This will give account of the contribution to the thermodynamic force in the absence of interactions, and a first approximation for each species. The resultant forces are applied to an AdResS system, to obtain a density profile where just μ^0 has been corrected.

- The remaining part of the chemical potential estimated using the resulting density (and concentration) profiles from the previous simulations. The logarithmic term can be directly evaluated from the concentration profiles, while for the functions f and g are treated empirically. Using a linear expansion in the densities of the functions f and g from Eqs. 5.3 and 5.4, it is possible to write

$$f^{mix}_{int}(c_{solvent}, c_{solute}) \approx \left[\frac{\partial f}{\partial c_{solvent}}\right]_{c^0_{solvent}, c^0_{solute}} \cdot \Delta c_{solvent} \tag{5.5}$$

$$g^{mix}_{int}(c_{solvent}, c_{solute}) \approx \left[\frac{\partial f}{\partial c_{solute}}\right]_{c^0_{solvent}, c^0_{solute}} \cdot \Delta c_{solute} \tag{5.6}$$

  that has to be added to the simple thermodynamic force to obtain its full form. The prefactors, denoted by K_t and K_s for the solvent and solute respectively, are determined empirically.

The first step was performed in the same way as for the one component case shown in the previous chapter: the discretization of the hybrid region permits the calculation of a histogram of chemical potentials, whose values are plotted on Figs. 5.18 and 5.19, accompanied with their respective thermodynamic forces.

The thermodynamics of the pure solvent system seems to have a greater dependence on the molecular representation, as expected since its change of

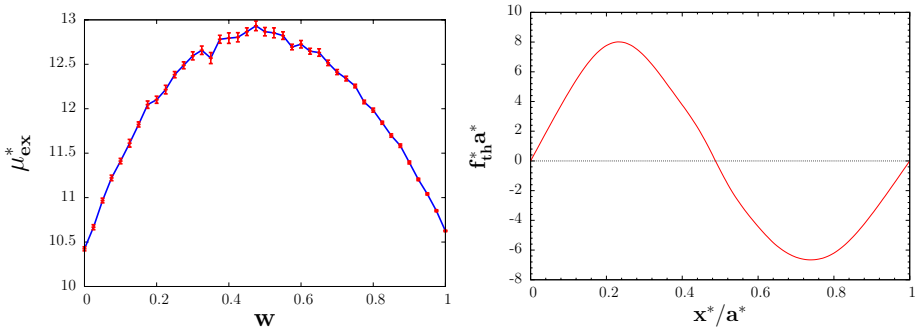

μ^0 $\mathbf{f}^0$

Figure 5.18: μ^0 and its respective thermodynamic force for the solvent.

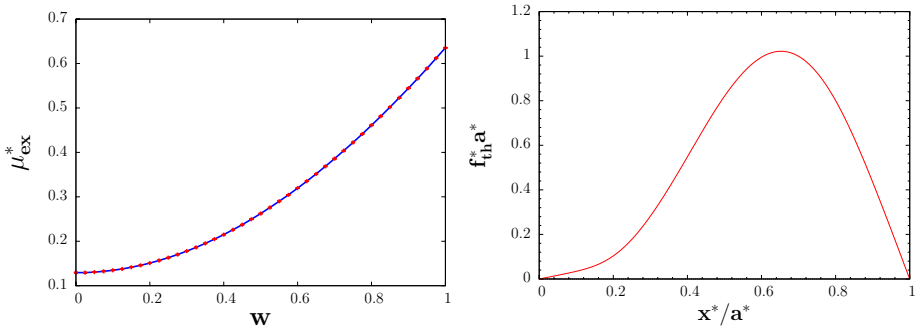

μ^0 $\mathbf{f}^0$

Figure 5.19: μ^0 and its respective thermodynamic force for the solute.

resolution is much deeper. For the solute, a small asymmetry is observed due the fact that atomistic and coarse-grained interactions differ only in a small tail.

The systems treated consists of boxes of size $36 \times 20 \times 20\sigma^3$ with 311 solutes in 2174 solvent particles. The width of the hybrid region was of 12 σ. 10 initial conditions were simulated over 7500τ, to obtain 15000 configurations that were averaged to give the density profiles shown in Fig. 5.20.

The corrective forces were obtained using the coefficients $K_t = 0.0017\epsilon$ and $K_s = 0.0259\epsilon$. The final shape of the forces is shown in Fig. 5.21. Finally, four AdResS simulations were performed over 20000τ that produced the density profiles displayed on Figs. 5.22. The stability of the result is also shown by the number of particles per region, plotted in Fig. 5.23. The free diffusion of each component is proven by the diffusion profiles depicted in Fig. 5.24.

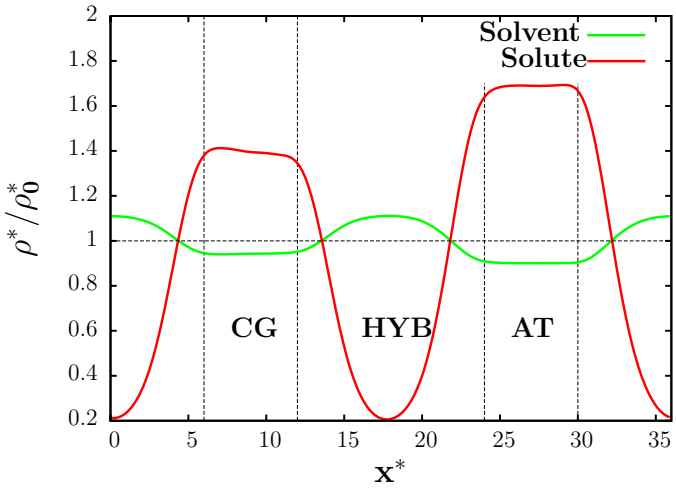

Figure 5.20: Solvent and solute density profiles after the correction of μ^0.

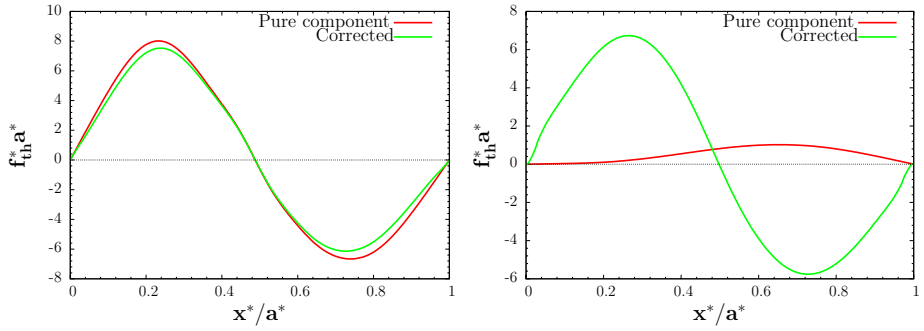

Figure 5.21: Final form of the thermodynamic forces.

5.5 Iterative approach

The iterative scheme can also be extended to multicomponent systems, with some minor features. The chosen procedure corrects the force of one species per iteration, starting from the densest to the most diluted. The force in step i on component α is then

$$\mathbf{f}_\alpha^i = -C_\alpha \nabla \rho_\alpha^i \tag{5.7}$$

The prefactor C_α has been chosen as $Kc_\alpha \frac{\partial p}{\partial \rho_\alpha}$. K is a value between 0 and 1 that will be tuned later in order to keep the stability of the method. Note that if the components are identical, $K = 1$ restores the one-component formula

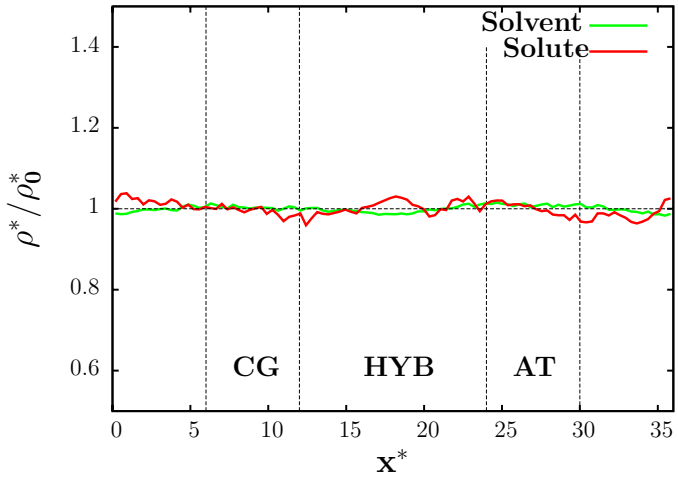

Figure 5.22: Solvent and solute density profiles under the exertion of the total thermodynamic force.

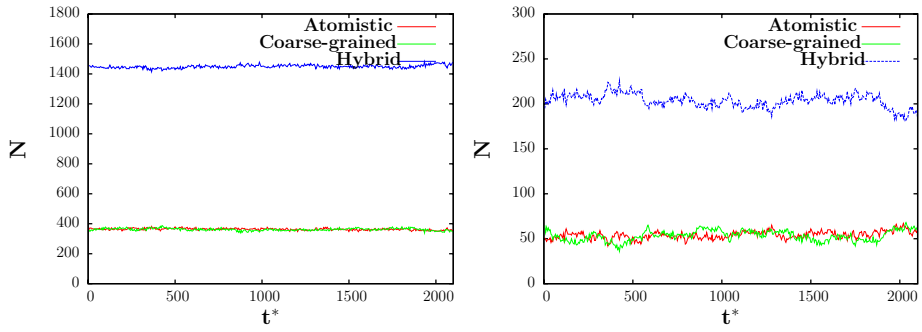

Solvent Solute

Figure 5.23: Number of particles per regime.

since $\rho_\alpha = c_\alpha \rho$.

When tested, $K = 1$ clearly overestimates the forces. Fig. 5.25 shows the density profiles of solute and solvent after two iterations on each specie. Each correction neglects its effect on the other component, leading to an uncontrolled change of density on it.

A direct solution to this problem is to simply choose K between 0 and 1. Its value, for simplicity, will be taken as the same for solvent and solute. The prefactors tested were of 0.1, 0.3 and 0.5.

For $K = 0.1$, the density profiles improve rapidly for the solvent, although for the solute there is no significant improvement from the third iteration. Fig. 5.26

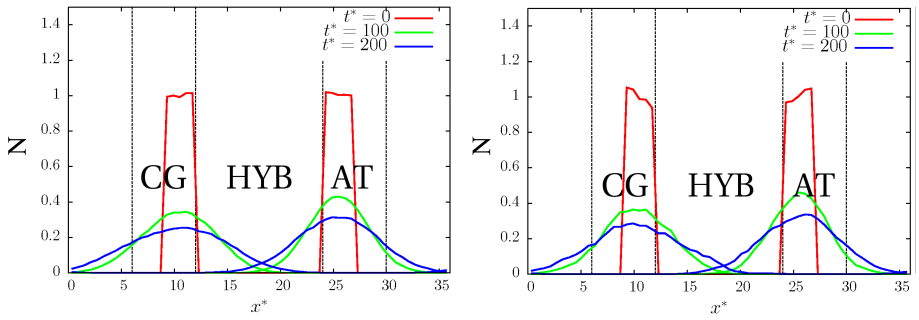

Solvent Solute

Figure 5.24: Diffusion profiles for both species in AdResS under the effect of thermodynamic force.

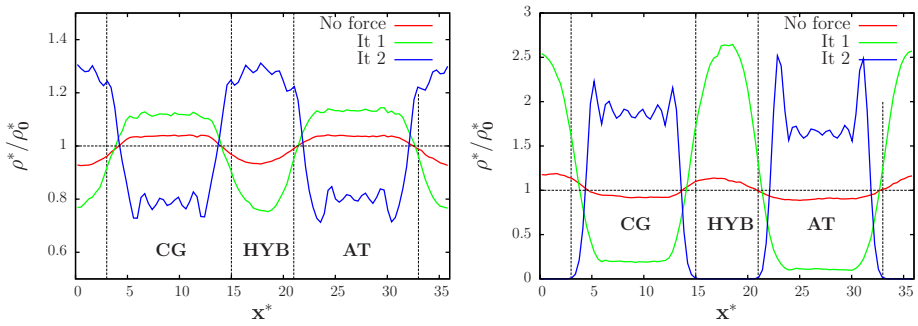

Solvent Solute

Figure 5.25: Density profiles from iterative procedure with $K = 1$

shows the improvement in both species for six iterations on each component.

The prefactor 0.3 gives the best results, allowing to reach a reasonably flat density profile in seven iterations. However, a small solute density bump inferior to the 5% is located at the borders of the coarse-grained region. The density profiles are shown in Fig. 5.27. The next two corrections do not improve the solute density. In fact, on every step, the correction on the solvent cancels the correction on the solute, and vice versa. Therefore, higher accuracy should be achieved by reducing the constant K. Fig. 5.28 shows how the density profiles can improve in one iteration with $K = 0.1$ after seven iterations with $K = 0.3$.

Finally, for $K = 0.5$, the corrections make the density profiles oscillate more drastically (see Fig. 5.29). However, convergence is not reached in the first ten iterations.

Although a prefactor K able to generate the thermodynamic forces in a reasonable number of iterations has been found empirically, it is clear that the

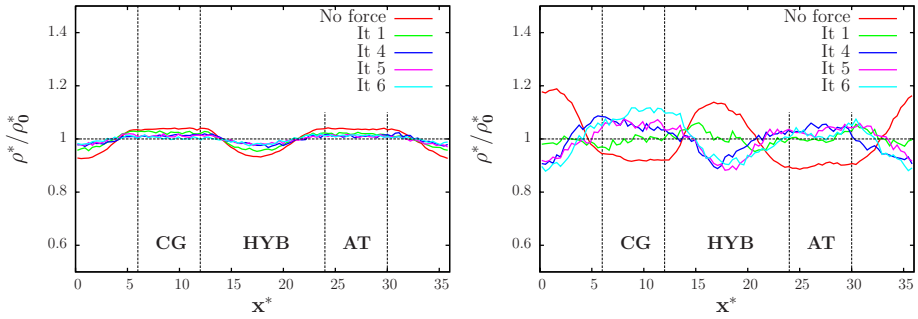

Figure 5.26: Density profiles from iterative procedure with $K = 0.1$

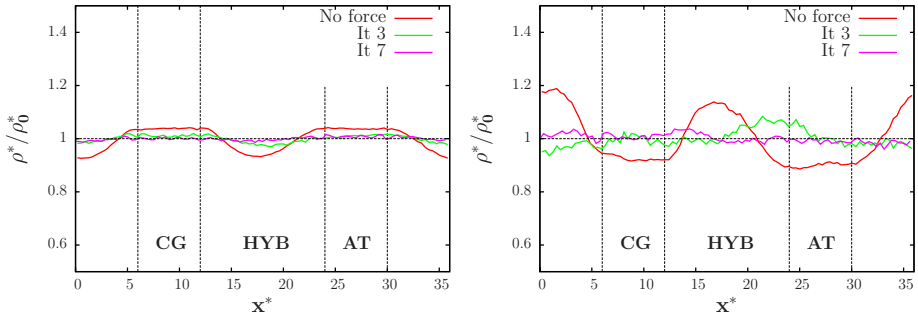

Figure 5.27: Density profiles from iterative procedure with $K = 0.3$.

prefactor that accompanies the density gradient does not differ form the one-component prefactor by more than an order of magnitude.

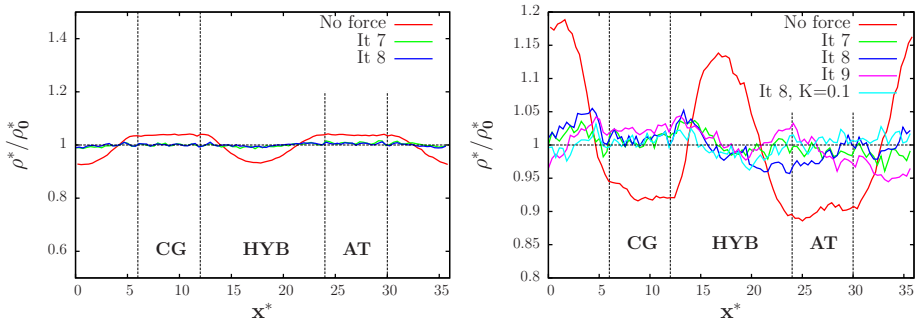

Solvent Solute

Figure 5.28: Fine tuning of the density profiles, with $K = 0.1$ after seven iterations with $K = 0.3$.

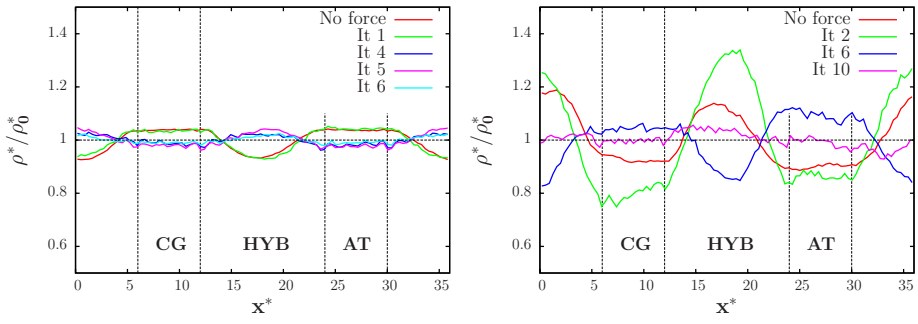

Solvent Solute

Figure 5.29: Density profiles from iterative procedure with $K = 0.5$.

Chapter 6

Adaptive resolution scheme of a model polymer: further development

In this chapter, further step towards the application of the AdResS to the simulation of more complex systems is developed.

A previous work has already studied a model polymer solvated in tetrahedral molecules able to change their representation under the AdResS [126]. The system was designed to keep the polymer in the atomistic representation, by defining the atomistic region as a sphere centered at the center of mass of the chain with a radius carefully determined. This setup is optimal for the simulation of a macromolecule where the structure of the solvent can be relevant for its functional properties. Additionally, the effects of the solute on the solvent can be crucial for the characterization of the solvation process [135]. Both situations can be studied describing with a detailed resolution only the first solvation shells around the solute.

In the present work, however, both solvent and polymer are allowed to change their representations. Such an application requires not only the change of resolution of a multicomponent system, but also the extension of AdResS to bonded interactions. The change of resolution is now through a flat geometry, more suitable to problems like the interaction of polymers with flat surfaces. The previous study of the interaction of polycarbonate with a nickel surface [52] is a clear example.

The chapter begins exposing the system setup chosen for this aim. Later on, the reparametrization of the required interactions will be described, followed by the results and their consequent improvement by the application of the interface correction [96]. Finally, the simulations will be corrected with the application of the thermodynamic force.

6.1 System setup

The model polymer is a bead-spring polymer chain, whose monomers are the solute particles described in Chapter 5. The bonded interactions are FENE bonds (see Eq. 3.11) with parameters $k_s = 30\epsilon/\sigma_s^2$ and $R_{0_s} = 1.5\sigma_s$, where $\sigma_s = 1.8\sigma$.

The system setup is illustrated in Fig. 6.1, where the polymer has been located at the center of the hybrid region, keeping its central monomer fixed. For the moment, this setting is enough for the test of the interactions and the analysis of certain statistical properties. Later applications will allow the chain to freely diffuse across the whole simulation box.

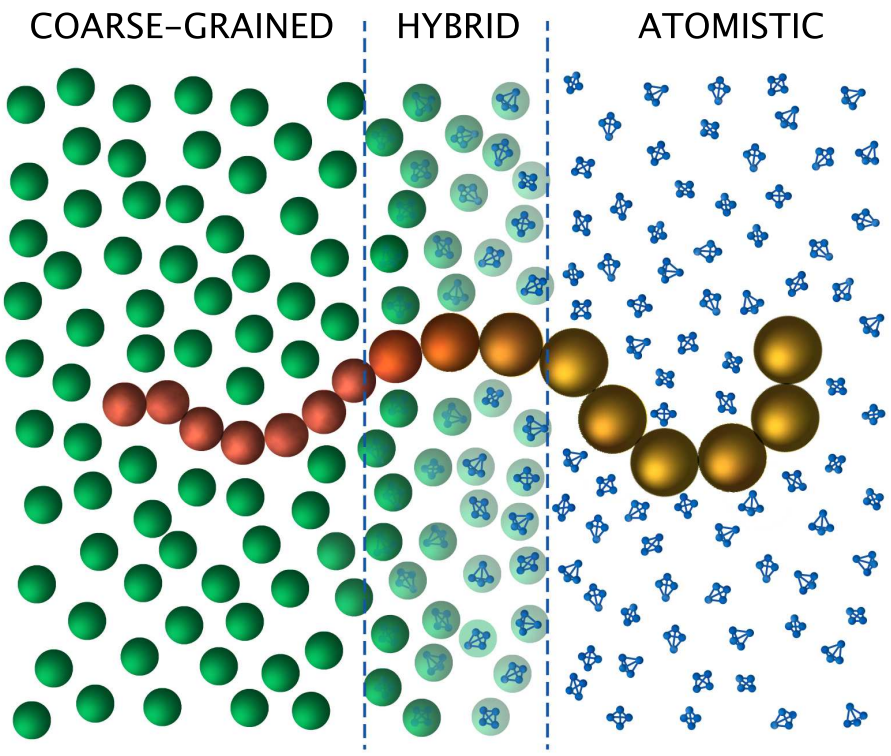

Figure 6.1: Polymer system setup. The monomers do not necessarily have the same excluded volume in both representations.

This configuration demands a complete reparametrization of the interactions in the coarse-grained region; namely, the non-bonded interactions between solvents and solutes, and the bonded potentials between the monomers of the model macromolecule. The former set of potentials has been systematically developed in the previous chapter, while the latter will be treated in the following

section.

The aim of the bonded coarse-grained interactions will be to reproduce the bond, angle and torsion distributions. In addition to this structure functions and the density profile, some statistical properties of the polymer will be monitored: the end-to-end distance

$$\langle R_E^2 \rangle = \langle (\mathbf{r}_N - \mathbf{r}_1)^2 \rangle, \tag{6.1}$$

where $\mathbf{r}_i$ is the position of the ith monomer and N is the number of monomer units; the hydrodynamic radius R_H,

$$\left\langle \frac{1}{R_H} \right\rangle = \frac{1}{N^2} \sum_{i \neq j} \left\langle \frac{1}{r_{ij}} \right\rangle \tag{6.2}$$

with $r_{ij} = |\mathbf{r}_i - \mathbf{r}_j|$, and the radius of gyration

$$\langle R_G^2 \rangle = \frac{1}{N} \sum_i \langle (\mathbf{r}_i - \mathbf{R})^2 \rangle \tag{6.3}$$

where $\mathbf{R}$ stands for the position of the center of mass of the polymer.

A deeper characterization of the chain structure can be done by inspecting the exponent ν that governs the scaling behavior of $\langle R_G^2 \rangle$ and $\langle R_E^2 \rangle$ through the relation

$$\langle R_E^2 \rangle \propto \langle R_G^2 \rangle \propto N^{2\nu} \tag{6.4}$$

Such a number can be obtained from the analysis of the static structure factor

$$S(q) = \frac{1}{N} \Big\langle \sum_{ij} e^{i\mathbf{q}\cdot(\mathbf{r}_i - \mathbf{r}_j)} \Big\rangle \tag{6.5}$$

which can be experimentally measured. In the regime $R_G^{-1} \ll q \ll b^{-1}$, with b the bond length, $S(q)$ is proportional to $q^{-1/\nu}$.

6.2 Two-body bonded interactions

The studied polymer, composed of 20 monomers, is solvated in 2800 tetrahedral molecules contained in a cubic box of side of length 25.261σ. The target bond length distribution was obtained from an atomistic simulation of 25000τ sampled every 1000 time steps. The Iterative Boltzmann Inversion was then applied to the bead-bead bond interaction starting from the potential of mean force, described in Chapter 3.

The procedure converged after three iterations. The initial and final interactions are shown on the left of Fig. 6.2. The agreement between the target and coarse-grained distributions is shown on the right.

The radial distribution functions, shown in Fig. 6.3 do not require further parametrizations. Structure factor and the statistical properties aforementioned are shown in Fig. 6.4 and Table 6.1 respectively, showing good agreement.

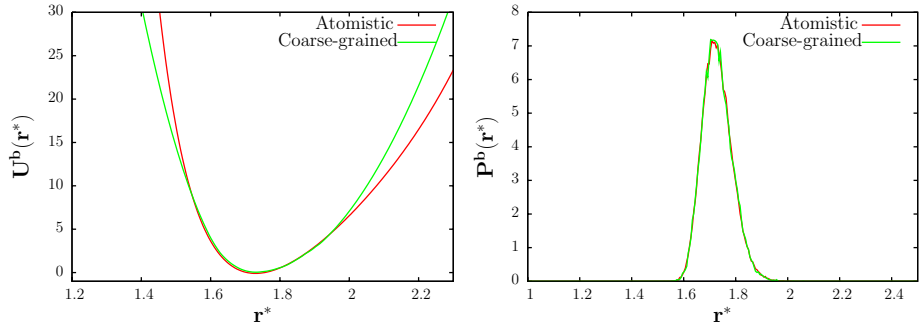

Bond potentials Bond length distribution

Figure 6.2: Results of the IBI for the bonded interaction between the monomers of the model polymer.

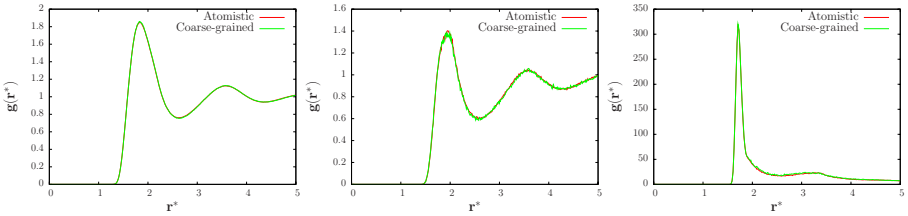

Solvent-Solvent Solvent-Solute Solute-Solute

Figure 6.3: Radial distribution functions.

System	Atomistic	Coarse-grained
p^*	1.98 ± 0.08	1.984 ± 0.002
$\langle R_E^2 \rangle^{1/2}$	10.7 ± 0.5	10.6 ± 0.2
$\langle R_G^2 \rangle^{1/2}$	4.2 ± 0.1	4.24 ± 0.06
$\langle R_H^{-1} \rangle^{-1}$	4.15 ± 0.05	4.17 ± 0.05
ν	0.56	0.57

Table 6.1: Summary of some polymer statistical properties. Pressure is included to show agreement. The chain consists of 20 monomer units.

The value of ν, that is 0.5 for a θ solvent and approximately 0.588 for a good solvent [83, 136, 137], is closer to the latter. The discrepancy could come from the finite size of the chain, as it has been previously observed [126], together with the quality of the solvent.

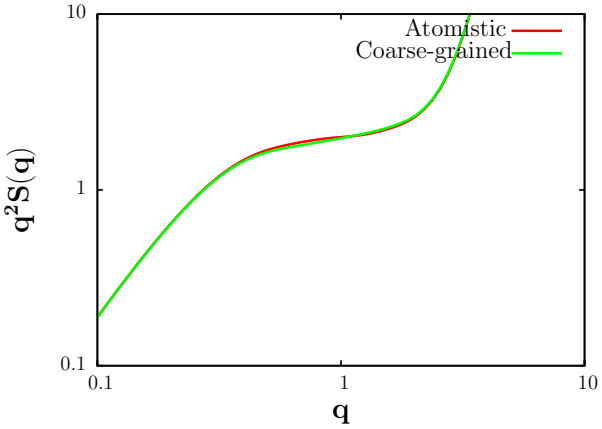

Figure 6.4: Structure factor in Kratky representation.

6.3 AdResS simulation of the model polymer

The AdResS simulations are performed in a box of the same size as in the atomistic calculations, while the hybrid region has a width of 4σ in the x direction. Six different initial conditions were integrated for 10000τ after an equilibration of 2500τ. Each configuration was saved every 1000 steps.

The density profile, shown in Fig. 6.5 shows reasonably good agreement with the atomistic simulations, considering that in the transition region it is expected a lack of solvent and a consequent excess of solute due the nature of their non bonded interactions, as observed previously in the multicomponent system. There is no asymmetry produced by the inclusion of the bonded interactions. Every profile shows a density "spike" coming from the fixed particle at the center of the hybrid zone. On the other hand, the bond distribution function and the structure factor (Fig. 6.3) do not seem affected by the adaptive regime. These functions can be compared with the resulting forms of a purely hybrid simulation, at $w = 0.5$. It is well known that at this point, the disagreement with the atomistic results is high, if not maximum [96]. However, the bond distribution shows a nice agreement between AdResS, atomistic and purely hybrid simulations. This is consistent with the fact that the interaction between solutes does not change greatly between atomistic and coarse-grained representations, as in the case of the solvent particles.

6.4 AdResS simulation with interface-pressure correction

Finally, the simulation is performed under the influence of the interface-pressure correction. Since the bond distribution does not change appreciably in the

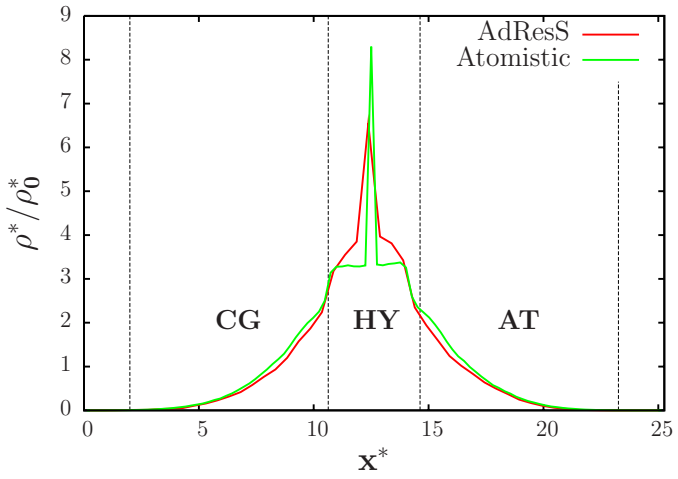

Figure 6.5: Monomer density profile of the model polymer on AdResS simulation.

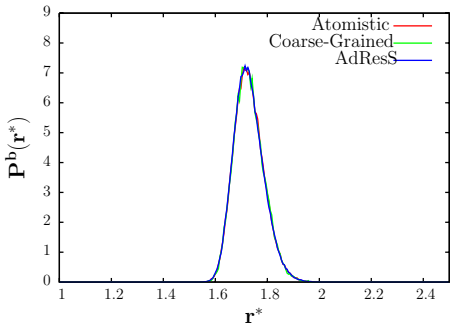

Figure 6.6: Bond length distribution

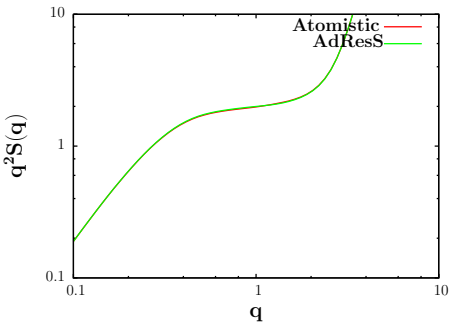

Figure 6.7: Structure factor in Kratky representation

purely hybrid simulation previously shown, the correction is applied only to the non-bonded interactions.

Simulations of 10000τ were performed for the same six initial conditions. The properties of the polymer, on Table 6.2 are again in good agreement with the atomistic values, while the bond distribution and structure factor do not display any change compared with the result without interface correction. In addition, the monomer density profile of Fig. 6.8 shows a considerable improvement, matching almost perfectly the atomistic result.

System	Atomistic	AdResS	AdResS-ic
p	1.98 ± 0.08	2.05 ± 0.02	2 ± 0.02
$\langle R_E^2 \rangle^{1/2}$	10.7 ± 0.5	10.1 ± 0.3	10.1 ± 0.4
$\langle R_G^2 \rangle^{1/2}$	4.2 ± 0.1	4.07 ± 0.07	4.07 ± 0.09
$\langle R_H^{-1} \rangle^{-1}$	4.15 ± 0.05	4.08 ± 0.04	4.05 ± 0.05
ν	0.56	0.54	0.53

Table 6.2: Summary of some statistical properties for AdResS simulation using interface-pressure correction. The polymer is composed of 20 monomers.

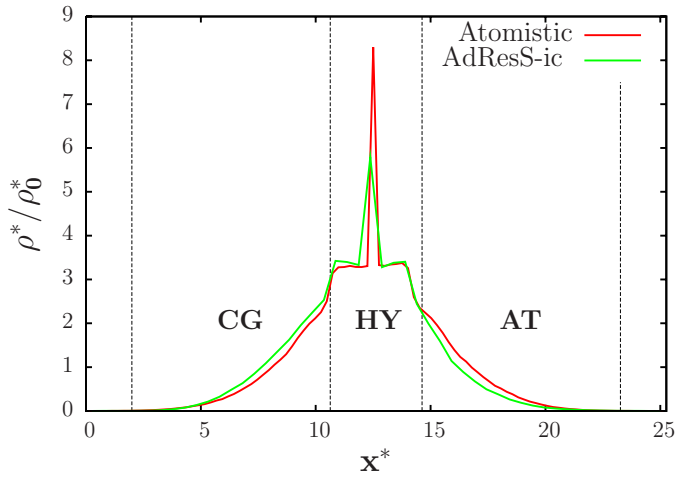

Figure 6.8: Monomer density profile of the model polymer on AdResS simulation with interface correction.

6.5 AdResS simulation under thermodynamic forces.

The thermodynamic force has been developed for the most diluted mixture, with 20 monomers solvated in 2400 solute particles in a box of dimensions $40.1 \times 20.05 \times 20.05\sigma^3$. The weighting function is the same used in the previous mixture study, with a hybrid region width of 12σ. The form of the chemical potentials is given by the Eqs. 5.3 and 5.4 presented in the previous chapter. However, this time, the mixing terms are expressed in terms of the density

$$f_{int}^{mix}(\rho_{solvent}, \rho_{solute}) \approx \left[\frac{\partial f}{\partial \rho_{solvent}}\right]_{\rho^0_{solvent}, \rho^0_{solute}} \cdot \Delta\rho_{solvent} \tag{6.6}$$

$$g_{int}^{mix}(\rho_{solvent}, \rho_{solute}) \approx \left[\frac{\partial f}{\partial \rho_{solute}}\right]_{\rho^0_{solvent}, \rho^0_{solute}} \cdot \Delta\rho_{solute} \tag{6.7}$$

which gives a correction to the thermodynamic force of the form $-K_i \nabla \rho_i$ for the component i. Therefore, including the term of the chemical potential of the pure species, plus the logarithm due to the entropy of mixing and above shown term proportional to the density of each component, it is possible to obtain the full thermodynamic forces shown in the left of Fig. 6.9. The constants were of $K_t = 26\epsilon\sigma^{-3}$ and $K_s = 0.3\epsilon\sigma^{-3}$ for the solvent and solute respectively. The density profiles of the AdResS simulations is shown in the right of Fig. 6.9.

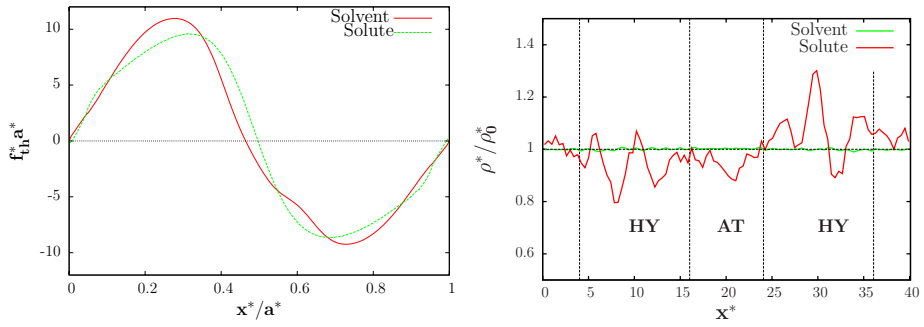

Thermodynamic forces Density profiles

Figure 6.9: Results for the thermodynamic forces in the most diluted mixture.

The solute density shows a noisy profile due to its low concentration. However, the density profile of the major component, which mainly determines the physics of the system, is practically homogeneous.

As a first step, the effect of the thermodynamic force is studied in a polymer characterized by the same interactions developed in the previous sections. The system consists of a chain composed of 50 monomers solvated in 7000 tetrahedral molecules. The box dimensions are of $36 \times 33.458 \times 33.458\sigma^3$ with a hybrid region width of 12σ. The target distributions and quantities were collected from three atomistic simulations integrated over 25000τ. Since the bonded interactions have been added, and the volume has changed in comparison to the system on which the thermodynamic forces were developed, it is expected that these forces will require certain refinement. That can be done by adding on to the force on component α the correction $\Delta \mathbf{f}_\alpha = -C_\alpha \nabla \rho_\alpha$ iteratively. The chosen prefactor is the one chosen for the iterative procedure on the mixture presented at the end of the previous chapter, $C_\alpha = 0.3 \frac{1}{\rho_T} \frac{\partial p}{\partial \rho_\alpha}$ evaluated in the coarse-grained representation. In this case, it was enough to correct the solute density over two steps, with a prefactor of $C_{solute} = 33.975\epsilon\sigma^3$.

For the AdResS systems, six initial conditions were integrated over 2500τ for equilibration and 12500τ for production. The density profiles obtained with this corrected thermodynamic force are compared for different systems in Fig. 6.10. Statistical properties are listed in Table 6.3. Bond distributions and structure factor are plotted in Fig. 6.11.

The agreement in the density profiles is almost perfect. It is worthy to note,

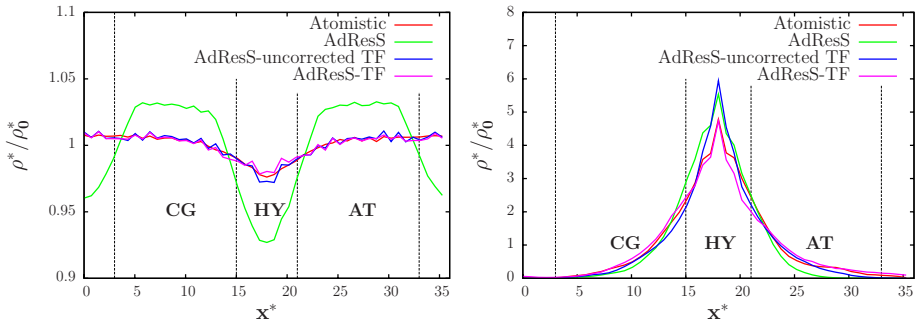

Figure 6.10: Density profiles for a 50 bead chain without angular interactions. The results are compared also for uncorrected and final forms of the thermodynamic forces.

System	Atomistic	AdResS	AdResS-TF
$\langle R_E^2 \rangle^{1/2}$	16.2 ± 0.6	15.5 ± 0.4	15.7 ± 0.6
$\langle R_G^2 \rangle^{1/2}$	7.06 ± 0.2	6.7 ± 0.2	6.8 ± 0.2
$\langle R_H^{-1} \rangle^{-1}$	6.09 ± 0.09	5.9 ± 0.1	5.9 ± 0.1
ν	0.56	0.56	0.54

Table 6.3: Some statistical properties of the 50 bead chain without angular interactions in atomistic and AdResS simulations.

additionally, that the solvent density resembles the atomistic profile in both hybrid regions, considering that the solute is concentrated in the center of the box. Therefore, the same thermodynamic force applied to the solvent could lead to different results in the absence of the minor component. However, this is not the case, showing the robustness method.

The value of ν shows no increase with respect to the exponent of the shorter chain, suggesting that the deviation with respect to a good solvent could come from the solvent quality.

Bond distributions are also well reproduced in AdResS simulations. Structural properties agree satisfactorily, although the structure factor is slightly perturbed with respect to the target function. This is expected since the structure of both solvent and solute differ in the hybrid region. However, such difference does not seem affected by the action of the thermodynamic forces. Note also that the end-to-end distance is in every case bigger than the width of the hybrid region.

To conclude this chapter, the same polymer is studied with angular and

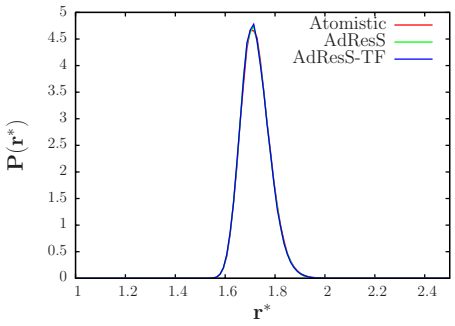

Bond distribution

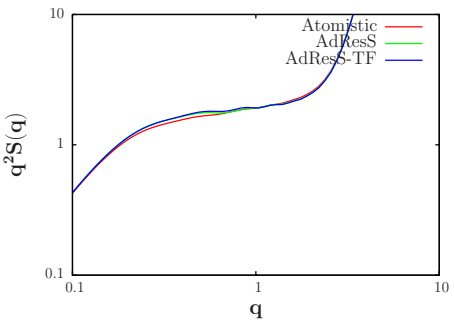

Structure factor in Kratky representation

Figure 6.11: Structural functions for the 50 bead polymer without angular interactions.

torsion interactions. The angular potential is given by

$$U^a(\theta) = \frac{k_\theta}{2}(\theta - \theta_0)^2 \tag{6.8}$$

where $k_\theta = 3rad^{-2}\epsilon$ and $\theta_0 = \frac{2}{3}\pi$. The torsion potential is, on the other hand,

$$U^t(\phi) = K_\phi[1 + \cos(\phi)] \tag{6.9}$$

with $K_\phi = 2\epsilon$.

Such force fields are able to satisfactorily reproduce their respective distributions in the coarse-grained representation. Hence, the AdResS interpolation of forces is not applied to these forces.

The thermodynamic forces, on the other hand, are iteratively corrected using the same formula as before, starting from the parametrized forces for the previously studied polymer. As it can be seen in the density profiles of Fig. 6.12, the thermodynamic forces produce the desired effect after two iterations.

Statistical properties, listed in Table 6.4 also show good agreement with atomistic results.

System	Atomistic	AdResS	AdResS-TF
$\langle R_E^2 \rangle^{1/2}$	16.8 ± 1	16.4 ± 0.5	18.2 ± 0.6
$\langle R_G^2 \rangle^{1/2}$	8.8 ± 0.3	8.9 ± 0.3	9.3 ± 0.2
$\langle R_H^{-1} \rangle^{-1}$	7.5 ± 0.2	7.6 ± 0.1	7.7 ± 0.1

Table 6.4: Some statistical properties of the 50 bead chain in presence of angles and torsions.

Finally, the bond distribution and structure factor are found in Fig. 6.13, while the angle and torsion distributions are depicted in Fig. 6.14.

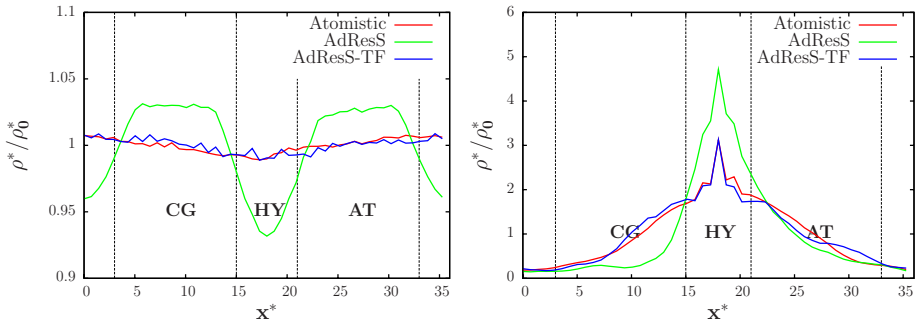

Solvent Solute

Figure 6.12: Density profiles for a 50 bead chain with three and four body interactions.

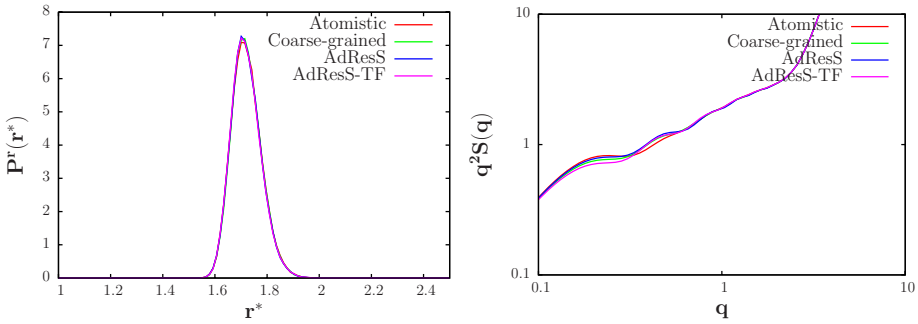

Bond distribution Structure factor in Kratky representation

Figure 6.13: Structural functions for the 50 bead polymer with angles and torsions.

Bond and torsion distributions seem almost perfectly matched in the coarse-grained and AdResS simulations. Angle distributions are also satisfactorily reproduced, although a small difference of less than 4% is present in the second peak that comes form the coarse-grained parametrization. This small difference is inherited in the AdResS simulations and not affected by the thermodynamic force. A similar case is observed in the structure factor, where the mismatch between AdResS and atomistic simulations is not improved by the thermodynamic force.

The structure factor does not allow to calculate ν precisely. However, it must be considered that the system setup and length of the simulations has been designed to test the effects of the AdResS forces and the thermodynamic forces on the basic structure and density profiles.

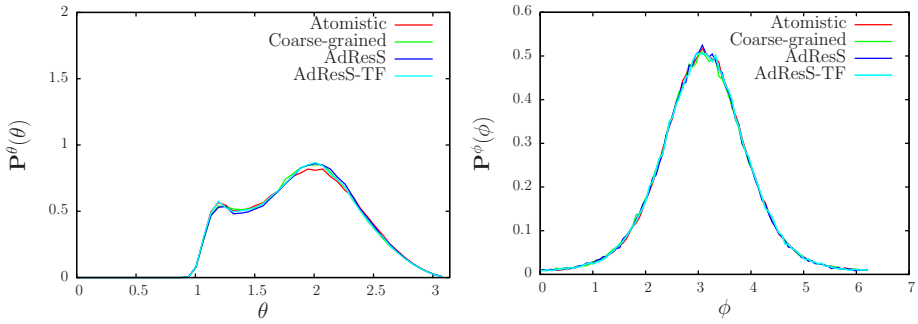

Angle distribution Torsion distribution

Figure 6.14: Some polymer distribution functions.

It is possible to conclude that, in general, the thermodynamic forces can be obtained in a systematic way to correct the density inhomogeneities of systems with bonded interactions. However, care must be taken when reproducing structural properties, specially in the hybrid region where, in general, they can be altered by the interpolation of forces.

Chapter 7

Implementation of the Adaptive Resolution Scheme in ESPResSo

A description of the numerical implementation of AdResS in the ESPResSo package [138] is presented in this chapter. Technical details about the interface commands, integrator and parallelization scheme are listed in the Appendix.

The chapter begins with a description of the general overview of the system and how the equations of motion are integrated. Later on, the parallelization scheme is described, continued by the implementation of the thermostat. After that, the initialization of the internal degrees of freedom when a molecule transits form coarse-grained to a hybrid domain is briefly discussed, to conclude with the treatment of bonded forces. Interface pressure correction and thermodynamic forces deserve a purely technical discussion that is included in the corresponding appendix.

It is worthy to point that the implementation can greatly help to understand better the physics of the AdResS and to have a more complete picture of it.

7.1 General setup

The system is composed of molecules with only one mapping point, located at the center of mass. The basic idea behind this implementation is the treatment of each molecule with a *double resolution*, i.e., every molecule will be composed of its atoms and a *virtual particle* that corresponds to its center of mass. The latter is nothing else than a mapping point needed for the calculation of the force at this point, which is properly distributed among the atoms later. Hence, the potential between two particles i and j belonging to different molecules α and β can be written as

$$V_{ij} = V^{ex}(\mathbf{r}_i, \mathbf{r}_j, ...) + V^{vs}(\mathbf{r}^{vs}(\mathbf{r}_i, \mathbf{r}_j, \ldots)) \tag{7.1}$$

where V^{ex} is the atomistic potential between them, and V^{vs}, the potential between the virtual sites, whose position $\mathbf{r^{vs}}$ is a function of the positions of the atoms of its molecule.

Therefore, the force on atom i is distributed according to

$$\begin{aligned} \mathbf{F}_i &= -\frac{\partial(V^{ex}+V^{vs})}{\partial \mathbf{r}_i} \\ &= \mathbf{F}_i^{ex} + \mathbf{F}^{vs}\frac{\partial \mathbf{r}^{vs}}{\partial \mathbf{r}_i} \\ &= \mathbf{F}_i^{ex} + \frac{m_i}{\sum_{i\in\alpha} m_i}\mathbf{F}^{vs} \end{aligned} \tag{7.2}$$

This choice avoids the creation and deletion of atoms, which is a highly expensive operation that involves an active manipulation of the memory. Therefore, the AdResS is reduced to the proper calculation and distribution of forces on the atomistic atoms, according to equation 1 in Chapter 3. The virtual sites' positions are simply updated from the positions of the atoms. Naturally, the intermolecular atomistic forces will not be calculated in the coarse-grained region, since they are not involved in the dynamics. The same holds for the coarse-grained force fields in the atomistic domain.

The intramolecular forces are calculated in the whole simulation box, independently of the representation of the molecule. They are not included in the interpolation scheme dictated by the AdResS equations, and their inclusion helps to stabilize the system.

7.2 Thermostat

The Langevin thermostat [27] has been chosen for the AdResS simulations, mainly due its local nature. This feature makes sure that the stationary velocity distribution of each particle will be consistent with the temperature of the thermostat, independent from the rest of the system[1]. In this case, the thermostat forces act only over the atoms across the whole simulation box. Once these degrees of freedom have the correct velocity distribution, the thermalization of the centers of mass is straightforward. The same features can be obtained by the application of a DPD [34, 40] thermostat.

Counting with this global setup, there are two tested options for the initialization of the atoms' velocities (and positions) when a molecule crosses from the coarse-grained to the hybrid regime[2]:

- Copy the atom's velocities relative to the center of mass of a molecule from a random molecule from the atomistic region [118]. This guarantees that the intramolecular degrees of freedom will be sampled from distributions consistent with the atomistic regime that is properly thermalized.

[1] Since the forces are not homogeneous neither conservative, this choice would prevent any eventual temperature profile that a global thermostat could generate.

[2] That is, the reintroduction of the integrated degrees of freedom

- Leave the positions and velocities untouched, that is a justified choice since the thermostat generates the correct velocity distribution regardless the representation of a molecule.

Both approaches give no difference in the velocity distributions in the hybrid region neither the density profiles, as shown in Fig. 7.1. However, the latter results considerably faster than the former. Another important feature is the parallelization scheme: since the ESPResSo package divides the simulation box into several domains that are distributed among the processors, the presence of atomistic molecules is guaranteed in all of them. Consequently, the second choice is more plausible for parallel simulations.

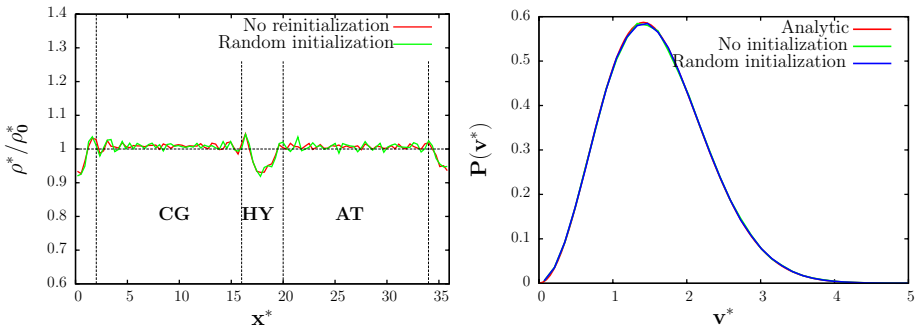

Density profiles Velocity distribution of hybrid particles

Figure 7.1: Comparison of distributions for AdResS simulations of tetrahedral systems, under the two initialization schemes.

7.3 Bonded Interactions

The bonded interactions between atoms that belong to the same molecule are fully considered since they are not affected by equation 1 from Chapter 3. This is required for the stability of the molecules in the coarse-grained region.

For more complex systems, like the polymer of Chapter 6, the bonded interactions are interpolated between the two representations whenever the atoms involved belong to different molecules, whose virtual sites have different identities.

Chapter 8

Conclusions

This thesis work was devoted to conceptual and technical advances of the Adaptive Resolution Scheme.

Conceptually, the thermodynamic consistency of the method was verified in the tetrahedral system, which allowed the introduction of the Thermodynamic Force. Such force was successfully applied in this system and in a simpler model, where both representations contain the same number of degrees of freedom. The application of the force reduces almost completely the density artifacts produced by the interpolation of forces that characterize AdResS. Special care has to be taken when this correction is applied: the reported finite size effects manifested through the formation of density patterns suggest that the width of the hybrid region must be large enough.

The concept of Thermodynamic Force was generalized and expressed in terms of pressure consistency, which allowed to establish numerical consistency between AdResS and molecular dynamics simulations of open systems. Additionally, this lead to the development of an iterative procedure for obtaining the Thermodynamic Force, that has also been applied to more complex systems like water [132]. The local physics of the atomistic region was compared with the results of purely atomistic simulations. Radial distribution functions and velocity distributions show a good agreement, while the particle number fluctuation in the subvolume, pressure and density profiles improve considerably under the application of the Thermodynamic Force, since it restores the target density in the whole simulation domain, and in particular, in this region.

Concerning multicomponent systems, a model mixture of spherical solutes was the subject of study. The development of the interactions, which is by itself a non-trivial issue, was performed systematically through successive applications of the Iterative Boltzmann Inversion correcting the pressure at each step, giving good results over a wide range of concentrations. The effects of AdResS were also listed for this set of mixtures, specially in the most concentrated case. There, the interface-correction and the Thermodynamic Force were also applied successfully to the most concentrated mixture, requiring a slightly more delicate treatment than in the pure component systems.

Finally, it was shown that the sole interpolation of forces of the AdResS can be applied to two-body bonded interactions. The distributions that characterize the model polymer treated are not affected in the hybrid zone, showing good agreement with purely atomistic simulations. Further application of the Thermodynamic Force on this system did in practice not affect the basic structure of the polymer.

Concerning the technical issues, a reference implementation of AdResS was incorporated to the ESPResSo simulation package, allowing its parallelization and implementation in a more standard way.

Appendix: Technical Details and Interface of the Implementation of AdResS in ESPResSo.

A deeper and more technical description of the AdResS implementation in the ESPResSo package [129, 138] is presented below. The integrator and parallelization scheme are described with more detail in a systematic way, while the commands developed for the TCL [139] interface of ESPResSo are also included. The appendix is structured in the same way as Chapter 7, where the conceptual aspects were explained.

General setup

The AdResS feature is enabled in ESPResSo by adding the line

```
#define ADRESSO
```

to the configuration file `myconfig.h`. Later on, the AdResS has to initialized at the `tcl` level through the line

```
adress set topo $kind width $width $hybrid_width \
center x $R_x wf $wf
```

where `kind` defines the general setup of the AdResS simulation. They can be
0 disabled
1 constant weight function
2 one dimensional geometry
3 spherical geometry
and `wf` the weighting function type:
0 conventional cosine-squared function
1 defined by the user
`hybrid_width` and `width`, on the other hand, are the widths of the hybrid and atomistic region respectively.

Integrator

The integrator used by ESPResSo corresponds to a standard velocity Verlet algorithm [14, 15], that can be summarized in four steps as

1. $v(t + \Delta t/2) = v(t) + \Delta t/2 \cdot f(t)/m$
2. $p(t + \Delta t) = p(t) + \Delta t\, v(t + \Delta t/2)$
3. Calculate $f(t + \Delta t)$ from $p(t + \Delta t)$, $v(t + \Delta t/2)$
4. $v(t + \Delta t) = v(t + \Delta t/2) + \Delta t/2 \cdot f(t + \Delta t)/m$

However, when the virtual sites are present, this has to be slightly modified to

1. $v(t + \Delta t/2) = v(t) + \Delta t/2\, f(t)/m$
2. $p(t + \Delta t) = p(t) + \Delta t\, v(t + \Delta t/2)$

2b. Recalculate and update the positions, velocities and weighting functions $w(\mathbf{R})$ of the virtual sites.

3. Calculate $f(t + \Delta t)$ from $p(t + \Delta t)$, $v(t + \Delta t/2)$

3b. Distribute the force of the virtual sites to its corresponding atoms.

4. $v(t + \Delta t) = v(t + \Delta t/2) + \Delta t/2\, f(t + \Delta t)$

Therefore, the integrator works only on the atomistic particles, while the virtual sites are merely dummy points employed in the force calculation.

Parallelization scheme and cut-offs

As mentioned in Chapter 7, the parallelization scheme used by ESPResSo consists in a partition of the simulation domain into several boxes of fixed volume. Each of these sub-volumes is surrounded by a *ghost layer* that contains a copy of the particles of the adjacent sub-volumes required for the calculation of the forces. Evidently, the thickness of this layer will depend of the cut-off range of the interactions.

The parallelization scheme requires two additional features in the presence of the virtual sites. The first concerns to the communication of the *ghost particles*, which positions must be known by each processor for the calculation of the virtual sites. Therefore, the properties of these particles must be updated, which requires a second communication.

The second issue consists on the redefinition of the ghost layer thickness. The implementation has to guarantee that every molecule that contains at least one non-ghost atom must be fully included in the processor. This is required for the calculation of the virtual sites and for the distribution of the forces. Consequently, the maximum cut-off between the non-bonded interactions has to be increased by approximately the size of a molecule. In practice, this is

performed by increasing the maximal cutoff by twice the maximal cut-off of the bonded interactions.

The molecular cut-off between particles type `type1` and `type2` can be set to `cut-off` through the sentence

```
inter $type1 $type2 molcut 1 $cut-off
```

This is a versatile implementation that allows the definition of an arbitrary cut-off between molecules. However, a more simple implementation requires only the inclusion of the line

```
#define MOL_CUT
```

in the configuration file `myconfig.h`.

Thermostat

The thermostat, as explained in Chapter 4, acts only on the atomistic representation of the molecules. The Langevin thermostat is initialized with the sentence

```
thermostat langevin $temperature $friction
```

while the DPD variant requires

```
thermostat dpd $temperature $friction $cutoff
```

where, in both cases, `temperature` is the temperature and `friction` is the friction coefficient required by the forces [27,34,40]. `cutoff` is the cut-off of the DPD pair interaction.

Molecule definition

The molecules can be defined in the standard way provided by ESPResSo. A simple tetrahedral molecule, for example, can be declared with

```
set molecule_topology $molecule_type
part 1 pos $pos1x $pos1y $pos1z virtual 0
lappend molecule_topology 1
part 2 pos $pos2x $pos2y $pos2z virtual 0
lappend molecule_topology 2
part 3 pos $pos3x $pos3y $pos3z virtual 0
lappend molecule_topology 3
part 4 pos $pos4x $pos4y $pos4z virtual 0
lappend molecule_topology 4
part 5 pos $pos5x $pos5y $pos5z virtual 1
lappend molecule_topology 5
eval analyze set $molecule_topology
analyze set topo_part_sync
```

The position of the virtual site can be initialized by calling

```
integrate 0
```

while the usual command

```
integrate $nsteps
```

integrates `nsteps` steps of the equations of motion, properly updating the positions of the centers of mass.

Interface pressure correction

The interface pressure correction supports only tabulated force fields. Therefore, coarse-grained and interface-corrected coarse-grained force fields must be defined in this way, included in the file `filename`. The command

```
inter $type1 $type2 adress_tab_ic $filename
```

initializes the coarse-grained force between the virtual particles of kind `type1` and `type2`. The file must be written in the same format as the tabulated interactions of ESPResSo: the first four lines are the special character `#`, the number of points N and the minimum and maximum separation distances r_{min} and r_{max}. Below, the two potentials are introduced in five columns as r, $\mathbf{F}^{CG}/r$, U^{CG}, $\mathbf{F}^{IC}$, U^{IC}. The number of points and the cut-off radius are assumed to be the same for both potentials, while the values of r are equally distributed between r_{min} and r_{max} with a fixed distance $(r_{max}-r_{min})/(N-1)$. The position and the potential columns are ignored in the calculations; their inclusion is only for the sake of readability.

Thermodynamic force

```
thermodynamic_force $type $filename $prefactor
```

where `type` is the type of the particle on which the force specified in `filename` will be exerted. `prefactor` is a coefficient defined by the user that multiplies the force. The format is consistent with the usual tabulated potential format in ESPResSo: the initial four consist in the special character `#`, followed by the minimum and maximum distances r_{min} and r_{max}. Then, three columns are entered: s, $-\frac{dU}{ds}$ and U. s corresponds to the dimensionless position in the hybrid region $\frac{x}{d_{hy}}$, with d_{hy} its width, ranging from 0 to 1. The derivative of the potential has to be expressed in terms of this variable. The third column is the potential associated with this field; it has no effect on the equations of motion and is included only for readability.

Bibliography

[1] K. Huang. *Statistical Mechanics.* John Wiley and Sons, 1987.

[2] I. R. McDonald J. P. Hansen. *Theory of Simple Liquids.* Academic Press, 2 edition, 1986.

[3] D. McQuarrie. *Statistical Mechanics.* Harper and Row, 1976.

[4] J. O. Hirschfelder, C. F. Curtiss, and R. B. Bird. *Molecular Theory of Gases and Molecules.* John Wiley and Sons, 1964.

[5] L. E. Reichl. *A Modern Course in Statistical Physics.* Wiley-VCH, 2 edition, 2004.

[6] P. A. Egelstaff. *An Introduction to the Liquid State.* Clarendon Press, 2 edition, 1992.

[7] P. Attard. Pair-hypernetted-chain closure for three-body potentials: Results for argon with the axilrod-teller triple-dipole potential. *Phys. Rev. A*, 45, 1992.

[8] H. Goldstein. *Classical Mechanics.* MA: Addison-Wesley, 1950.

[9] J. B. Marion and S. T. Thornton. *Classical Dynamics of Particles and Systems.* Harcourt Brace Jovanovich, 3 edition, 1988.

[10] R. L. C. Akkermans and G. Ciccotti. On the equivalence of atomic and molecular pressure. *J. Phys. Chem. B*, 108:6866, 2004.

[11] R. G. Winkler. Virial pressure of periodic systems with long range forces. *J. Chem. Phys.*, 117:2449, 2002.

[12] M. P. Allen and D. J. Tildesley. *Computer Simulation of Liquids.* Clarendon Press, 1987.

[13] D. P. Landau and K. Binder. *A Guide to Monte Carlo Simulations in Statistical Physics.* Cambridge University Press, 2002.

[14] D. Frenkel and B. Smit. *Understanding Molecular Simulation: From Algorithms to Applications.* Academic Press, San Diego, 2002.

[15] D. C. Rapaport. *The Art of Molecular Dynamics Simulation*. Cambridge University Press, 2 edition, 2004.

[16] R. W. Hockney and J. W. Eastwood. *Computer Simulations Using Particles*. Mc-Graw-Hill, New York, 1981.

[17] L. Verlet. Computer "experiments" on classical fluids. i. thermodynamical properties of lennard-jones molecules. *Phys. Rev.*, 159:98, 1967.

[18] W. C. Swope, H. C. Andersen, P. H. Berens, and K. R. Wilson. A computer simulation method for the calculation of equilibrium constatns for the formation of physical clusters of molecules: Application to small water clusters. *J. Chem. Phys.*, 76:637, 1994.

[19] M. Tcukerman, B. J. Berne, and G. J. Martyna. Reversible multiple time scale molecular dynamics. *J. Chem. Phys.*, 97:1990, 1992.

[20] H. C. Andersen. Molecular dynamics at constant pressure and/or temperature. *J. Chem. Phys.*, 72:2384, 1980.

[21] D. J. Evans and G. P. Morris. *Statistical Mechanics of Non-Equilibrium Liquids*. Academic Press, London, 1990.

[22] S. Nosé. A unified formulation of the constant temperature molecualr dynamics. *J. Chem. Phys.*, 81:511, 1984.

[23] W. G. Hoover. Canonical dynamics: Equilibrium phase-space distributions. *Phys. Rev. A*, 31:1695, 1985.

[24] G. J. Martyna, M. L. Klein, and M. E. Tuckerman. Nosé-hoover chains: The canonical ensemble via continouus dynamics. *J. Chem. Phys.*, 97:2635, 1992.

[25] H. J. C. Berendsen, J. P. M. Pootma, A. DiNola, and J. R. Haak. Molecular dynamics with coupling with and external bath. *J. Chem. Phys.*, 81:3684, 1984.

[26] G. Bussi, D. Donadio, and M. Parrinello. Canonical sampling through velocity rescaling. *J. Chem. Phys.*, 126:014101, 2007.

[27] B. Dünweg. Langevin methods. In B Dünweg, A. I. Milchev, and D. P. Landau, editors, *Computer Simulations of Surfaces and Interfaces: Proceedings of the NATO Advanced Study Institute, Albena, Bulgaria, from 9 to 20 September 2002*, page 77. Springer Netherlands, 1 edition, February 2004.

[28] T. Schneider and E. Stoll. Molecular-dynamics study of a three-dimensional one-component model for distortive phase transitions. *Phys. Rev. B*, 17:1302, 1978.

[29] B. A. Mann, E. Everaers, C. Holm, and K. Kremer. Scaling in polyelectrolyte networks. *Europhys. Lett.*, 67:786, 2004.

[30] H. Risken. *The Fokker-Planck equation.* Berlin:Springer-Verlag, 1984.

[31] P. Español and P. Warren. Statistical mechanics of dissipative particle dynamics. *Europhys. Lett.*, 30:191, 1995.

[32] A. Kopf, B. Düenweg, and W. Paul. Dynamics of polymer "isotope" mixtures: Molecular dynamics simulation and rouse model analysis. *J. Chem. Phys.*, 107:6945, 1997.

[33] M. Pütz, K. Kremer, and G. S. Grest. What is the entanglement length in a polymer melt? *Europhys. Lett.*, 49:735, 2000.

[34] T. Soddemann, B. Dünweg, and K. Kremer. Dissipative particle dynamics: A useful thermostat for equilibrium and nonequilibrium molecular dynamics simulations. *Phys. Rev. E*, 68:046702, 2003.

[35] B. Dünweg. Molecular dynamics algorithms and hydrodynamics screening. *J. Chem. Phys.*, 99:6977, 1993.

[36] P. J. Hoogerbrugge and J. M. V. A. Koelman. Simulating microscopic hydrodynamic phenomena with dissipative particle dynamics. *Europhys. Lett.*, 19:155, 1992.

[37] P. Español. Hydrodynamics from dissipative particle dynamics. *Phys. Rev. E*, 52:1734, 1995.

[38] R. Groot and P. Warren. Dissipative particle dynamics: Bridging the gap between atomistic and mesoscopic simulation. *J. Chem. Phys.*, 107:4423, 1997.

[39] I. Pagonabarraga, M. H. J. Hagen, and D. Frenkel. Self-consistent dissipative particle dynamics algorithm. *Europhys. Lett.*, 42:377, 1998.

[40] C. Junghans, M. Praprotnik, and K. Kremer. Transport properties controlled by a thermostat: An extended dissipative particle dynamics thermostat. *Soft Matter*, 4:156, 2008.

[41] M. Karplus and J. A. McCammon. Molecular dynamics simulations of biomolecules. *Nat. Struct. Biol.*, 9:646, 2002.

[42] X. Daura, B. Jaun, D. Seebach, W. F. van Gunsteren, and A. E. Mark. Reversible peptide folding : When simulation meets experiment. *J. Mol. Biol.*, 280:925, 1998.

[43] H. Fan and A. E. Mark. Refinement of homology based protein structures by molecular dynamics simulation techniques. *Protein Science*, 13:211, 2004.

[44] X. Daura, W. F. van Gunsteren, and A. E. Mark. Folding-unfolding termodynamics of a beta-heptapeptide from equilibrium simulations. *Proteins: Struct. Funct. Genet.*, 34:269, 1999.

[45] G. Colombo, D. Roccatano, and A. E. Mark. Folding and stability of the three-stranded b-sheet peptide betanova: Insights from molecular dynamics simulations. *Proteins: Struct. Funt. Genet.*, 46:380, 2002.

[46] A. V. Verde and D. Frenkel. Simulation study of micelle formation by bile salts. *Soft Matter.*

[47] S. Fujiwara, T. Itoh, M. Hashimoto, and Y. Tamura. Molecular dynamics simulation of micelle formation in amphiphilic solution. *Mol. Sim.*, 33:115, 2007.

[48] R. Pool and P.G. Bolhuis. Can purely repulsive soft potential predict micelle formation correctly? *Phys. Chem. Chem. Phys.*, 8:941, 2006.

[49] P. Bolhuis and D. Frenkel. Microscopic and mesoscopic simulation of entropic micelles. *Physica A*, 244:45, 1997.

[50] R. Braun, D. Engelman, and K. Schulten. Molecular dynamics simulations of micelle formation around dimeric glycophorin a transmembrane helices. *Biophys. J.*, 87:754, 2004.

[51] H. Christen and H. Eicke. Monte-carlo model of micelle formation. *J. Phys. Chem.*, 78:1423, 1974.

[52] L. Delle Site, C. F. Abrams, A. Alavi, and K. Kremer. Polymers near metal surfaces: Selective adsorption and global conformations. *Phys. Rev. Lett.*, 89:156103, 2002.

[53] L. Delle Site, S. Leon, and K. Kremer. Bpa-pc in a ni(111) surface: The interplay between adsorption energy and conformational entropy for different chain end modifications. *J. Am. Chem. Soc.*, 126:2944, 2004.

[54] D. Andrienko, S. León, L. Delle Site, and K. Kremer. Adhesion of polycarbonate blends on a nickel surface. *Macromolecules*, 38:5810, 2005.

[55] X. Zhou, D. Andrienko, L. Delle Site, and K. Kremer. Dynamic surface decoupling in a sheared polymer melt. *Europhys. Lett.*, 70:264, 2005.

[56] X. Zhou, D. Andrienko, L. Delle Site, and K. Kremer. Flow boundary conditions for chain-end adsorbing polymer blends. *J. Chem. Phys.*, 123:104904, 2005.

[57] J. J. Nicholas, K. E. Gubbins, W. W. Streett, and D. J. Tildesley. Equation of state for the lennard-jones fluid. *Mol. Phys.*, 37:1429, 1979.

[58] E. J. Meijer, D. Frenkel, R. A. LeSan, and H. J. C. Ladd. Location of melting point at 300k of nitrogen by monte carlo simulation. *J. Chem. Phys.*, 92:7570, 1990.

[59] A. J. C. Ladd and L. V. Woodcock. Ttriple-point coexistence properties of the lennard-jones system. *Chem. Phys. Lett.*, 51:155, 1977.

[60] J. A. C. Veerman and D. Frenkel. Phase diagram of a system of hard spherocylinders by computer simulation. *Phys. Rev. A*, 41:3237, 1990.

[61] M. Rovere, D. W. Hermann, and K. Binder. The gas-liquid transition of the two-dimensional lennard-jones fluid. *J. Phys.:Condens. Matter*, 2:7009, 1990.

[62] B. B. Laird and A. D. J. Haymet. Phase diagram for the inverse sixth power potential system from molecular dynamics simulations. *Mol. Phys.*, 75:71, 1992.

[63] S. Toxvaerd. Molecular dynamics calculation of the equation of state of alkanes. *J. Chem. Phys.*, 93:4290, 1990.

[64] M. J. P. Nijmeijer, A. F. Bakker, C. Bruin, and J. H. Sikkenk. A molecular dynamics simulation of the lennard-jones liquid-vapour interface. *J. Chem. Phys.*, 89:3789, 1998.

[65] A. Belonoshko. Molecular dynamics of silica at high pressures: Equation of state, structure, and phase transitions. *Geochimica et Cosmochimica Acta*, 58:1557, 1994.

[66] M. Matsui, S. C. Parker, and M. Leslie. The md simulation of the equation of state of mgo: Application as a pressure calibration standard at high temperature and high pressure. *American Mineralogist*, 85:312, 2000.

[67] T. P. Straatsma, H. J. C. Berendsen, and J. P. M. Postma. Free energy of hydrophobic hydration: A molecular dynamics study of noble gases in water. *J. Chem. Phys.*, 85:6720, 1986.

[68] K. S. Shing and K. E. Gubbins. Free energy and vapour-liquid equilibria for a quadrupolar lennard-jones fluid. *Mol. Phys.*, 46:1109, 1992.

[69] C. H. Bennett. Efficient estimation of free energy differences from monte carlo data. *J. Comp. Phys.*, 22:245, 1976.

[70] D. Frenkel and A. J. C. Ladd. New monte carlo method to compute the free energy of arbitrary solids. application to the fcc and hcp phases of hard spheres. *J. Chem. Phys.*, 81:3188, 1984.

[71] A. D. Bruce, N. B. Wilding, and G. J. Ackland. Free energy of crystalline solids: A lattice-switch monte carlo method. *Phys. Rev. Lett.*, 79:3002, 1997.

[72] G. Orkoulas and A. Z. Panagiotopoulos. Free energy and phase equilibria for the restricted primitive model of ionic flids from monte carlo simulations. *J. Chem. Phys.*, 101:1452, 1994.

[73] ed. K. Binder. *Monte Carlo and molecular dynamics simulations in polymer science*. Oxford University Press, New York, 1995.

[74] G. Brannigan, L. C.-L. Lin, and F. L. H. Brown. Implicit solvent simulation models for biomembranes. *Eur. Biophys. J.*, 35:104–124, 2006.

[75] G. Brannigan, P. F. Philips, and F. Brown. Flexible lipid bilayers in implicit solvent. *Phys. Rev. E*, 72:011915, 2005.

[76] B. Roux and T. Simonson. Implicit solvent models. *Biophys. Chem.*, 78:1–20, 1999.

[77] P. Ferrara, J. Apostolakis, and A. Caflisch. Evaluation of a fast implicit solvent model for molecular dynamics simulations. *Proteins*, 46:24–33, 2002.

[78] D. Bechor and N. Ben-Tal. Implicit solvent model studies of the interactions of the influenza hemagglutin in fusion peptide with lipid bilayers. *Biophys. J.*, 80:643–655, 2001.

[79] B. J. Reynwar, G. Illya, V. A. Harmandaris, M. M. Mueller, K. Kremer, and M. Deserno. Aggregation and vesiculation of membrane proteins by curvature-mediated interactions. *Nature*, 477:461, 2007.

[80] M. Praprotnik, L. Delle Site, and K. Kremer. Multiscale simulation of soft matter: From scale bridging to adaptive resolution. *Annu. Rev. Phys. Chem.*, 59:545, 2008.

[81] B. Lambeth, C. Junghans, K. Kremer, C. Clementi, and L. Delle Site. *submitted*.

[82] C. Peter and K. Kremer. Multiscale simulation of soft matter systems. *Faraday Discuss.*, 144:9, 2010.

[83] P. Gilles de Gennes. *Scaling concepts in polymer physics*. Cornell University Press, 1979.

[84] A. A. Louis. Beware of density dependent pair potentials. *J. Phys.: Condens. Matter*, 14:9187, 2002.

[85] S. Izvekov and G. A. Voth. A multiscale coarse-graining method for biomolecular systems. *J. Phys. Chem. B*, 109:2469, 2005.

[86] W. G. Noid, J.-W. Chu, G. S. Ayton, and G. A. Voth. Multiscale coarse-graining and structural correlations: Connections to liquid-state theory. *J. Phys. Chem. B*, 111:4116, 2007.

[87] S.J. Marrink, H.J. Risselada, S. Yefimov, D.P. Tieleman, and A.H. de Vries. The martini forcefield: coarse grained model for biomolecular simulations. *J. Phys. Chem. B*, 111:7812, 2007.

[88] B. Hess, S. León, N. van der Vegt, and K. Kremer. Long time atomistic polymer trajectories from coarse grained simulations: bisphenol-a polycarbonate. *Soft Matter*, 2:409, 2006.

[89] D. Fritz, V. Harmandaris, K. Kremer, and N. van der Vegt. Coarse-grained polymer melts based on isolated atomistic chains: Simulation of polystyrene of different tacticities. *Macromolecules*, 42:7579, 2009.

[90] R. L. Henderson. A uniqueness theorem for fluid pair correlation functions. *Phys. Lett. A*, 49:197, 1974.

[91] V. Ruehle, C. Junghans, A. Lukyanov, K. Kremer, and D. Andrienko. Versatile object-oriented toolkit for coarse-graining applications. *J. Chem. Theor. Comp.*, 5:3211, 2009.

[92] A. Lyubartsev and A. Laaksonen. Calculation of effective interaction potentials from radial distribution functions: A reverse monte carlo approach. *Phys. Rev. E*, 52:3730, 1995.

[93] D. Reith, M. Puetz, and F. Mueller-Plathe. Deriving effective mesoscale potentials from atomistic simulations. *J. Comput. Chem.*, 24:1624, 2003.

[94] R. Faller. Automatic coarse graining of polymers. *Polymer*, 45:3869, 2004.

[95] W. Tschoep, K. Kremer, J. Batoulis, T. Burger, and O. Hahn. Simulation of polymer melts. i. coarse-graining procedure for polycarbonates. *Acta Polym.*, 49:61, 1998.

[96] M. Praprotnik, L. Delle Site, and K. Kremer. Adaptive resolution scheme for efficient hybrid atomistic-mesoscale molecular dynamics simulations of dense liquids. *Phys. Rev. E*, 73:066701, 2006.

[97] H. Wang, C. Junghans, and K. Kremer. Comparative atomistic and coarse-grained study of water: What do we lose by coarse-graining? *Euro. Phys. J. E*, 28:221, 2009.

[98] M. Johnson, T. Head-Gordon, and A. A. Louis. Representability problems for coarse-grained water potentials. *J. Chem. Phys.*, 126:144509, 2007.

[99] Q. Sun, J. Ghosh, and R. Faller. Coarse-graining of condensed phase and biomolecular systems. Springer Netherlands, 1 edition, 2009.

[100] F. Stillinger, H. Sakai, and S. Torquato. Statistical mechanical models with effective potentials: Definitions, applications, and thermodynamic consequences. *J. Chem. Phys.*, 117:288, 2002.

[101] V. Harmandaris and K. Kremer. Dynamics of polystyrene melts through hierarchical multiscale simulations. *Macromolecules*, 42:791, 2009.

[102] K. Tarmyshov and F. Müller-Plathe. Interface between platinum(111) and liquid isopropanol(2-propanol): A model for molecular dynamics studies. *J. Chem. Phys.*, 126:074702, 2007.

[103] J. Rogal, K. Reuter, and M. Scheffler. Co oxidation on pd(100) at technologically relevant pressure conditions: First-principles kinetic monte carlo study. *Phys. Rev. B*, 77:155410, 2008.

[104] K. Reuter, D. Frenkel, and M. Scheffler. The steady state of heterogeneous catalysis, studied by first-principles statistical mechanics. *Phys. Rev. Lett.*, 93:116105, 2004.

[105] L. Ghiringhelli, B. Hess, N. van der Vegt, and L. Delle Site. Competing adsorption between hydrated peptides and water onto metal surfaces: From electronic to conformational properties. *J. Am. Chem. Soc.*, 130:13460, 2008.

[106] O. Alexiadis, V. Harmandaris, V. Mavrantzas, and L. Delle Site. Atomistic simulation of alkanethol self-assembled monolayers on different metal surfaces via a quantum, first-principles parametrization of the sulfur-metal interaction. *J. Phys. Chem. C*, 111:6380, 2007.

[107] G. Lu, E. B. Tadmor, and E. Kaxiras. From electrons to finite elements: A concurrent multiscale approach for metals. *Phys. Rev. B*, 73:024108, 2006.

[108] G. Csanyi, T. Albaret, M. C. Payne, and A. D. Vita. "learn on the fly": A hybrid classical and quantum-mechanical molecular dynamics simulation. *Phys. Rev. Lett.*, 93:175503, 2004.

[109] G. De Fabritiis, R. Delgado-Buscalioni, and P. Coveney. Multiscale modeling of liquids with molecular specificity. *Phys. Rev. Lett.*, 97:134501, 2006.

[110] R. Delgado-Buscalioni and G. De Fabritiis. Embedding molecular dynamics within fluctuating hydrodynamics in multiscale simulations of liquids. *Phys. Rev. E*, 76:036709, 2007.

[111] E. Villa, A. Balaeff ad L. Mahadevan, and K. Schulten. Multiscale method for simulating protein-dna complexes. *Multiscale Model. Simul.*, 2:527–553, 2004.

[112] M. Neri, C. Anselmi, M. Cascella, A. Maritan, and P. Carloni. Coarse-grained model of proteins incorporating atomistic detail of the active site. *Phys. Rev. Lett.*, 95:218102, 2005.

[113] H. Rafii-Tabar, L. Hua, and M. Cross. A multi-scale atomistic-continuum modelling of crack propagation in a two-dimensional macroscopic plate. *J. Phys: Cond. Matt.*, 10:2375, 1998.

[114] J. Broughton, F. Abraham, N. Bernstein, and E. Kaxiras. Concurrent coupling of length scales: Methodology and application. *Phys. Rev. B*, 60:2391–2403, 1999.

[115] J. Smirnova, L. V. Zhigilei, and B. Garrison. A combined molecular dynamics and finite element method technique applied to laser induced pressure wave propagation. *Comp. Phys. Comm.*, 118:11–16, 1999.

[116] S. O'Connell and P. Thompson. Molecular dynamics–continuum hybrid computations: A tool for studying complex fluid flows. *Phys. Rev. E*, 52:R5792–R5795, 1995.

[117] N. G. Hadjiconstantinou. Combining atomistic and continuum simulations of contact-line motion. *Phys. Rev. E*, 59:2475–2478, 1999.

[118] M. Praprotnik, L. Delle Site, and K. Kremer. Adaptive resolution molecular-dynamics simulation: Changing the degrees of freedom on the fly. *J. Chem. Phys.*, 123:224106, 2005.

[119] M. Praprotnik, K. Kremer, and L. Delle Site. Adaptive molecular resolution via a continuous change of the phase space dimensionality. *Phys. Rev. E*, 75:017701, 2007.

[120] B. Ensing, S. O. Nielsen, P. Moore, M. Klein, and M. Parrinello. Energy conservation in adaptive hybrid atomistic/coarse-grain molecular dynamics. *The Journal of Chemical Physics*, 132:114101, 2010.

[121] A. Heyden and D. Truhlar. A conservative algorithm for an adaptive change of resolution in mixed atomistic/coarse-grained multiscale simulations. *J. Chem. Theor. Comput.*, 4:217, 2008.

[122] A. Poma and L. Delle Site. Classical to path-integral adaptive resolution in molecular simulation: Towards a smooth quantum-classical coupling. *Phys. Rev. Lett.*, 104:250201, 2010.

[123] R. Bulo, B. Ensing, J. Sikkema, and L. Visscher. Toward a practical method for adaptive qm/mm simulations. *J. Chem. Theo. Comp.*, 5:2212, 2009.

[124] M. Praprotnik, K. Kremer, and L. Delle Site. Fractional dimensions of phase space variables: a tool for varying the degrees of freedom of a system in a multiscale treatment. *J. Phys. A: Math. Theor.*, 40:F281, 2007.

[125] H. Weber and G. Arfken. *Mathematical methods for physicists*. Academic Press, 5 edition, 1995.

[126] M. Praprotnik, L. Delle Site, and K. Kremer. A macromolecule in a solvent: Adaptive resolution molecular dynamics simulation. *J. Chem. Phys.*, 126:134902, 2007.

[127] S. Matysiak, C. Clementi, M. Praprotnik, K. Kremer, and L. Delle Site. Modeling diffusive dynamics in adaptive resolution simulation of liquid water. *J. Chem. Phys.*, 128:024503, 2008.

[128] B. Hess, C. Kutzner, D. van der Spoel, and E. Lindahl. Gromacs 4: Algorithms for highly efficient, load-balanced, and scalable molecular simulation. *J. Chem. Theory Comput*, 4(3):435–447, 2008.

[129] C. Junghans and S. Poblete. A reference implementation of the adaptive resolution scheme in espresso. *Comp. Phys. Comm., accepted*, 2010.

[130] T. Munakata. Mechanical and Langevin thermostats: Gulton staircase problem. *Phys. Rev. E*, 59:5048, 1999.

[131] R. Miller. The jackknife-a review. *Biometrika*, 61:1, 1974.

[132] S. Poblete, S. Fritsch, C. Junghans, K. Kremer, G. Ciccotti, and L. Delle Site. *In preparation.*

[133] B. D. Todd, D. J. Evans, and P. J. Daivis. Pressure tensor for inhomogeneous fluids. *Phys. Rev. E*, 52:1627, 1995.

[134] S. Poblete, M. Praprotnik, K. Kremer, and L. Delle Site. Coupling different levels of resolution in molecular simulations. *J. Chem. Phys.*, 132:114101, 2010.

[135] G. Careri. *Hydration processes in biology: Theoretical and experimental approaches.* edited by M. C. Besillient-Funel(IOS, Amsterdam), 1999.

[136] M. Doi and S. F. Edwards. *The theory of polymer dynamics.* Clarendon Press, Oxford, 1986.

[137] *Monte Carlo and Molecular Dynamics simulation in Polymer Science.* Clarendon Press, Oxford, 1995.

[138] H.J. Limbach, A. Arnold, B.A. Mann, and C. Holm. ESPResSo–an extensible simulation package for research on soft matter systems. *Computer Physics Communications*, 174:704, 2006.

[139] Tcl/Tk. Tool command language/toolkit, 2003.